IMAGE: A MAP OF THE STARS OF THE ORION CONSTELLATION

JournalPreview

London Journal of Research in Science: Natural & Formal

Volume 24 | Issue 9 | Compilation 1.0

Great Britain Journals Press

WWW.JOURNALSPRESS.COM

Journal Content
In this Issue

Great Britain Journals Press

Autonomous Phase Identification in X-ray Diffraction: A Hybrid Approach with Bayesian FusionNet and Feature-Optimized Ensemble Learning

Dr. Subhash Khatarkar & Dr. Kamlesh Ahirwar

ABSTRACT

X-ray diffraction (XRD) plays a pivotal role in material characterization, offering valuable insights into crystalline structures. This study introduces a comprehensive framework for autonomous phase identification through a machine learning-guided approach. The proposed methodology comprises four key stages. In the pre-processing phase, raw data undergoes meticulous cleaning to eliminate noise, followed by normalization and smoothing procedures to ensure data integrity. Feature extraction involves a multi-faceted approach. Peak identification meticulously captures critical features such as peak position, intensity, and width within XRD patterns. Statistical features, encompassing mean, standard deviation, skewness, and kurtosis, provide a robust characterization of the dataset. The incorporation of Discrete Wavelet Transform further enriches the feature space by capturing both high and low-frequency information. For feature selection, a Hybrid Optimization Approach, combining the Kookaburra Optimization Algorithm (KOA) and White Shark Optimizer, is employed. This ensures an optimal subset of features for subsequent analysis. Phase identification is facilitated by a Bayesian FusionNet, integrating the strengths of Improved GhostNetV2, Bayesian Neural Network (BNN), and Feedforward Neural Network (FNN). The outcomes from these models are aggregated by taking the mean, enhancing the reliability and accuracy of phase identification.

Keywords: X-ray diffraction, Discrete wavelet transform, ghost NetV2, BNN, FNN, KOA.

Classification: LCC Code: TA418.9.N35

Language: English

Great Britain Journals Press

LJP Copyright ID: 925691
Print ISSN: 2631-8490
Online ISSN: 2631-8504

London Journal of Research in Science: Natural & Formal

Volume 24 | Issue 9 | Compilation 1.0

Autonomous Phase Identification in X-ray Diffraction: A Hybrid Approach with Bayesian FusionNet and Feature-Optimized Ensemble Learning

Dr. Subhash Khatarkar[α] & Dr. Kamlesh Ahirwar[σ]

ABSTRACT

X-ray diffraction (XRD) plays a pivotal role in material characterization, offering valuable insights into crystalline structures. This study introduces a comprehensive framework for autonomous phase identification through a machine learning-guided approach. The proposed methodology comprises four key stages. In the pre-processing phase, raw data undergoes meticulous cleaning to eliminate noise, followed by normalization and smoothing procedures to ensure data integrity. Feature extraction involves a multi-faceted approach. Peak identification meticulously captures critical features such as peak position, intensity, and width within XRD patterns. Statistical features, encompassing mean, standard deviation, skewness, and kurtosis, provide a robust characterization of the dataset. The incorporation of Discrete Wavelet Transform further enriches the feature space by capturing both high and low-frequency information. For feature selection, a Hybrid Optimization Approach, combining the Kookaburra Optimization Algorithm (KOA) and White Shark Optimizer, is employed. This ensures an optimal subset of features for subsequent analysis. Phase identification is facilitated by a Bayesian FusionNet, integrating the strengths of Improved GhostNetV2, Bayesian Neural Network (BNN), and Feedforward Neural Network (FNN). The outcomes from these models are aggregated by taking the mean, enhancing the reliability and accuracy of phase identification. This innovative framework not only automates phase identification in X-ray diffraction but also showcases the efficacy of a hybridized machine learning approach, amalgamating optimization algorithms and neural networks for enhanced performance and interpretability. The proposed methodology holds significant promise for advancing material science research and facilitating efficient analysis in diverse applications.

Keywords: X-ray diffraction, Discrete wavelet transform, ghost NetV2, BNN, FNN, KOA.

Author α: Department of Physics, J.H. Government Post Graduate College Betul (M.P.) 460001.
σ: J.H. Government Post Graduate College Betul (M.P.) India 460001.

I. INTRODUCTION

An XRD is a useful non-destructive analytical technique for analyzing crystal structure, phase composition, and orientation of powder, solid, and liquid materials [1]. Tiny crystallites include a wide variety of materials. The term "phase" refers to these crystals' structural type and chemical makeup. Materials may consist of both crystalline and non-crystalline components, and they may be single phase or multiphase mixes [2]. An X-ray diffractometer can distinguish between different crystalline phases by their respective diffraction patterns [3]. Phase identification is often carried out by comparing reference database patterns to X-ray diffraction patterns acquired from unidentified materials. This method is comparable to the procedure of comparing fingerprints at a crime scene [4]. XRD is the

London Journal of Research in Science: Natural & Formal

result of constructive interaction between crystalline sample and X-rays. The wavelength of the X-rays used is equal to the distance between atoms in crystalline lattice [5]. The resulting diffraction pattern may be analyzed in several ways, most popular being the application of widely recognized Bragg's Law, which is used to measure crystals and their phases [6]. An X-ray source, XRD detector, and sample container are the three main parts of X-ray apparatus. X-rays that the source emit light the sample. After that, sample phase diffracts it so that it may get into detector [7]. Adjusting sample, tube, and detector to change diffraction angle determines the intensity and collects diffraction data. Depending on sample type and diffractometer's geometry, the angle between incident beam and sample can be either constant or variable and is commonly matched with diffracted beam angle [8].

Algorithms for machine learning are ideal for analyzing big and complicated datasets because they can recognize patterns and correlations in the data. They have been used in materials research to solve a variety of issues, such as the processing of imaging data and the prediction of material characteristics [9]. Machine learning has been applied to X-ray diffraction for the purpose of classifying diffraction patterns and analyzing crystal structure [10]. An interpretable machine learning model can enable data-driven quantification of empirical expert knowledge, and a quick and easy machine learning approach can categorize crystal systems and space groups based on powder XRD patterns with high accuracy. The powder XRD pattern need to be employed as material descriptor for machine learning (ML)-based symmetry detection and property prediction [11]. Recent years have seen a major increase in the interest of material scientists and engineers in machine learning as well as high-throughput testing and computation. It is common practice to create suitable material descriptors for the systematic representation of materials in prospective machine learning models [12]. As long as actual or theoretical standard powder XRD patterns are available, knowledge-based material descriptors cannot be extracted for use in ML [13]. Full-profile powder XRD patterns, which indicate the material identity, may be used in place of conventional descriptors that need complex knowledge-based extraction processes. It is difficult to create a flexible ML model that can predict properties and identify symmetry for all typical inorganic materials [14]. The incorporation of ML techniques into XRD pattern analysis has been driven by need for accurate phase identification, quantification of multiphase mixtures with varying raw data quality, and expansion the amount of data that is available [15]. Processing XRD observations has become increasingly dependent on ML over past 10 years as processing power has increased and both XRD and ML have been made simpler and better.

This study introduces a novel framework for autonomous phase identification in XRD, leveraging a hybrid approach that combines feature-optimized ensemble learning with a Bayesian FusionNet. The primary aim of this research is to develop a self-sufficient method for phase detection in XRD by utilizing machine learning and optimization approaches. Beyond simple automation, a hybrid technique combining the best aspects of feature-optimized ensemble learning and Bayesian FusionNet is being researched and developed.

1.1. Contribution of Study

The following is an overview of the study's contributions:

- The paper discusses the necessity of automating the X-ray diffraction phase identification procedure. The paper contributes significantly to simplifying XRD pattern analysis, which is essential for material characterization, by presenting a complete framework incorporating machine learning-led techniques.
- The use of a Hybrid Optimization Approach, combining the Kookaburra Optimization Algorithm (KOA) and White Shark Optimizer for feature selection, is a notable contribution. By doing this, the efficiency and efficacy of the phase identification process are maximized since the most pertinent subset of characteristics is chosen for further examination.

- ❖ Phase identification is made more accurate and reliable by using ensemble learning, namely by averaging the results from Improved GhostNetV2, BNN, and FNN. An improved forecast is produced by using ensemble approaches, which lessen the biases and mistakes of individual models.
- ❖ The suggested approach has plenty of potential for developing material science research. The study enhances an efficacy and efficiency of material analysis by automating and improving phase identification procedure in XRD.

1.2. Structure of Paper

The remaining part of paper is structured as follows: In Section 2, relevant existing works are provided; proposed methodology is covered in Section 3; Section 4 provides an explanation of the findings; Finally, Section 5 includes a conclusion and suggestions for further research.

II. LITERATURE REVIEW

The study of literature provides an extensive overview of what is currently known about autonomous phase identification in X-ray diffraction. By laying out the background, offering a historical viewpoint, and critically assessing the most recent approaches, it prepares the reader for the later sections of the work. In the end, it justifies the novelty and applicability of suggested hybrid approach using Bayesian FusionNet and Feature-Optimized Ensemble Learning.

In 2020, Hocine *et al.*, [16] described the application of operando X-ray diffraction in laser-assisted 3D printing. Operando X-ray diffraction, according to authors, is a method that enables real-time observation of structural alterations that take place during printing. To optimize the printing settings and raise the caliber of printed goods, the study emphasized how crucial it is to comprehend these alterations. Operando X-ray diffraction can offer insightful information about the printing process and help enhance 3D printing technology, according to conclusion.

In 2019, Oviedo *et al.*, [17] presented a novel approach that makes use of deep neural networks and data augmentation to identify tiny X-ray diffraction datasets. This study provided a quick and easy-to-understand method that raises classification accuracy. This paper identified potential differences between experimental thin film XRD patterns and simulated XRD powder patterns by proposing a physics-informed strategy for data augmentation that expands limited, focused experimental and simulated datasets. The process entails training a deep neural network to categorize the diffraction patterns and artificially growing dataset using data augmentation techniques. The efficiency and precision of X-ray diffraction analysis in materials science research may be improved by using this method.

In 2020, Lee *et al.*, [18] presented a simple, quick methodology based on deep learning methods to solve complicated multiphase inorganic compound challenges including phase identification and measurement. A viable powder XRD pattern simulation was performed on 170 inorganic compounds in Sr-Li-Al-O quaternary compositional pool, where potential LED phosphors have been discovered. Finally, 1,785,405 synthetic XRD patterns were produced by combinatorially merging simulated powder XRD patterns of 170 inorganic compounds. This large prepared dataset was used to build and train convolutional neural network (CNN) models. The fully trained CNN model accurately and rapidly detects component phases while working with complex multiphase inorganic substances.

In 2022, Sivaraman *et al.*, [19] addressed the difficulties in figuring out relationships between structure and properties of amorphous and liquid metal oxides. This study was suggested predicting chemically realistic structures for HfO_2 by ML with Gaussian Approximation Potential (GAP). The GAP model used training datasets to achieve Density Functional Theory-Strongly Constrained and Appropriately Normed (DFT-SCAN) theoretical level. This topology was shown to be consistent with structure of a

range of liquid and amorphous transition metal oxides with different ion sizes, including TiO2 and ZrO2.

In 2020, Utimula *et al.*, [20] highlighted the use of ML clustering to analysis of powder XRD pattern to determine ThMn12-type alloys of compositions. This paper investigates the potential applications of this method to further materials science's knowledge of alloy composition. The XRD spectrum patterns are subjected to a clustering approach employing dynamic-time-wrapping (DTW) analysis to determine microscopic structures of substituents added to main phase of magnetic alloys. This methodology developed here was not exclusive to system under consideration; rather, it may be broadly applied to systems whose attributes are to be adjusted by atomic replacements within a phase.

In 2022, Dong *et al.*, [21] delivered a deep learning algorithm that can be used to predict XRD spectrum based only on a material's composition. This algorithm can then be used to infer important structural features for structural analysis that occurs later on, such as classification of crystal systems or space groups, calculation of crystal lattice parameters, or prediction of material properties. This DeepXRD algorithm may obtain good performance for XRD prediction as assessed across test sets according to benchmark tests on two datasets. Therefore, it may be applied to high-throughput screening for identification of novel materials in the vast materials composition space.

In 2023, Utimula *et al.*, [22] designed autoencoder to build a feature space describing XRD patterns. In this paper, the training of an autoencoder to detect systematics resulting from atomic changes inside single phase without structural transitions was presented. The trained autoencoder builds a feature space that correctly identifies substitution compositions of XRD patterns. A projected XRD pattern to a point and compositions interpolated in feature space coincide rather well. After that, interpolated point in feature space is used by autoencoder to create a virtual XRD pattern. When feature space was effectively tailored by enough training data, the autoencoder predicts an XRD pattern with concentration that is difficult to quantify using potential resolution of supercell technique of ab initio calculations.

In 2022, Massuyeau *et al.*, [23] established a machine learning-based method that uses powder X-ray diffraction patterns to automatically identify if an unknown substance is a perovskite type. RF and CNN models were used to identify the different perovskite structure types based on the hybrid lead halide powder X-ray diffraction patterns. The structural types of novel unknown compounds might be predicted from their experimental powder XRD patterns once a deep learning network had been trained on a dataset of known compounds. In an array of novel hybrid lead halides, this technique was employed to discern perovskite-type materials.

In 2021, Banko *et al.*, [24] Applied variational autoencoders (VAE) to analyze thin-film data from experiments and simulations for XRD. The structural similarity of textured diffraction patterns is one example of latent information that may be revealed by using crystal structure representations that a VAE has learnt. Although other artificial intelligence (AI) agents are effective in classifying XRD data into known phases, similarly conditioned VAE excels at understanding what it does not know. It can identify novel phases and blends, as well as data outside the distribution it was trained on, very rapidly. These characteristics highlighted the value of VAE as an AI for deciphering XRD data and supporting materials discovery both "on the fly" and during post hoc analysis.

In 2020, Wang *et al.*, [25] presented a convolutional neural network (CNN) model that uses sparse experimental data to quickly identify metal-organic framework (MOF) XRD patterns. The noise collected from experimental spectra was added to theoretical data to train the model. The investigation additionally examined the CNN model's activation properties using class activation maps (CAMs) and utilized neighbourhood component analysis (NCA) to cluster XRD data from the same MOF. The potential of CNNs for individual material identification is demonstrated by this work.

2.1 Problem Statement

The statement of problem emphasizes how important it is to develop phase identification techniques to stay up with the increasing diversity and complexity of materials under study. X-ray diffraction analysis might undergo a revolutionary change with the help of this hybrid solution that attempts to close the gap between conventional methods and the rapidly changing area of machine learning. Table 1 illustrates the features and limitations of various existing techniques.

Table 1: Comparison of various existing methods

Author	Method	Features	Challenges
[16] Hocine *et al.*, 2020	operando	The laser settling time may be ascertained with this experiment.	This approach becomes particularly critical for modeling tiny structures.
[17] Oviedo *et al* 2019	physics-informed data augmentation	▪ Accessible assessment of errors. ▪ A technique for augmenting data that facilitates quick and precise categorization.	The framework may be expanded to include any spectrum with information-rich characteristics that need to be classified, in addition to XRD classification.
[18] Lee *et al* 2020	CNN	▪ Recognizing the many stages of inorganic multiphase structures. ▪ Observe trends and formulate forecasts.	It is not applicable to highly entropy systems.
[19] Sivaraman *et al* 2022	ML with GAP	It offers a way to generate an ML-IP with ab initio accuracy by directly validating model during active learning process.	Long-range electrostatics must be explicitly included in modeling of non-isotropic chemical environments
[20] Utimula *et al* 2020	DTW	▪ Differentiate between substituent concentrations. ▪ The predictive power of framework is higher.	The contraction causes a shift in peak locations, which is not picked up by system.
[21] Dong *et al* 2022	DeepXRD	▪ Research using two datasets as benchmarks to assess performance. ▪ Examination of potential for XRD spectrum prediction.	▪ It is expensive to experimentally characterize crystal structures using XRD. ▪ Restricted to rather small systems; it is not suitable for extensive screening.
[22] Utimula *et al* 2023	Autoencoder	▪ Determining doping levels. ▪ Elucidating pointlessness of each top. ▪ Producing synthetic XRD patterns.	It was unable to provide a plausible explanation for XRD's physics-related irrelevance.
[23] Massuyeau *et al* 2022	RF and CNN	▪ Automatically identify the perovskite type of a given material. ▪ It had the capability to forecast the kinds of	Powder XRD patterns could not distinguish between perovskites and non-perovskites without laborious structural determination.

		structures of novel, unidentified chemicals.	
[24] Banko *et al* 2021	VAE	▪ It may be applied to real-time examination of distribution of dataset among several structures.	veracity and efficacy of high-throughput diffraction must be increased.
[25] Wang *et al* 2020	CNN	▪ Observed that the presence of noise and reduced crystallinity had a significant impact on categorization accuracy.	The identification of individual XRD patterns from a large database of spectra is a challenging task.

III. PROPOSED METHODOLOGY

This study proposes a novel and complete framework for autonomous phase identification in XRD, using ML-guided approaches for improved interpretability and accuracy. There are four main phases in this technique, and each one adds to the overall stability and effectiveness of the phase identification process. Pre-processing (data cleaning, normalization, and smoothing), feature extraction (peak identification, statistical features, and discrete wavelet transform), feature selection (via a hybrid optimization approach utilizing Kookaburra Optimization Algorithm and White Shark Optimizer), and Bayesian FusionNet-based phase identification (combining Improved GhostNetV2, Bayesian Neural Network, and Feedforward Neural Network, with results aggregated by taking the mean) are the four essential stages. This novel method of automating phase identification demonstrates the convergence of neural networks, optimization methods, and machine learning. The approach is a potent tool for scholars and practitioners, with the potential to further material science research and enable effective analysis in a range of applications. The advancement of material characterisation techniques is facilitated by the combination of various approaches, which improve phase identification efficiency, interpretability, and reliability. The proposed architecture is displayed in Fig. 1.

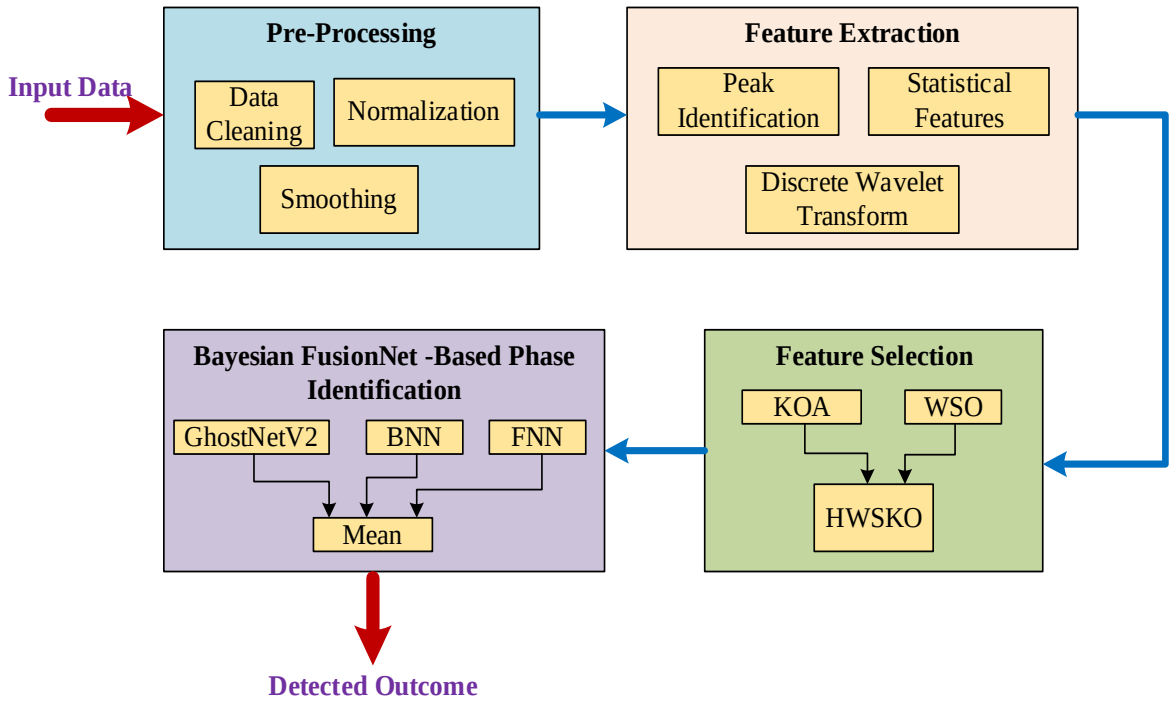

Figure 1: System model of Proposed technique

3.1. Preprocessing

Pre-processing for Autonomous Phase Identification in X-ray Diffraction is a method that makes use of machine learning to help with and enhance material characterisation. This makes it possible to automatically interpret experimental data using methods like XRD. This technique combines analysis and diffraction such that measurements are guided toward characteristics that raise confidence of model that has been trained for recognize crystalline phases. This allows for utilization of early experimental data. The methodology entails integrating a physical diffractometer with an ML algorithm to facilitate the detection of transient intermediate phases generated in solid-state processes on-site, utilizing a standard diffractometer located within the organization. Accurate identification of minute quantities of components in multi-phase mixtures at short measurement durations is also made possible by the faster phase detection process. The preprocessing stage includes data cleaning, normalization, and smoothing.

A. Data Cleaning

The process of eliminating or rectifying outdated, inadequate, or incorrect information from the raw diffraction pictures is known as data cleaning in X-ray diffraction preprocessing. This procedure is necessary because the precision and dependability of the structure determination are greatly impacted by the quality of the data utilized in X-ray diffraction. The following are a few of the procedures in data cleaning for X-ray Diffraction preprocessing:

i. *Spot finding:* This process eliminates any background pixels and noise by locating and determining the strengths of the diffraction spots on each image.
ii. *Indexing:* In this stage, each spot is given a distinct set of three integers, or Miller indices, based on experimental setup.
iii. *Parameter refinement:* This stage determines the estimated errors associated with each reflection's integrated intensity, which is the total of all the spots' intensities that correspond to the same reflection.
iv. *Integration:* The integrated intensity of each reflection, which is the total of the intensities of all the spots that belong to the same reflection, is calculated in this phase along with an estimation of the related errors.
v. *Scaling and Merging:* This process merges the data from multiple images into a single dataset and corrects the intensity data for a number of variables, including absorption, polarization, and exposure duration.

B. Normalization

A technique for data processing called normalization seeks to lessen the impact of artifacts and intensity variations in XRD patterns. Phase identification, peak fitting, and structural determination are few of the XRD analyses that can benefit from normalization's increased precision and dependability. The category and source of XRD patterns determine which normalization approach is used for XRD data. Some of the most popular techniques for normalizing are:

i. *Normalization by the background intensity:* The measured intensity is divided by the background intensity, which may be calculated by fitting a polynomial or spline function to the XRD pattern's baseline. This approach accounts for fluctuations in background noise and artifacts. Applications of this technique include micro-XRD patterns obtained from liquid phase in-situ studies.
ii. Normalization by the total scattered intensity: The measured intensity is divided by the total scattered intensity (which may be computed by integrating the complete XRD pattern) in this approach to account for differences in sample transmission and absorption. This technique works

well with ultrafast XRD patterns obtained from thin-film materials utilizing a plasma source powered by a laser.

iii. Normalization by the incident beam intensity: The incident beam intensity, which can be seen by a beam stop or a reference detector, is divided by the measured intensity in this technique to account for fluctuations in the X-ray source intensity. Conventional XRD patterns obtained from solid materials in an ambient setting can be used with this approach.

Normalization is a crucial preprocessing procedure for XRD data since it improves the comparability of various XRD patterns and the signal-to-noise ratio. Normalization can also help with application of ML methods for XRD data interpretation.

C. Smoothing

Data noise is minimized by the use of digital filter smoothing, also known as Savitzky-Golay smoothing. The application uses the variance approach to assess the amount of noise in the pattern and automatically modifies the smoothing settings based on that level. Different smoothing parameters are employed for the crystalline and amorphous components of the pattern, if the user chooses to match them (for the amorphous instance, often more smoothing is applied).

3.2. Feature Extraction

A crucial part of medical image analysis is feature extraction. From the previously processed data, features are extracted. The process of converting pre-processed XRD data into a more compact and useful representation that can be utilized for additional analysis is known as feature extraction. This stage includes peak identification, statistical features, and discrete wavelet transform.

A. Peak identification

The technique of identifying the distinctive peaks in an X-ray diffraction (XRD) pattern that represents a material's crystal structure and content is called peak identification. It is possible to extract and use as features for a variety of studies the peak position, intensity, and width of these peak.

i. Peak Position: The peak position (also known as the diffraction angle) depends on separation between reflection planes when wavelength is constant. Consequently, the distance of peak location and reflection plane coincide. Peak location is often determined using following techniques:

- Estimating peak position directly from angle of diffraction.
- Calculating peak position using maximum angle after smoothing.
- Using mathematical functions fitted to measured line.

ii. Peak Intensity: The maximum intensity is height at which an XRD peak is at its highest point. Frequently, it lines up with height at Bragg's angle. The geometric relationship between an XRD peak's total intensity and HW, Imax, and Sc is as follows:

$$I_{peak} = I_r k F_w M T \left(\frac{1}{v^2}\right)\left(\frac{1}{\rho}\right)|A|^2\left(1 + cos^2 2\theta\right)\left(\frac{1}{\sin sin\, 2\theta}\right)\varphi\left(\frac{1}{\mu^*}\right)\left(\frac{S_c}{HW}\right) \quad (1)$$

Where, I_r represents raw intensity of XRD; k is physical constant; F_w denotes weight fraction; T means temperature factor; M represents multiplicity factor; volume of unit cell is denoted by v; ρ stands for density; $|A|$ represents modulus of amplitude scattering in the direction of angle θ; φ represents distribution factor; μ^* symbolizes mean mass absorption coefficient; S_c is shape of SRD peak; HW means Width at half maximum intensity.

iii. Width

Divergence magnitude is dictated by the aperture of the divergence and the effective focal width of the source. The mathematical formula of maximum width is given in following Eqn. (2)

$$W = \frac{K\gamma}{Lcos\theta} \tag{2}$$

In above equation, width is represented by W; K denotes constant; γ represents wavelength; $Lcos\theta$ denotes diffraction line.

B. Statistical Features:

i. *Mean:* The arithmetic average of the data set is calculated using the mean. It refers to the total number of values divided by the sum of all the values. The mean is quite simple. Its estimation of the data values is excellent.

$$\bar{\mu} = \sum_{i=1}^{n} \frac{\mu_i}{n} \tag{3}$$

ii. *Standard deviation:* This is a statistical technique used to measure degree of dispersion or variation for a set of data points. When describing spread or breadth of diffraction peaks in an XRD examination, the standard deviation is frequently employed to provide details about the homogeneity and crystalline quality of a material.

$$SD = \sqrt{\frac{\sum_{i=1}^{n}\left(\mu_i - \bar{\mu}\right)^2}{n-1}} \tag{4}$$

iii. *Skewness:* Skewness quantifies how dissimilar a real-valued random variable's probability distribution is from one another. The skewness can be calculated using following Eqn.

$$Skewness = \frac{n}{(n-1)(n-2)} \sum_{i=1}^{n} \left(\frac{\mu_i - \bar{\mu}}{SD}\right)^3 \tag{5}$$

iv. *Kurtosis:* Kurtosis is a statistical metric that quantifies the peak or flatness of a real-valued random variable's probability distribution. The following equation can be used to determine the kurtosis.

$$K = \frac{n(n+1)}{(n-1)(n-2)(n-3)} \sum_{i=1}^{n} \left(\frac{\mu_i - \bar{\mu}}{SD}\right)^4 - \frac{3(n-1)^2}{(n-2)(n-3)} \tag{6}$$

Where, n represents number of data; μ_i denotes individual data; $\bar{\mu}$ is mean of data; standard deviation of data is represented by SD.

C. Discrete Wavelet Transform

A mathematical method known as the Discrete Wavelet Transform (DWT) can divide a signal up into its frequency components. Wavelet transform uses a series of basic functions, termed wavelets, which are scaled and shifted replicas of a mother wavelet to capture both high-frequency and low-frequency information. The wavelets are limited in duration and can adjust to the specific characteristics of the signal locally. At every stage of decomposition, the DWT processes the signal through a number of filters to provide a comprehensive information at each level as well as a coarse approximation. The low-frequency information is contained in coarse approximation, while high-frequency information is contained in detailed information. The DWT may be utilized for variety of tasks and applied to wide range of data kinds, including vibrations, images, and noises.

DWT may be practically implemented using two filters: one for low-pass and one for high-pass. Wavelet dilation and shifting operations are used to create a wavelet of a prototype signal, sometimes referred to as a "mother" or "single modeling" wavelet y (t). The following formula illustrates this connection.

$$\varphi(j,k)(t) = \frac{1}{\sqrt{2^j}}\varphi\left(\frac{(t-k2^j)}{2^j}\right) \tag{7}$$

Where, j represents scaling factor; t denotes time; k is shifting parameter; $\varphi(t)$ denotes function of mother wavelet; DWT may be calculated mathematically by convolving the signal $x(t)$ with the mother-wavelet $\varphi(j,k)$ dilated, reflected, and normalized. The mother-wavelet convolution of the data gives Equation (8).

$$dwt(j,k)(t) = y[n] = (x * \varphi(j,k)(t))[n] = \frac{1}{\sqrt{2^j}}\int x(t)\varphi\left(\frac{(t-k2^j)}{2^j}\right)dt \tag{8}$$

The signals are broken down by filters into approximation and detail coefficients, whose computation is given as

$$y_{low}[n] = (x * g)[n] = \sum_{k=-\infty}^{\infty} x[k]g[2n-k] \tag{9}$$

$$y_{high}[n] = (x * h)[n] = \sum_{k=-\infty}^{\infty} x[k]h[2n-k] \tag{10}$$

The aforementioned equations may be more precisely described using following convolution technique that stated in Eqn. (11) and (12).

$$y_{low} = (x * g)\downarrow 2 \tag{11}$$

$$y_{high} = (x * h)\downarrow 2 \tag{12}$$

The high-frequency and low-frequency components are represented by the low- and high-pass filters in equations (9) and (10) respectively. The outputs provide the approximation (from the low-pass filter) and detail (from the high-pass filter) coefficients. Fig. 2 depicts the 2-level DWT decomposition process.

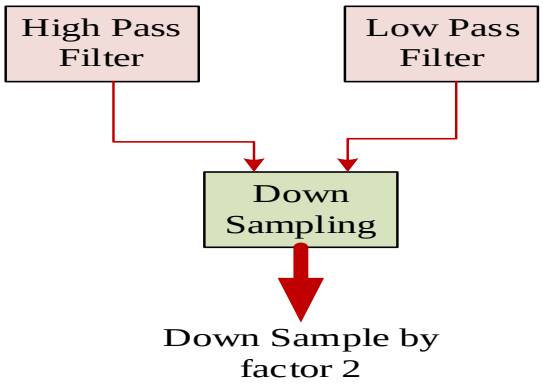

Figure 2: DWT decomposition procedure

The patterns of diffracted X-rays from a crystalline material can be examined using DWT in XRD. The phase composition and crystal structure of material are disclosed using XRD data, which may be seen as 1D signal. It may be divided into several frequency bands that correlate to various spatial scales of crystal lattice by DWT on XRD data. The overall phase composition and average lattice parameters are

revealed by low-frequency bands, and crystal structural and local fluctuations defects are shown by high-frequency bands. It is also possible to identify and quantify the diffraction peaks more easily using DWT to lower noise and improve peaks and in XRD.

3.3. Feature Selection

Feature selection is a method of reducing dimensionality strategy that selects a subset of useful characteristics by eliminating noisy, redundant, or irrelevant features from the original set. Feature selection frequently leads to higher learning accuracy, increased model interpretability, and lower processing costs. It is possible to reduce data effectively by using feature selection techniques. This helps locate precise information. Feature selection can reduce measurement and storage requirements, training and utilization durations, and curse of dimensionality to improve prediction performance. It can also help with data presentation and interpretation.

In feature selection, hybrid optimization is a methodology that combines many approaches to improve efficiency and performance. In this study, Hybrid White Shark Optimizer and Kookaburra Optimization Algorithm (HWSKO) is introduced to provide effective feature selection. It is a novel feature selection method that combines the advantages of two metaheuristic algorithms: White Shark Optimizer (WSO) and Kookaburra Optimization Algorithm (KOA). The benefits of this HWSKO are described as follows:

- The process can reduce computational complexity and storage needs of models by removing characteristics that are irrelevant, redundant, and noisy from original feature space.
- It may choose the ideal collection of characteristics to improve classification model performance and lower error rates.
- The many behaviours of white shark and Kookaburra, such as hunting Strategy, exploitation, chasing, and speed of movement may be used by HWSKO to balance exploration and exploitation of search space. This can improve the global optimization impact and keep algorithm from being stuck in local optima.
- HWSKO can interact with variety of classifiers and handle several data sets, including numerical data, text, and image.

The White Shark and Kookaburra optimization algorithm are discussed in following section:

3.3.1. White Shark Optimizer

A meta-heuristic technique called White Shark Optimizer (WSO) is used for effectively solve Optimal Power Flow (OPF) problem. WSO is a novel optimization system designed to help white sharks in the ocean depths, modelled after their scholarly hunting patterns in the wild. This algorithm was created to address optimization issues in the real world that are challenging to resolve using existing methods, both restricted and unconstrained. A large variety of engineering optimization problems, especially those with high dimensionality, may be solved with WSO thanks to its mathematical methodology. The global optimum problems for difficult optimization problems should be easily and exactly identified by it thanks to its durability and simplicity. This section includes details on mathematical models developed to characterize hunting behaviours of white sharks and used to support proposed WSO to solve OPF problem. Tracking and killing prey are involved in this.

a) Movement Speed Towards the Prey

A white shark may identify the position of its prey by listening for a halt in the wave is given in Equation (13).

$$W_{k+1}^{i} = \sigma\left[W_{k}^{i} + \rho_1\left(L_{best_k} - L_{k}^{i}\right) \times C_1 + \rho_2\left(L_{best}^{v_k^i} - L_{k}^{i}\right) \times C_2\right] \quad (13)$$

Where, L represents location of sharks; The i^{th} index vector of sharks reaching the ideal spot is v^{i}.

b) Movement Towards Best Possible Prey

The behavior of white sharks as they approach prey was described in this context using location update mechanism given in Eqn. (14).

$$P^{i}_{k+1} = \{P^{i}_{k.} \to \oplus P_{0} + w.a + l.b; \quad rand < mv\, P^{i}_{k} + \frac{W^{i}_{k}}{f; \qquad rand \geq mv} \tag{14}$$

$$mv = \frac{1}{\left(a_{0}+e^{\frac{\left(\frac{k}{2-k}\right)}{a_{1}}}\right)} \tag{15}$$

Where, $\oplus$ denotes bitwise EX-OR operation; f represents frequency of shark's wavy motion. The location constants a_{0} and a_{1} are employed to manage exploitation and exploration.

c) Movement Towards Optimal Shark

Sharks can maintain their position ahead of most favourable individual at close proximity to the target. The expression for this phenomenon may be found in equation (16).

$$P^{'i}_{k+1} = P_{bestk} + r_{1}\vec{D}_{p} sgn\left(r_{2} - 0.5\right) r_{3} < R_{p} \tag{16}$$

$$R_{p} = \left|1 - e^{\left(\frac{-a_{2}\times k}{k}\right)}\right| \tag{17}$$

Where, D_{p} is the distance between shark and target, a_{2} denotes a location factor used to control exploitation and exploration, and R_{p} represents a parameter used to reflect power of white sharks.

3.3.2. Kookaburra Optimization Algorithm

The Dacelo genus of birds includes the carnivorous Kookaburra, which is a member of the Alcedininae and Coraciiformes families of terrestrial tree kingfishers. These birds are primarily terrestrial. Australia and New Guinea are the natural habitats of this bird. They live in a variety of settings, including as wet forests and desert savannahs, as well as next to streams and in neighbourhoods with plenty of tall trees. This bird essentially warns its foes not to approach its area by making a sound that is comparable to human laughing.

a. Initialization

The KOA method is a population-based optimizer that generates suitable solutions for optimization problems repeatedly by conducting random search in problem-solving space. Every Kookaburra in KOA population is a possible vector-based solution since they are all arranged in problem-solving space so that, depending on where they are, they may each decide the values for decision variables. The KOA population matrix, which is made up of kookaburras may be modelled according to equation (18). The starting placements of kookaburras are randomly determined at beginning of KOA implementation using Equation (19).

$$X = \begin{bmatrix} X_{1} \\ \vdots \\ X_{i} \\ \vdots \\ X_{N} \end{bmatrix} = \begin{bmatrix} x_{1,1} & \cdots & x_{1,d} & \cdots & x_{1,m} \\ \vdots & \ddots & \vdots & \iddots & \vdots \\ x_{i,1} & \cdots & x_{i,d} & \cdots & x_{i,m} \\ \vdots & \iddots & \vdots & \ddots & \vdots \\ x_{N,1} & \cdots & x_{N,d} & \cdots & x_{N,m} \end{bmatrix} \tag{18}$$

$$x_{i,d} = lb_d + rand.\left(Ub_d - Lb_d\right) \quad (19)$$

Where, r is random number in the interval [0, 1], Ub_d *and* Lb_d are the upper and lower bounds of d^{th} decision variable, respectively. X denotes KOA population matrix, X_i represents i^{th} kookaburra, and $x_{i,d}$ is its d^{th} dimension in search space.

Given that every kookaburra's location inside the issue-solving space represents a potential solution for the related kookaburra problem, it is possible to assess the problem's objective function. Equation (20) may be used to express the set of evaluated values for problem's objective function as a vector.

$$F = \left[F_1 \vdots F_i \vdots F_N\right] = \left[F\left(X_1\right) \vdots F\left(X_i\right) \vdots F\left(X_N\right)\right] \quad (20)$$

According to above equation, F_i represents the evaluated objective function based on i^{th} kookaburra, and F stands for evaluated objective function vector.

An appropriate criterion for assessing the caliber of population members and potential solutions is the assessed values for objective function. The best member is one who has highest assessed value for objective function, and worst member is one who has the lowest evaluated value for objective function. The position of kookaburras in problem-solving space and function of issue are modified throughout each iteration, and best member of population is also updated based on comparison of new values.

b. KOA Mathematical Modeling

The KOA technique changes the positions of kookaburras to enhance potential solutions based on modeling of genuine kookaburra behaviours in following two phases: exploration and exploitation. This is done through an iterative process.

i. Phase I: Hunting technique (Exploration)

The carnivorous kookaburra bird eats other tiny birds, insects, reptiles, frogs, and mice. Even in situations where its legs are weak, this bird's muscular neck aids in hunting. Because of their attack strategy and way of choosing their prey, kookaburras cover a lot of ground when in position. This approach is represented by idea of exploration, which stands for global search. In order to discover primary optimal zone, one must carefully scan problem-solving space to avoid becoming stuck in local optimal. In KOA design, each kookaburra considers the position of other kookaburras who have a higher objective function value, as prey location, simulating kookaburra hunting behavior. The Eqn. (21) shows calculation for available prey set of every kookaburra.

$$PC_i = \left\{B_k : F_k < F_i \, and \, k \neq i\right\} \quad (21)$$

In above equation, F_k is the objective function value, and PC_i denotes a set of potential prey for the i^{th} kookaburra.

Every kookaburra is thought to choose its target at random and launch an assault on it according to the KOA design. Equation (22) is used to determine the kookaburra's new position based on the simulation of its progress towards prey in hunting strategy.

$$x_{i,d}^{P1} = x_{i,d} + rand \cdot \left(SPC_{i,d} - N \cdot x_{i,d}\right) \quad (22)$$

Where, $PC_{i,d}$ is d^{th} dimension of selected prey for i^{th} kookaburra, N represents a random number from set {1, 2}. $x_{i,d}^{P1}$ is its d^{th} dimension, and $rand$ stands for random number with normal distribution in range of [0, 1].

II. Phase II: Assuring the Death of Prey (Exploitation)

The second distinguishing feature of kookaburra behavior is that, following an assault, the animal carries the victim with it and ensures that it dies by striking it against tree several times. The prey is then firmly held between the kookaburra's claws before being crushed and consumed. This activity causes slight shifts in the posture of kookaburras when it occurs close to hunting area. This approach integrates local search with notion of exploitation, and it refers to potential of algorithm for provide better solutions near to identified solutions and promising regions. Equation (23) is used in the KOA design to determine a random position, simulating the movement of kookaburras about the hunting area.

$$x_{i,d}^{P2} = x_{i,d} + (1 - 2rand) \cdot \frac{Ub_d - Lb_d}{t} \tag{23}$$

Where, $x_{i,d}^{P2}$ is its d^{th} dimension, and t represents algorithm's iteration counter.

Once the target is attacked, the kookaburra drags the kill along with it and ensures that it is killed. After holding the prey firmly between its claws, the kookaburra smashes and consumes it. The drawback of KOA is that kookaburra bird has weak legs. This bird carries the prey in its claws but it has feeble legs. This may reduce the efficiency of attacking prey. To improve the efficiency of KOA, the WSO is hybrid with KOA in this study.

3.3.3. Hybrid White Shark Optimizer and Kookaburra Optimization Algorithm

In this study, the hybrid method of HWSKO is introduced. This hybrid algorithm combines both WSO and KOA to improve its efficiency. The equation (17) from WSO is optimized with equation (22) in KOA. The expression of hybrid HWSKO is given in equation (24).

$$x_{i,d}^{P1} = x_{i,d} + rand \cdot \left(R_p * SPC_{i,d} - N \cdot x_{i,d}\right) \tag{24}$$

In above equation, R_p represents the power reflector. This part is introduced in above equation to improve the power of claws. This HWSKO may employ movement speed to strike a balance between search space exploitation and exploration.

3.4. Bayesian FusionNet -Based Phase Identification

The phase identification process based on Bayesian FusionNet is a major advancement in automating and enhancing the precision of XRD analysis. This newly introduced method in this study integrates GhostNetV2, BNN, and FNN. In this study, the GhostNetV2 is improved for enhance the performance of suggested technique. This proposed method enables more effective and dependable phase detection in research by fusing modern neural network designs and utilizing their combined capabilities. This opens up significant novel possibilities for study with broad applicability.

3.4.1. GhostNetV2

A lightweight convolutional neural network (CNN) architecture is called GhostNetV2. High performance at low computational cost is the goal of GhostNetV2. Ghost modules and DFC attention

are only two of the methods it employs to do this. Ghost modules can minimize the number of channels in a convolutional layer by using a method known as "channel pruning". This contributes to lowering the necessary number of FLOPs and parameters without materially affecting accuracy. The goal of DFC is to be a new, effective attention mechanism that works well. Accuracy may be increased by capturing long-range relationships between features.

3.4.1.1. Improved GhostNetV2

In this study GhostNetV2 is improved by replacing DFC with transformer-based attention network in conventional DFC. This improved network Captures long-range dependencies effectively. It is more powerful technique and it models the links between features across various spatial locations by using self-attention processes. Fig. 3 shows the structure of Improved GhostNetV2.

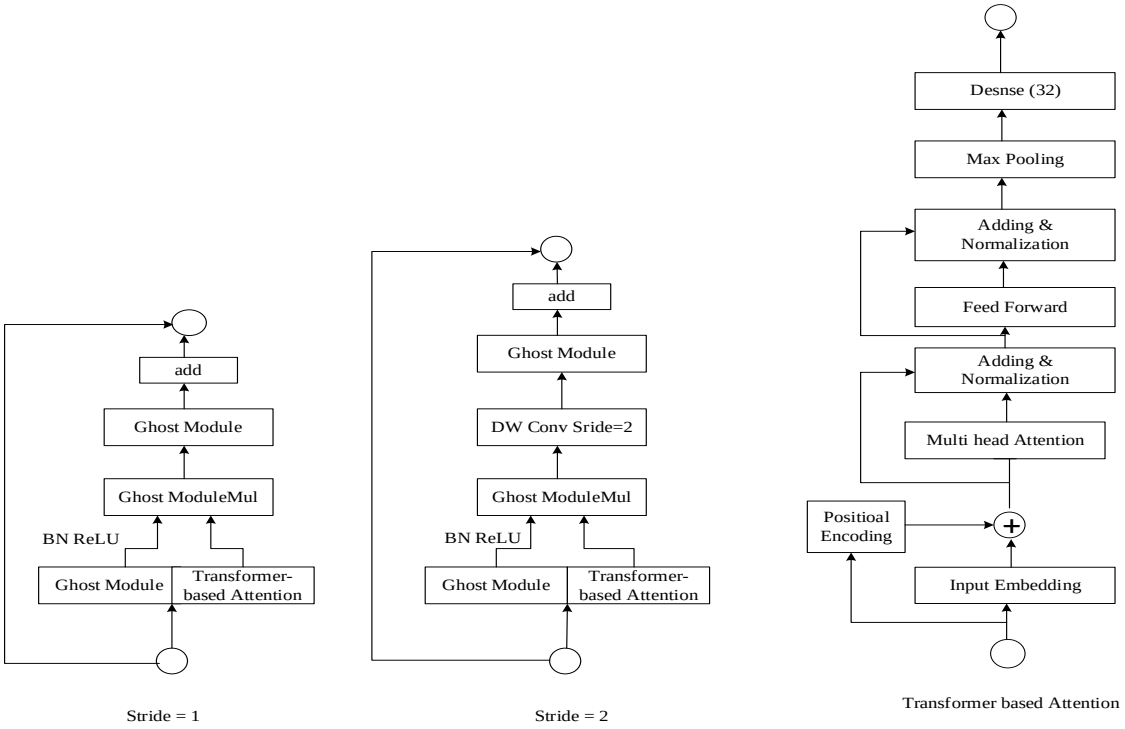

Figure 3: Architecture of Improved GhostNetV2

A model that can successfully extract minor information to distinguish between various materials is needed since XRD patterns can be noisy and complicated. The channel reduction and attention mechanisms of GhostNetV2 may be useful in this situation.

3.4.2. Bayesian Neural Network

The objective of classical learning is to identify a single optimal model parameter configuration, usually using maximum-likelihood optimization. As a result, the learner in the Bayesian framework observes the data D and then infers a posterior distribution $P(w|D)$ over the model's parameters w. The posterior distribution is determined by Bayes rule, which is as follows: $P(w|D)\alpha\ P(D|w)P(w)$, where $P(w)$ denotes prior distribution over parameters and $P(D|w)$ is the likelihood of D as determined by model with parameters w. The Bayesian model average (BMA) is then used to determine the model's predictions for a fresh test sample x.

$$P(y|x,\ D) = \int_{w} P(y|x,\ w)P(w|D)dw \tag{25}$$

Where, the predictive distribution for a specific value of the parameters w is denoted by $P(y|x,\ w)$. This BMA is especially persuasive in the context of Bayesian deep learning since, for a given issue, a contemporary neural network's posterior over parameters might reflect a multitude of complimentary solutions that correspond to various parameter values.

3.4.3. Feedforward Neural Network

FNN is one type of artificial neural network that is quite popular. Data moves through hidden layers of feedback-neutral network (FNN) in a single direction, from input layer to output layer. Numerous neurons make up each buried layer, which may be thought of as a linear change of the output from the layer before it. It is possible to characterize the basic functions of neurons as following equation (26).

$$h(X) = wX + b \tag{26}$$

Where, w stands for weight matrix, b is the bias vector, and X is the input vector.

A nonlinear processing of the neuron's output, controlled by activation function is necessary to increase the accuracy of network because many functions are linearly indivisible. The nonlinear transformation is then realized by converting the input, $h(X)$ to a different value. For phase identification, sigmoid function is used as the activation function and it can be expressed as following equation (27).

$$Sigmoid(x) = \frac{1}{1+e^{-x}} \tag{27}$$

The sigmoid function is frequently utilized in neural networks due to its stability and ease of derivation. A loss function is also necessary in order to assess the FNN's identification performance. In this FNN, cross-entropy function is selected as a loss function. A different loss function will be used to minimize the gradient since the sigmoid function's slope rapidly varies at both the upper and lower boundaries. The cross-entropy function may retain a high gradient because of its logarithmic nature, which is represented as following equation (28).

$$Loss = -\sum_{i=1}^{n} Y_i log\left(\hat{Y}\right) \tag{28}$$

Where, Y_i denotes ideal output; $\hat{Y}$ represents actual output.

The mean is probably used to integrate results or predictions from the three models (BNN, FNN, and Improved GhostNetV2). The structure of mean is displayed in Fig. 4. The ensemble technique, which averages the predictions from several models, can yield a more reliable and accurate forecast. Mathematically this can be expressed in following equation (29).

$$Mean = \frac{Y_1 + Y_2 + Y_3}{3} \tag{29}$$

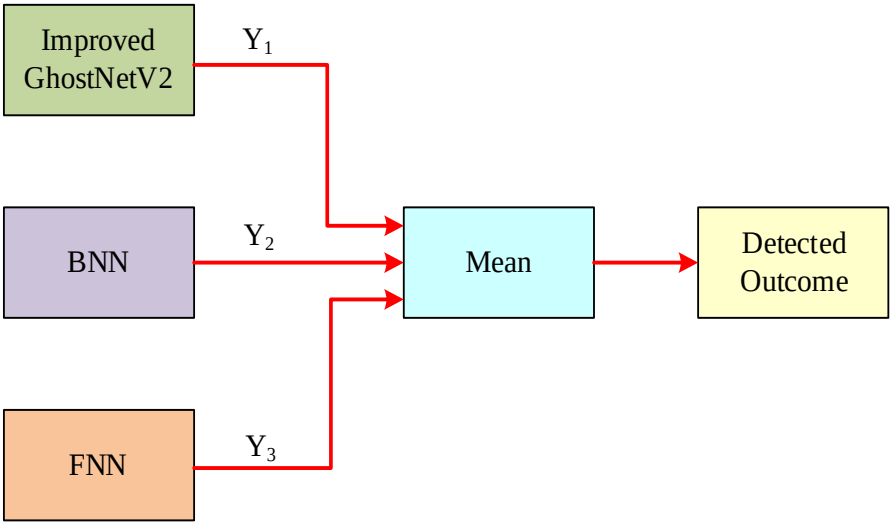

Figure 4: Structure of mean outcome

The mean reduces the biases and inaccuracies of individual models. This type of model averaging takes use of the variety of models that are used. The ensemble technique attempts to provide a more reliable and accurate overall forecast by integrating the strengths of each model, which may perform better in particular scenarios or with particular kinds of data.

III. RESULTS AND DISCUSSION

This section of this paper discusses about evaluation of results. The various metrices are taken for evaluate performance of proposed approach. The metrices are mainly used to analyse efficiency of suggested technique with various methods that are currently in use. The main objectives of this section are:

- Effectiveness of proposed technique using Sensitivity, Precision, Accuracy, Selectivity, FPR, NPV, F-score, MCC, and FNR;
- Comparison of the suggested approach with alternative existing techniques based on evaluation metrics.
- The execution is performed in python platform.

4.1. Evaluation of metrices

The following metrics are used in the assessment of the proposed attack detection system:

Accuracy: It represents a percentage of total number of two correct guesses to total number of predictions in Eqn. (25).

$$Accuracy = \frac{TN+TP}{TP+TN+FN+FP} \quad (25)$$

Where, FP for False Positive, TP stands for True Positive, TN for True Negative, and FN for False Negative, an accuracy ratio of 1 denotes perfect accuracy, and 0 for a random guess.

Precision: It is defined as the ratio of the total amount of abnormal and normal data detected to the quantity of normal data detected, as given in Eqn. (26).

$$Precision = \frac{TP}{TP+FP} \quad (26)$$

Sensitivity: It is defined as the ratio of total amount of data in dataset to number of normal data that were found, as shown in Eqn. (27).

$$Precision = \frac{TP}{TP+FN} \tag{27}$$

F-score: The harmonic mean of precision and recall metrics is known as F-measure. It is represented in following Eqn. (28).

$$F - Measure = \frac{2PR}{P+R} \tag{28}$$

Specificity: The percentage of real negative cases that model properly detected is called Specificity, which is often referred to as True Negative Rate or Selectivity. Specificity is a binary classification performance measure. The formula for calculating specificity is as follows:

$$Specificity = \frac{TN}{FP+TN} \tag{29}$$

MCC: Matthews Correlation Coefficient or MCC is a statistic used to assess how well binary classification model is doing. The following Eqn. (30) is used to compute it:

$$MCC = \frac{TP \times TN - FP \times FN}{\sqrt{(TP+FP)(TP+FN)(TN+FP)(TN+FN)}} \tag{30}$$

NPV: A performance measure called Negative Predictive Value (NPV) is used in binary classification to assess how well a model predicts the negative class, or the occurrences that lack a specific condition or characteristic. The True Negative Rate is another name for NPV. The following Eqn. (31) is utilized to determine Negative Predictive Value:

$$NPV = \frac{TN}{TN+FN} \tag{31}$$

FPR: The percentage of true negative occurrences that model mistakenly predicts as positive is called False Positive Rate (FPR), sometimes called False Alarm Rate. This performance statistic is utilized in binary classification. The below formula is used to compute it:

$$FPR = \frac{FP}{FP+TN} \tag{32}$$

FNR: In binary classification, the False Negative Rate (FNR) is a performance indicator that quantifies the percentage of true positive occurrences that the model mistakenly predicts as negative. It is also known as the Miss Rate. The following formula is used to get FNR:

$$FNR = \frac{FN}{FN+TP} \tag{33}$$

4.2. Evaluation of proposed technique with existing methods

The proposed technique is compared with various existing methods such as Improved GhostNetV2, BNN, and FNN to verify the performance of introduced strategy. For this purpose, the dataset is split for training and testing. Initially, the data is split as seventy percentage for training and thirty percent for testing. Further, the 80-percentage data was utilised for training purpose and the remaining data was used for testing. These split data was mainly used to ensure the effectiveness of developed method. The proposed and existing technique is analyzed with various evaluation metrices and these are discussed in following section. Table 1 depicts comparison result of proposed and existing method when data split is 70/30. The comparison between proposed and current methods when the data split is 80/20 is shown in Table 2.

Table 1: Percentage values of various methods for data split 70/30

Model	Bayesian FusionNet	Improved GhostNetV2	BNN	FNN
Accuracy	0.98685	0.95054	0.93023	0.90909
Precision	0.98702	0.94148	0.92105	0.92105
F-Score	0.98385	0.94588	0.92105	0.85
Specificity	0.9878	0.94	0.94	0.94175
Sensitivity	0.98101	0.9775	0.90323	0.85714
MCC	0.98205	0.94118	0.90323	0.92683
NPV	0.98155	0.95161	0.92857	0.95223
FPR	0.04541	0.06341	0.05341	0.07341
FNR	0.03294	0.07954	0.06954	0.08954

Table 2: Percentage values of various methods for data split 80/20

Model	Bayesian FusionNet	Improved GhostNetV2	BNN	FNN
Accuracy	0.99061	0.96591	0.94118	0.91023
Precision	0.98715	0.95588	0.9375	0.93878
F-Score	0.98719	0.95133	0.925	0.8534
Specificity	0.98281	0.94243	0.9434	0.9412
Sensitivity	0.98715	0.9612	0.93023	0.86364
MCC	0.989213	0.95082	0.92683	0.92563
NPV	0.989364	0.95455	0.93478	0.95238
FPR	0.03241	0.05341	0.03341	0.06341
FNR	0.02554	0.06954	0.04954	0.07954

The accuracy values of proposed, Improved GhostNetV2, BNN, and FNN are 0.98685, 0.95054, 0.93023, and 0.90909 respectively when 70 percentage data sets are involved for training and 30 percentage for testing. Similarly, when the data sets are split as 20 percentage for testing and 80 percentage for training, the accuracy values are denoted as 0.99061, 0.96591, 0.94118, and 0.91023 for proposed, Improved GhostNetV2, BNN, and FNN respectively. The aforementioned values states that the proposed method has highest accuracy than all other existing techniques. The graphical representation of accuracy analysis is shown in following Fig. 5.

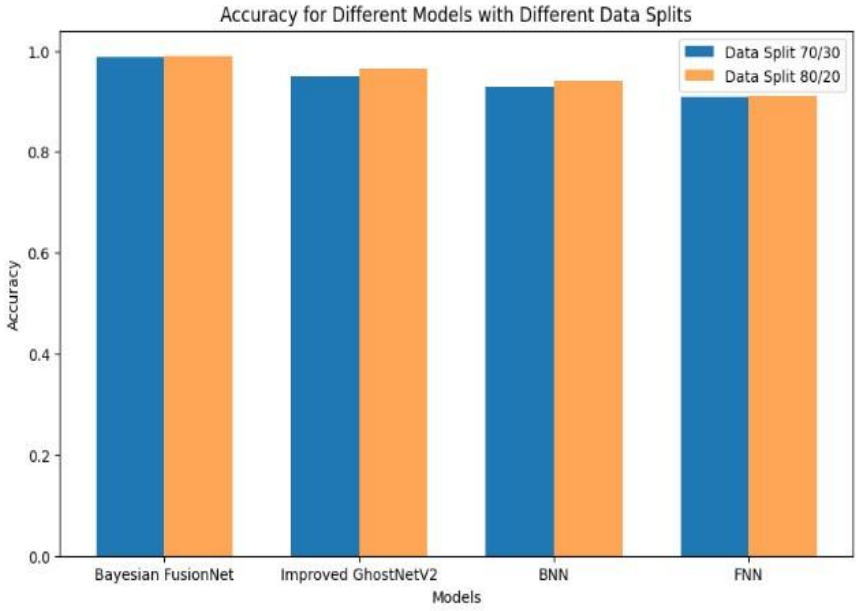

Figure 5: Analysis of accuracy

The suggested strategy, Improved GhostNetV2, BNN, and FNN have precision values of 0.98702, 0.94148, 0.92105, and 0.92105, respectively, when 70% of data sets are used for training and 30% are used for testing. Similar to this, precision scores for suggested method, Improved GhostNetV2, BNN, and FNN are stated as 0.98715, 0.95588, 0.9375, and 0.93878 correspondingly when the data sets are divided into 80 percent for training and 20 percent for testing. The results stated above indicate that the suggested method outperforms all other current methods in terms of precision. The following Fig. 6 displays precision analysis graphically.

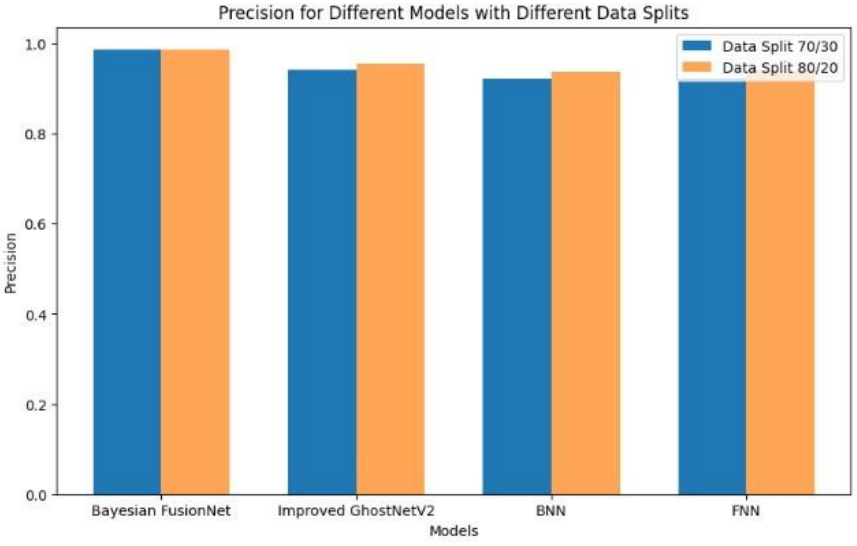

Figure 6: Analysis of precision

The F-score values of newly developed method, Improved GhostNetV2, FNN, and BNN are, respectively, 0.98385, 0.94588, 0.85, and 0.92105 with 70% of data sets are used for training and 30% for testing. Likewise, if data sets were divided into 80 percent for training and 20 percent for testing, the F-score results for suggested, BNN, Improved GhostNetV2, and FNN are stated as 0.98719, 0.925, 0.95133, and 0.8534 respectively. According to provided values, the suggested method is the most accurate F-score of all currently used methods. The F-score analysis is displayed graphically in Fig. 7 below.

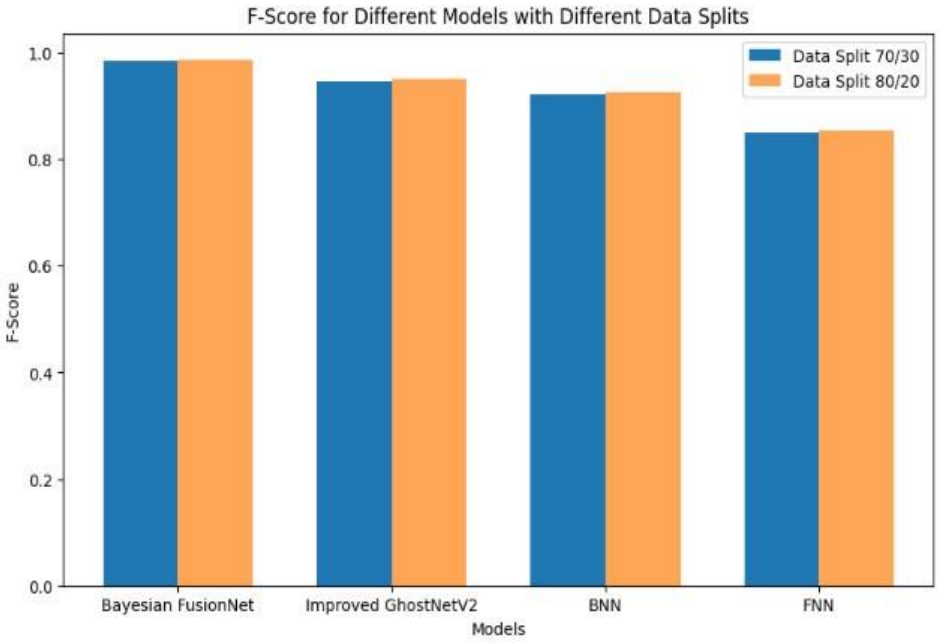

Figure 7: Analysis of F-score

FNN, BNN, Improved GhostNetV2, and proposed approach have specificity values of 0.94175, 0.94, 0.94, and 0.9878 respectively, with 70% of the data sets utilized for testing and 30% for training. Similarly, if 80 percent of data sets are used to training and 20 percent are used for testing, specificity for FNN, BNN, Improved GhostNetV2and, and proposed method are 0.9412, 0.9434, 0.94243, and 0.98281 respectively. The recommended approach has the highest specificity score among all presently employed methods, based on given information. Fig. 8 below shows a visual representation of the specificity analysis.

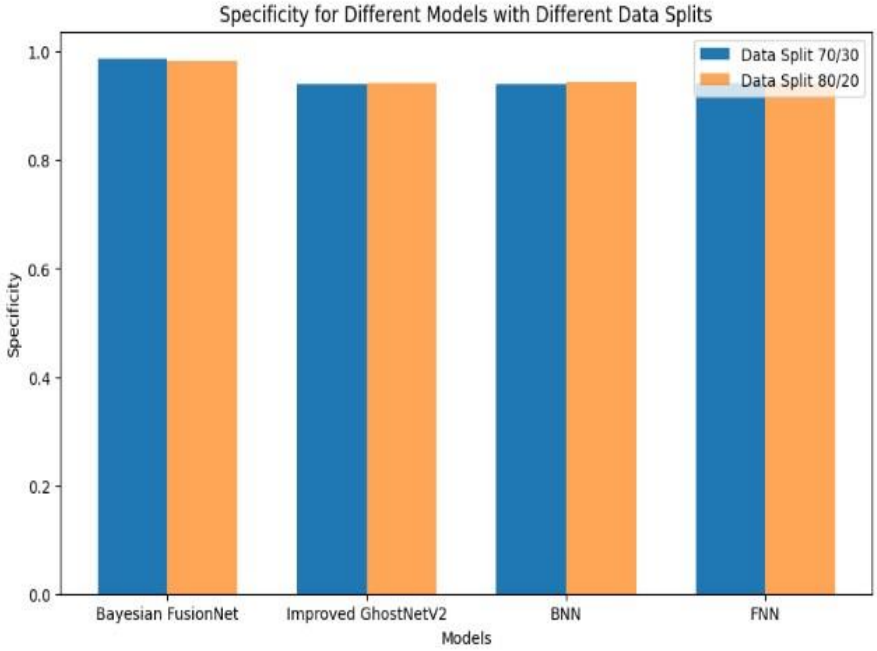

Figure 8: Analysis of specificity

Improved GhostNetV2, FNN, BNN, and established strategy have sensitivity values of 0.9775, 0.85714, 0.90323, and 0.98101 respectively, with 70% of the data sets employed for testing and 30% for t00.00raining. Similarly, the sensitivity for recommended, BNN, Improved GhostNetV2, and FNN are 0.980....715, 0.93023, 0.9612, and 0.86364 respectively, if the data sets are split into 80 percentage for training and 20 % for testing. The recommended approach has the highest sensitivity among all presently employed methods, based on aforementioned results. Figure 9 below shows a visual representation of the sensitivity analysis.

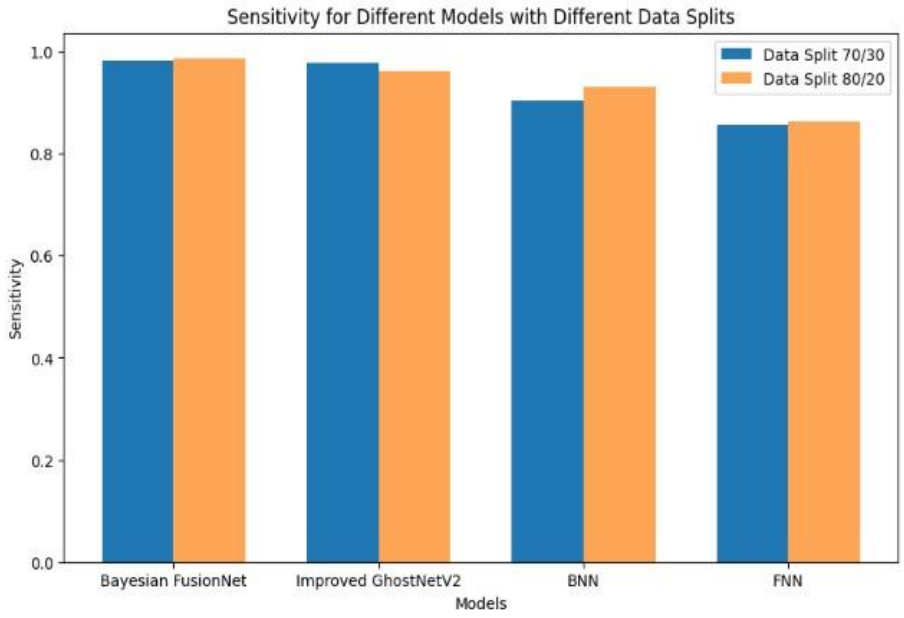

Figure 9: Analysis of sensitivity

The MCC values are listed as 0.98205 for proposed technique, 0.94118 for Improved GhostNetV2, 0.92683 for FNN, and 0.90323 for BNN with 70% of data sets utilized for training and 30 percentage for testing. Similarly, if data sets are split 80 percent for training and 20 percent for testing, the MCC values are 0.989213 for recommended approach, 0.92683 for BNN, 0.95082 for Improved GhostNetV2, and 0.92563 for FNN. Based on information provided above, the proposed approach has the highest MCC value among all presently available methods. Fig. 10 below shows an illustration of MCC evaluation.

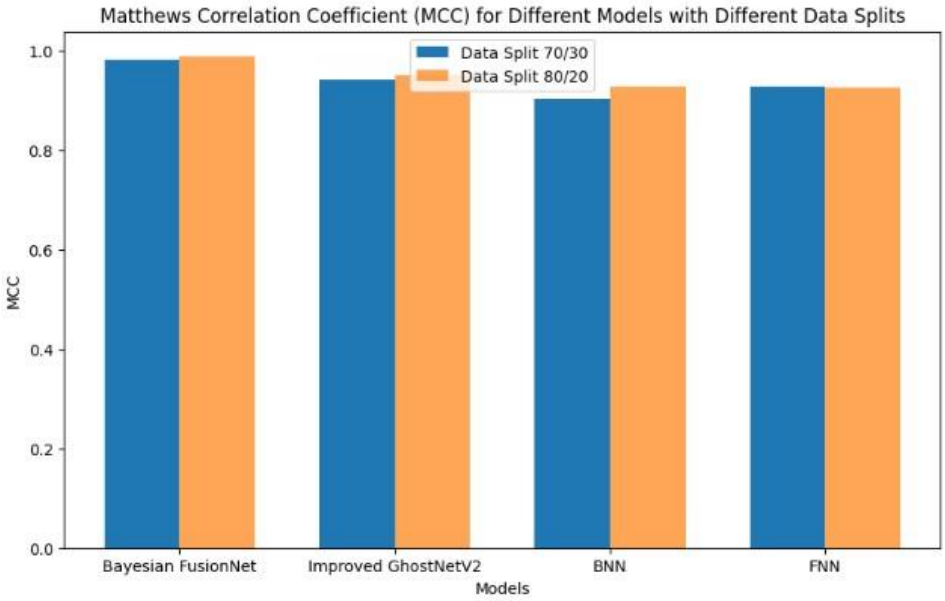

Figure 10: Analysis of MCC

The NPV values for 70% of data sets used for training and 30% for testing are 0.98155 for proposed approach, 0.95161 for Improved GhostNetV2, 0.95223 for FNN, and 0.92857 for BNN. Similar to this, the NPV values for recommended technique is 0.989364, 0.93478 for BNN, 0.95455 for Improved GhostNetV2, and 0.95238 for FNN if the data sets are divided 80 percent for training and 20 percent for testing. Out of all currently accessible approaches, the suggested strategy has the greatest NPV value according to information presented above. Figure 11 below provides an example of NPV evaluation.

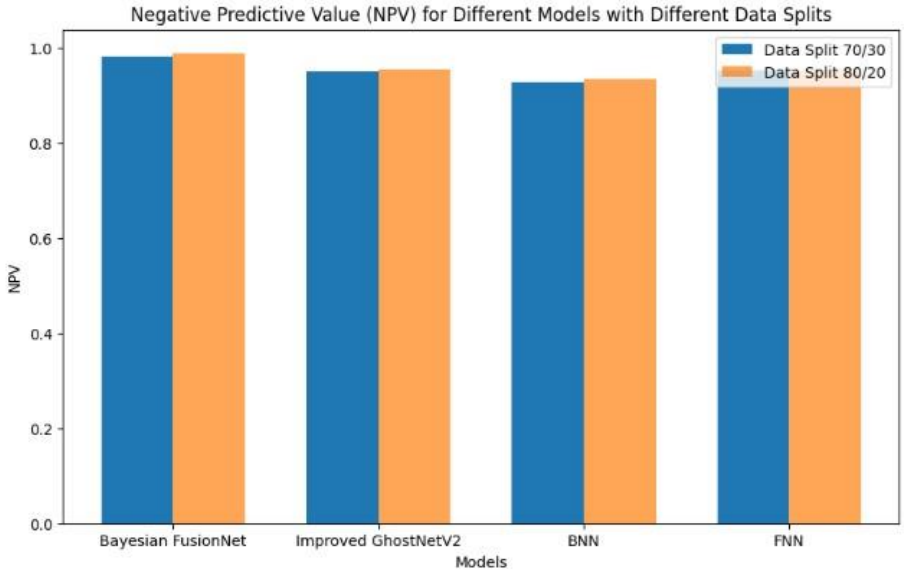

Figure 11: Analysis of NPV

When 70% of data sets are utilized for training and 30% are used for testing, the FPR values of proposed approach, FNN, BNN, and Improved GhostNetV2 are 0.04541, 0.07341, 0.05341, and 0.06341, respectively. Similarly, with the data sets split 80 percent for training and 20 percent for testing, the accuracy scores for the proposed technique, BNN, Improved GhostNetV2, and FNN are 0.03241, 0.03341, 0.05341, and 0.06341, respectively. The above-mentioned results show that the

recommended method performs more precisely than any other existing method. The subsequent Fig. 12 illustrates FPR analysis visually.

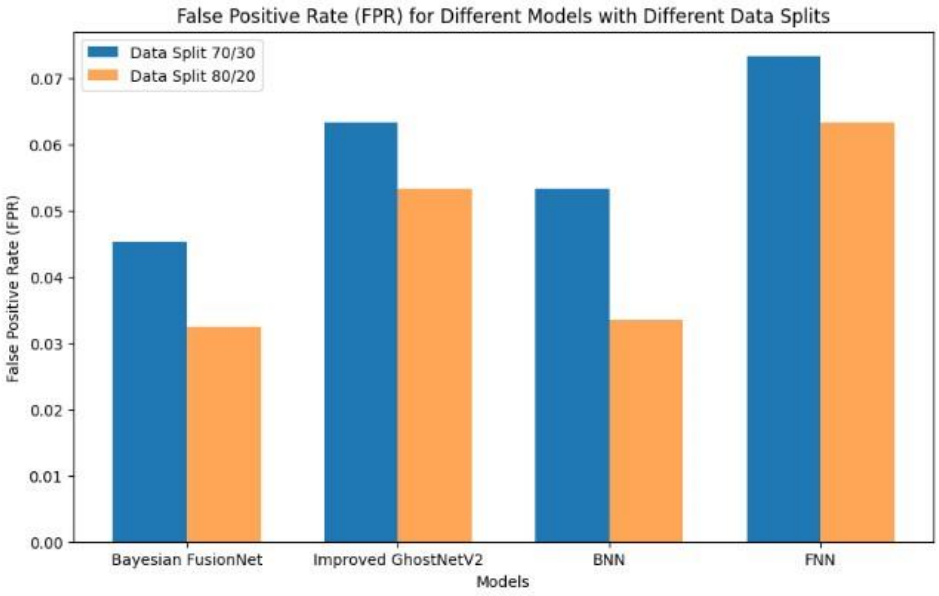

Figure 12: Analysis of FPR

The methods FNN, Improved GhostNetV2, BNN, and the recommended strategy have FNR values of 0.08954, 0.07954, 0.06954, and 0.03294, respectively, when 70% of data sets are utilized for training and 30% for testing. Similar to this, when the data sets are split into 80 percent for training and 20 percent for testing, FNR scores for recommended technique, BNN, Improved GhostNetV2, and FNN are reported as 0.02554, 0.04954, 0.06954, and 0.07954 accordingly. The aforementioned findings show that recommended strategy performs more precisely than any other existing approach in terms of FNR. The following Fig.13 is visually displayed the evaluation of FNR.

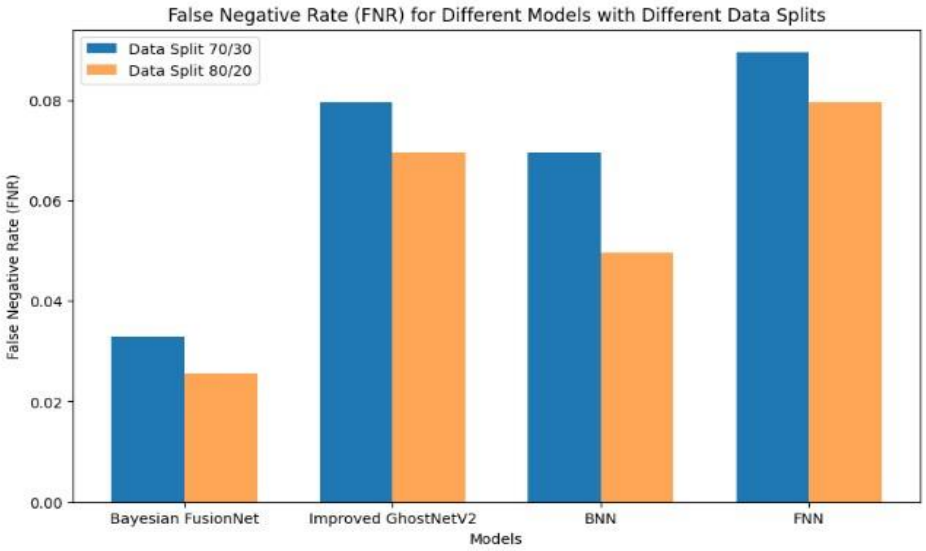

Figure 13: Analysis of FNR

From above evaluation results, the suggested approach exceeds current techniques in a range of assessment measures. The suggested method outperforms Improved GhostNetV2, BNN, and FNN in

terms of accuracy, precision, F-score, specificity, sensitivity, MCC, NPV, and reduced FPR when trained with 70% of the data. Even with 80% more training data, this pattern continues. Its solid performance across numerous assessment criteria is demonstrated by superiority of suggested technique in terms of F-score, accuracy, precision, sensitivity, specificity, MCC, reduced FPR, and NPV.

IV. CONCLUSION

This study presents a novel framework using a hybridized machine learning technique for autonomous phase detection in X-ray diffraction. The procedure includes a rigorous pre-processing step that includes data cleaning, normalization, and smoothing. This is followed by a multi-pronged feature extraction step that extracts important information such as peak position, intensity, and statistical characteristics. HWSKO, a novel hybrid optimization technique, is used to choose features, which successfully lowers computational complexity and improves model performance. Compared to previous techniques, the Bayesian FusionNet-based phase identification shows superiority across several assessment measures by integrating Improved GhostNetV2, Bayesian Neural Network, and Feedforward Neural Network. The outcomes demonstrate that the suggested method is successful even with a larger training dataset in terms of accuracy, precision, and other important parameters. This extensive framework highlights the promise of a hybridized machine learning technique for furthering material science research and enabling effective analysis across a range of applications, in addition to automating phase detection in X-ray diffraction.

Future studies might investigate the incorporation of increasingly more sophisticated designs to improve the Bayesian FusionNet as neural network technology advances. Further research into attention processes, recurrent neural networks, or innovative convolutional neural networks (CNNs) may improve the model's capacity to identify complex patterns in XRD data. An important step forward would be to improve the suggested technique for real-time applications. The process entails enhancing the Bayesian FusionNet computing performance to facilitate swift phase identification, hence making it suitable for real-time analysis in material science labs or industrial environments.

REFERENCES

1. Pandey, A., Dalal, S., Dutta, S. and Dixit, A., 2021. Structural characterization of polycrystalline thin films by X-ray diffraction techniques. *Journal of Materials Science: Materials in Electronics*, *32*, pp.1341-1368.
2. Panahi, S.L., Garcia-Ramón, M., Pineda, E. and Bruna, P., 2020. New (FeCoCrNi)-(B, Si) high-entropy metallic glasses, study of the crystallization processes by X-ray diffraction and Mössbauer spectroscopy. *Journal of Non-Crystalline Solids*, *547*, p.120301.
3. Londoño-Restrepo, S.M., Jeronimo-Cruz, R., Millán-Malo, B.M., Rivera-Muñoz, E.M. and Rodriguez-García, M.E., 2019. Effect of the nano crystal size on the X-ray diffraction patterns of biogenic hydroxyapatite from human, bovine, and porcine bones. *Scientific reports*, *9*(1), p.5915.
4. Gómez, Ó., Mesejo, P., Ibáñez, Ó. and Cordón, Ó., 2021. Deep architectures for the segmentation of frontal sinuses in X-ray images: Towards an automatic forensic identification system in comparative radiography. *Neurocomputing*, *456*, pp.575-585.
5. Kohn, V.G. and Smirnova, I.A., 2020. Theory of the Laue Diffraction of X Rays in a Thick Single Crystal with an Inclined Step on the Exit Surface. I: Numerical Solution. *Crystallography Reports*, *65*, pp.508-514.
6. Hiley, C.I., Hansford, G. and Eastaugh, N., 2022. High-resolution non-invasive X-ray diffraction analysis of artists' paints. *Journal of Cultural Heritage*, *53*, pp.1-13.

7. Martínez-Criado, G., 2020. Application of micro-and nanobeams for materials science. *Synchrotron light sources and free-electron lasers: accelerator physics, instrumentation and science applications*, pp.1719-1753.
8. Ciatto, G., Aubert, N., Lecroard, M., Engblom, C., Fontaine, P., Dubuisson, J.M., Abiven, Y.M., Janolin, P.E., Kiat, J.M., Dumont, Y. and Berini, B., 2019. FORTE–a multipurpose high-vacuum diffractometer for tender X-ray diffraction and spectroscopy at the SIRIUS beamline of Synchrotron SOLEIL. *Journal of Synchrotron Radiation*, *26*(4), pp.1374-1387.
9. Rao, C. and Liu, Y., 2020. Three-dimensional convolutional neural network (3D-CNN) for heterogeneous material homogenization. *Computational Materials Science*, *184*, p.109850.
10. Vecsei, P.M., Choo, K., Chang, J. and Neupert, T., 2019. Neural network based classification of crystal symmetries from x-ray diffraction patterns. *Physical Review B*, *99*(24), p.245120.
11. Zhao, Y., Cui, Y., Xiong, Z., Jin, J., Liu, Z., Dong, R. and Hu, J., 2020. Machine learning-based prediction of crystal systems and space groups from inorganic materials compositions. *ACS omega*, *5*(7), pp.3596-3606.
12. Oviedo, F., Ferres, J.L., Buonassisi, T. and Butler, K.T., 2022. Interpretable and explainable machine learning for materials science and chemistry. *Accounts of Materials Research*, *3*(6), pp.597-607.
13. Weber, S., Diaz, A., Holler, M., Schropp, A., Lyubomirskiy, M., Abel, K.L., Kahnt, M., Jeromin, A., Kulkarni, S., Keller, T.F. and Gläser, R., 2022. Evolution of Hierarchically Porous Nickel Alumina Catalysts Studied by X‐Ray Ptychography. *Advanced Science*, *9*(8), p.2105432.
14. Qian, X. and Yang, R., 2021. Machine learning for predicting thermal transport properties of solids. *Materials Science and Engineering: R: Reports*, *146*, p.100642.
15. Guccione, P., Lopresti, M., Milanesio, M. and Caliandro, R., 2020. Multivariate analysis applications in x-ray diffraction. *Crystals*, *11*(1), p.12.
16. Hocine, S., Van Swygenhoven, H., Van Petegem, S., Chang, C.S.T., Maimaitiyili, T., Tinti, G., Sanchez, D.F., Grolimund, D. and Casati, N., 2020. Operando X-ray diffraction during laser 3D printing. *Materials Today*, *34*, pp.30-40.
17. Oviedo, F., Ren, Z., Sun, S., Settens, C., Liu, Z., Hartono, N.T.P., Ramasamy, S., DeCost, B.L., Tian, S.I., Romano, G. and Gilad Kusne, A., 2019. Fast and interpretable classification of small X-ray diffraction datasets using data augmentation and deep neural networks. *npj Computational Materials*, *5*(1), p.60.
18. Lee, J.W., Park, W.B., Lee, J.H., Singh, S.P. and Sohn, K.S., 2020. A deep-learning technique for phase identification in multiphase inorganic compounds using synthetic XRD powder patterns. *Nature communications*, *11*(1), p.86.
19. Sivaraman, G., Csanyi, G., Vazquez-Mayagoitia, A., Foster, I.T., Wilke, S.K., Weber, R. and Benmore, C.J., 2022. A combined machine learning and high-energy x-ray diffraction approach to understanding liquid and amorphous metal oxides. *Journal of the Physical Society of Japan*, *91*(9), p.091009.
20. Utimula, K., Hunkao, R., Yano, M., Kimoto, H., Hongo, K., Kawaguchi, S., Suwanna, S. and Maezono, R., 2020. Machine‐Learning Clustering Technique Applied to Powder X‐Ray Diffraction Patterns to Distinguish Compositions of ThMn12‐Type Alloys. *Advanced Theory and Simulations*, *3*(7), p.2000039.
21. Dong, R., Zhao, Y., Song, Y., Fu, N., Omee, S.S., Dey, S., Li, Q., Wei, L. and Hu, J., 2022. DeepXRD, a Deep Learning Model for Predicting XRD spectrum from Material Composition. *ACS Applied Materials & Interfaces*, *14*(35), pp.40102-40115.
22. Utimula, K., Yano, M., Kimoto, H., Hongo, K., Nakano, K. and Maezono, R., 2023. Feature Space of XRD Patterns Constructed by an Autoencoder. *Advanced Theory and Simulations*, *6*(2), p.2200613.

23. Massuyeau, F., Broux, T., Coulet, F., Demessence, A., Mesbah, A. and Gautier, R., 2022. Perovskite or Not Perovskite? A Deep-Learning Approach to Automatically Identify New Hybrid Perovskites from X-ray Diffraction Patterns. *Advanced Materials*, *34*(41), p.2203879.
24. Banko, L., Maffettone, P.M., Naujoks, D., Olds, D. and Ludwig, A., 2021. Deep learning for visualization and novelty detection in large X-ray diffraction datasets. *Npj Computational Materials*, *7*(1), p.104.
25. Wang, H., Xie, Y., Li, D., Deng, H., Zhao, Y., Xin, M. and Lin, J., 2020. Rapid identification of X-ray diffraction patterns based on very limited data by interpretable convolutional neural networks. *Journal of chemical information and modeling*, *60*(4), pp.2004-2011.

This page is intentionally left blank

Measuring Local People Perception toward Wildlife and Conservation at the Periphery of the Dja Biosphere Reserve, East Region, Cameroon

Epanda Manfred Aimé, Mukam Fotsing André Junior, Ladi Ngwah Adi, Daniel Frynta, Jacob Willie & Stijn Speelman

Charles University of Prague

ABSTRACT

The Dja Biosphere Reserve is home to immense natural resources. Increasing poaching and other human activities like shifting cultivation and industrial agriculture are major problems in this area. This study addresses the need to explore the attitude and perception of local residents toward wildlife and conservation. Questionnaires, surveys and field observations were used in data collection. A total of 400 people was conveniently selected in 16 villages from October to December 2015. Data analysis relied mainly on factor analysis and structural equation modelling in SPSS 21 and Smart-PLS software. The main findings indicate a significant positive relationship between wildlife education, community wildlife sensitization and the local attitude on community involvement in conservation, which in turn have a strong and positive significant impact on the perception of the local people towards wildlife and conservation. Moreover, the perception of local people has a significant positive impact on the level of discipline towards wildlife and conservation.

Keywords: wildlife conservation, perception of wildlife, dja faunal reserve, local community implication, wildlife education.

Classification: LCC Code: QH75-77

Language: English

Great Britain Journals Press

LJP Copyright ID: 925691
Print ISSN: 2631-8490
Online ISSN: 2631-8504

London Journal of Research in Science: Natural & Formal

Volume 24 | Issue 9 | Compilation 1.0

Measuring Local People Perception toward Wildlife and Conservation at the Periphery of the Dja Biosphere Reserve, East Region, Cameroon

Epanda Manfred Aimé [α] Mukam Fotsing André Junior [σ], Ladi Ngwah Adi[ρ], Daniel Frynta [Ↄ], Jacob Willie[§] & Stijn Speelman [χ]

ABSTRACT

The Dja Biosphere Reserve is home to immense natural resources. Increasing poaching and other human activities like shifting cultivation and industrial agriculture are major problems in this area. This study addresses the need to explore attitude and perception of local residents toward wildlife and conservation. Questionnaires surveys and field observations were used in data collection. A total of 400 people was conveniently selected in 16 villages from October to December 2015. Data analysis relied mainly on factor analysis and structural equation modelling in SPSS 21 and Smart-PLS software. The main findings indicate a significant positive relationship between wildlife education, community wildlife sensitization and the local attitude on community involvement in conservation, which in turn have a strong and positive significant impact on the perception of the local people towards wildlife and conservation. Moreover, the perception of local people has a significant positive impact on the level of discipline towards wildlife and conservation. The results also suggest that local people perception index is not one-dimensional but can be considered as a three-dimensional construct affected by intention, wildlife threat and community involvement. Strategies aiming to change the perception of local people toward wildlife and conservation therefore need integrated approaches. This research points the involvement of local communities in wildlife management as an essential strategy to shape positive perception toward wildlife. Anti-poaching strategies will be easier if local people had a good perception towards wildlife and conservation. Wildlife education and sensitization are also essential in any conservation strategy, as they are key drivers of positive perception toward wildlife and conservation.

Keywords: wildlife conservation, perception of wildlife, dja faunal reserve, local community implication, wildlife education.

*Author*α: Tropical Forest and Rural Development.
ασρ: Centre de Recherche pour la Conservation et le Développement.
Ↄ: Department of Zoology, Faculty of Science, Charles University of Prague, Prague, Czech Republic.
§: Department of Biology, Faculty of Science, Ghent University, Centre for Research and Conservation, Royal Zoological Society of Antwerp.
αχ: Department of Agricultural Economics, Faculty of Bioscience Engineering, Ghent University.

I. INTRODUCTION

African wildlife conservation has long reclined on protected areas (Gueneau and Jacobe, 2005; Duan et al., 2022). They were imposed by governments with the view of effectively protecting, developing and maintaining representative samples of various biotopes in the area where they were installed (vodouhê et *al.,* 2010). Communities had restricted access to their livelihood resources, and they were sometimes relocated elsewhere without any appropriate compensation and suffered from crop damage by wildlife

(Kumssa and Bekele, 2014). Interventions to counteract poaching principally relied on law enforcement patrolling to deter, detect and punish poachers (Steinmetz et *al.,* 2014). The army was deployed to prevent people from exploiting wildlife resources. All these created negative perceptions among locals and promoted bad attitudes toward protected areas. Conflicts therefore emerged between protected areas and surrounding communities (Infield and Namara, 2001). Today, there is a considerable debate on the extent to which protected areas delivers conservation outcomes in terms of habitat and species protection (Geldmann et *al.,* 2013). Many conservationists now think that local people's participation is a major factor in the success or failure of any conservation project (Baloda et *al.,* 2011). In response, new strategies, often referred to as community-based conservation (CBC), have evolved over the past two decades (Infield and Namara, 2001). CBC aims to simultaneously achieve development and conservation goals, therefore meeting the objectives of both local communities and conservationists (Nilsson et *al.,* 2016). This strategy is inclusive rather than exclusive and seeks to provide more participation to local communities. People are therefore at the centre of all conservation practices (Tichaawa and Mhlanga, 2015) and assessment of their perceptions towards conservation has become an important aspect in designing conservation interventions (Ebua et *al.,* 2011). Indeed, local communities' perception of protected areas influences the interactions that people have with them and therefore the effectiveness of conservation efforts (Vodouhê et *al,* 2010).

To date, many studies have focused on examining perceptions and attitudes of local communities toward protected areas **(**Vodouhê et *al.,* 2010; Ebua et *al.,* 2011; Kumssa and Bekele, 2014; Tichaawa and Mhlanga, 2015, infield and Namara, 2001; Gemeda et *al.,* 2016). Their interest was mainly on accessing general knowledge, perceptions and attitudes of locals toward conservation and the factors associated with them. However, little research has been focused on the specific status of the Dja Biosphere Reserve and little is known about the perception of local residents toward this protected area. The Dja Biosphere Reserve has been established as a faunal reserve in 1950 and a UNESCO World Heritage site in 1981. Since the creation of this protected area, there has been many interventions in attempts to deter poaching from local communities. Although the government along with national and international organisations have spent billions of US dollars, the level of poaching in this protected area continue to threaten threatened and endangered species (Nasi et *al.*, 2008). Some species populations are drastically declining and other are on the brink of extinction. In recent years, understanding that militarised and exclusionary approaches were not successful, conservationists now integrate local communities to try to accommodate their aspirations in hopes they form a better perception of biodiversity and conservation.

This study, therefore, aims to examine to what extent education, sensitization and attitude of the local people through community involvement influence their perceptions toward wildlife and conservation; to investigate the impact of their perceptions on community discipline toward wildlife and conservation; and to construct and validate the psychometric properties of the measurement scale on the perceptions of local people toward wildlife and its conservation.

Based on the results from previous studies, we formulated 3 hypotheses (1) there is a relationship between education, sensitization and attitude of local people to their perceptions toward wildlife and conservation; (2) the perception of local people is intimately linked to their discipline toward it; (3) the perception of local people toward wildlife and conservation is not one-dimensional.

II. MATERIAL AND METHODS

1.1. The Study Area

The study was conducted at the northern periphery of the Dja Biosphere Reserve (Fig 1) in the Messamena Sub-division, Upper Nyong Division of the East Region of Cameroon. The Dja Biosphere

Reserve is located in the East and South regions of Cameroon, between 2°50 and 3°30 latitude North, and 12°20 and 13°40 longitude East. This protected area is a vital home for critically endangered great apes and is one of the most emblematic and endangered landscape in the world. Apart from the critically endangered Western Lowland Gorilla (*Gorilla gorilla*) and endangered chimpanzee (*Pan Troglodytes troglodytes*), other flagship species in this UNESCO World Heritage Site include the forest elephant (*Loxondonta africana cyclotis*), grey parrot (*Psithacus erithacus*), giant pangolin (*Loxondonta africana cyclotis*), and leopard (*Panthera pardus).* This forested reserve which encompasses 5,260 sq. km is classified among the largest protected areas of the Guinea-Congolian tropical rain forests and designated an important bird area. It was created on the 26 June 1950 by decree No. 319 of the French High commissioner for Cameroon, and in 1981, at the instigation of the Cameroon branch of UNESCO's Man and Biosphere program, it became a UNESCO biosphere reserve. The UNESCO world heritage sites scheme was extended to the Dja Biosphere Reserve in 1987. The study area has an altitude ranging from 600 to 700 m above the sea level. The population of the Messamena Sub-division is estimated at 26 153 inhabitants including 13 441 males and 12 712 females (BUCREP, 2005). The population density is not high, including about 1.5 inhabitants/ sq. km. The major ethnic groups, the Badjoue and the Baka people live side by side in and outside the reserve. The climate is of the humid equatorial type with 4 seasons: a long-wet season from August to November, a long dry season from November to March, a short-wet season from March to June and a short dry season from June to August (Epanda, 2004). The average annual rainfall is 1563 mm and the average temperature vary between 19, 8°C and 27°C (Willie et *al.,* 2012). The hydrography is dominated by the Dja River which form a natural boundary to the reserve from the south, west and north. As in many rural areas in Cameroon, the livelihood of local people relies on a mixture of activities such as agriculture, livestock keeping, hunting, fishing, Non-Timber Forest Products (NTFP) valorisation and handicraft. The main crops grown in the area are cassava (*Manihot esculenta),* cocoa (*Theobroma cacao*), coffee (*Coffeeae* spp.), cocoyam (*Xanthosoma sagittifolium),* groundnut (*Arachis hypogaea)* and plantain (*Mussa* spp.*).* The poor condition of roads is not favourable to the commercialisation of agricultural products. As a result, a high proportion of the harvest is mainly for consumption and the remaining part is sold as a very low price (Mukam, 2017). Bushmeat is hunted mainly for subsistence; only a small proportion is sold (Avila et *al.,* 2017). Commercial logging, mining, poaching, industrial agriculture and infrastructure development are among the most important threats to the reserve and are the main contributing factors to habitat loss and fragmentation. Recent human population growth has increased deforestation and also exacerbated the impacts of poaching and the illegal bush meat trade.

Since 2010 the population of the study area has been involved through the NGO Tropical Forest and Rural Development (TF-RD) in a community-centred conservation program that aimed to improve local people's livelihood and perception and therefore divert them from poaching. Actions to reduce poaching were based on the creation of alternative income sources, groups training and structuring and awareness rising through education and sensitization. Alternative sources of income were introduced through the valorization of cocoa-based agroforest enriched with plantain and other local fruit trees and the valorization of non-timber forest products. Local people engaged in these activities were trained in sustainable agricultural practices, provided support in the creation of community enterprises and given access to high-value markets that would otherwise be inaccessible.

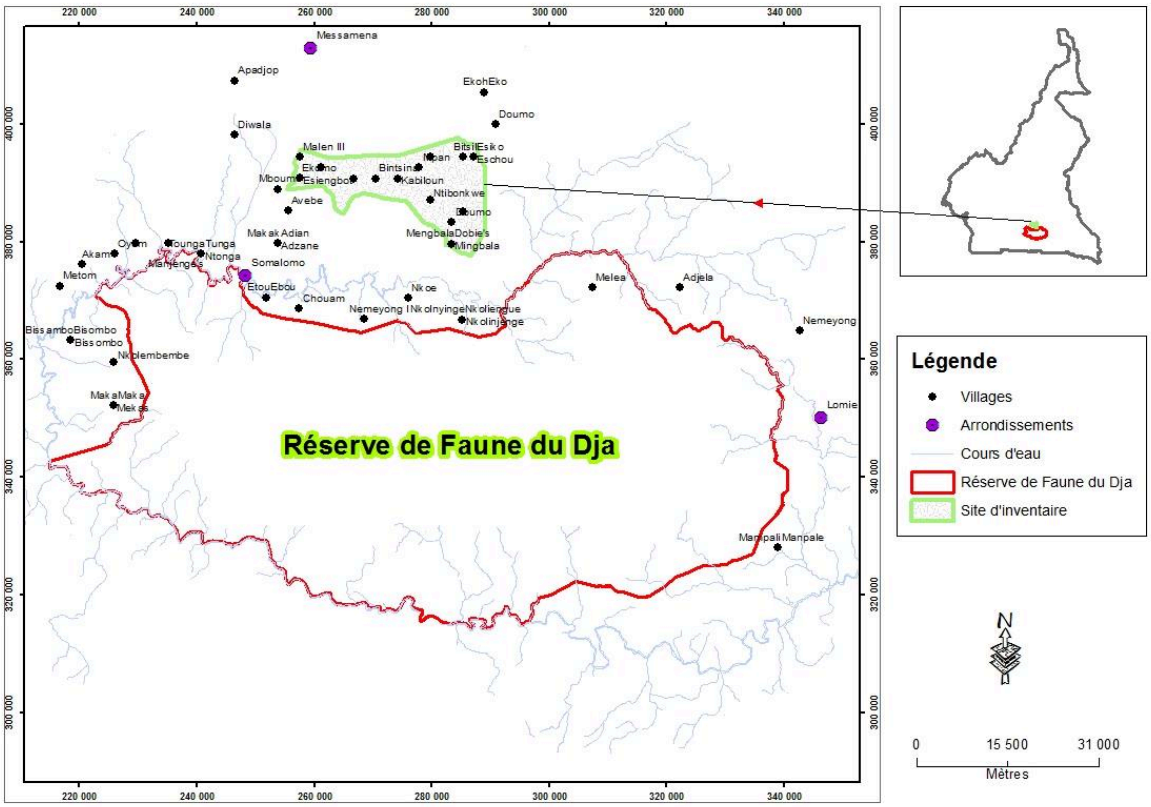

Figure 1: Localization of the study area at the Northern Buffer zone of the Dja biosphere reserve

1.2. Methods

A questionnaire survey was carried out from October to December 2015 in 16 villages around the northern periphery of the Dja Biosphere Reserve. The total population of the study area was estimated at 3655 inhabitants using information of the 2005 national census (BUCREP, 2005) which was actualised using the population rate of increment, which was 15, 6 % between 2005 and 2017 (BUCREP, 2011). Four hundred people were surveyed yielding a sampling intensity of 10,94 %. Out of the 400 participants, only 334 properly responded to the entire questionnaire. The other 66 were excluded from the analysis. Convenience sampling was found adequate and reasonable to be used because the members of the population were difficult to reach, given that they are mostly farmers and hunters (Knapp & al, 2017). The advantages of the use of this technique of non-probabilistic sampling are that it is easy and convenient to rely upon the judgement of the experts to draw the sample. The population were divided into clusters of villages, and a purposive sampling was applied in selecting each element within the sample frame. The villages included in the sample frame were: Bintsina, Bitsil, Doumo Mama, Doumo Pierre, Echou, Kabilone II, Kompia, Madjuh II, Malen II, Malen V, Medjoh, Mimpalla, Nemeyong, Ngloumінanga, Ntibonkeuh and Djassa. Interviews were conducted in French since it is the second language spoken by the population after the local language (Bajoue). To avoid misinterpretation problems, interviewers were accompanied by a person native of the area who served as interpreter when necessary. Respondents were asked questions about household demographics, education, employment, income generating activities and their perception toward wildlife and its conservation. To capture information on perceptions and attitude toward wildlife conservation, we used a five points liker-scale (from strongly disagree to strongly agree). Collecting information on sensitive topics like wildlife conservation is enormously challenging (wilfed & Maccoll, 2010) not only because of the illegal nature of hunting activities, but also because people do not always want to reveal real information concerning them. Since people commonly fear social rejection from other in the

village, they choose to withhold truthful information. Data collected in such situations are therefore biased. To avoid such bias, the purpose of the study was introduced to the participants and they were insured of full anonimity for any incriminating information they may disclose. In addition, participant observation was carried out to triangulate information collected. The first author has been working with the communities of the study area since 2003 and have earned their trust. With respect to that, no payment of any kind was given to the respondents, and all were willing to answer the questionnaire. Moreover, since there is no law enforcement organisation in the study area, and the communities have been involved in a community-centred conservation approach, none of the respondents were afraid of being arrested. Therefore, they talked freely about wildlife and hunting activities and their perception toward conservation.

III. DATA ANALYSIS

All the analysis were performed in SPSS 21 and Smart PLS software. The former was used to conduct structural equation modelling while SPSS 21 was used to calculate frequencies and to run principal component analysis (PCA). We used partial least square approach to structural equation modelling (SEM -PLS) otherwise known as soft modelling. This method has several advantages which include the normality of data distribution not assumed. In addition, this approach of data analysis can include a larger number of indicator variables even higher than 50 items. It is used when dealing with weak theory, and it is a more robust and relax modelling approach (Afthanorhan, 2013). This method was accompanied by covariance-based approach of structural equation model (CB –SEM) which is well known for its accurate measurement of goodness-of-fit indices.

Before modelling with smart PLS, the 49 items of the questionnaire on perceptions of local people towards wildlife and conservation scale were subjected to principal component analysis (PCA) to gather information on the interrelationship of the variables. Prior to performing PCA, the suitability of the data for factor analysis was assessed by inspecting the correlation matrix, Bartlett's test of sphericity and Kaiser-Meyer-Oklin (KMO) value. These finding revealed the presence of many correlation coefficients above 0.5, confirming the theoretical expectation. Additionally, the KMO value was 0.77 exceeding the cut-off criteria, while Bartlett's test of sphericity reached statistical significance (P = 0.000), supporting the factorability of the correlation matrix. The 49 items were reduced into 16 components (or factor), with the associated Eigen value greater than 1. Only items with a loading factor of 0.5 or more were returned in this study for further analysis. The validity and reliability of the scale were also accessed. Convergent validity refers to the degree of agreement in two or more indicators of the same construct. Evidence of convergent validity was assessed by inspecting the average variance extracted (AVE) for each factor. According to Fornell and Larcker (1981), convergent validity is established, if the variance-extracted value exceeds 0.50. The results from this study (Table 1) revealed that the variance extracted for six constructs (or variables) ranged from 0.45 to 0.79. The variance extracted of measure of local people perception was the only variable below 0.5, though it can be approximated to 0.5. The individual construct Cronbach Alpha reliability score, considered as the lower bound for all the constructs, was found to be sufficiently significant for all the constructs, loading extremely high for community discipline (α = 0. 75) and low on wildlife knowledge (α =0.68). The composite reliability which is considered as the upper bound and more robust was found to be significantly higher than Cronbach alpha for all the constructs.

To verify if the perception index of local people is a one-dimensional construct or not, factors extracted using PCA were subjected to a second order confirmatory factor analysis (Structural Equation Modelling). However, to determine if the model will be accepted or rejected, at least 3 to 4 tests are recommended (Hair et *al.,* 2010). In this study, we used both absolute fit indices and adjusted goodness-of-fit indices (Table 2). These measures are direct measures of how well the model of

perception index specified by the researcher reproduced the observed data. Result in table 2 show that all measures of absolute fit indices are significant, meaning that the measurement model proposed by the researcher fit the data. All the measures of incremental indices were also found to be significant except normed fit index, which fails to meet with the cut-off criteria.

Table 1: Average Variance Extracted and reliability indexes

Variables	AVE	Composite Reliability	Cronbach's Alpha
Community Discipline	0.56	0.83	0.75
Intention	0.56	0.81	0.70
Local People Attitude	0.79	0.88	0.73
Local People Perception	0.45	0.69	0.68
Wildlife Sensitization	0.58	0.62	0.64
Wildlife knowledge	0.56	0.77	0.63
Community Involvement	0.55	0.78	0.59

Table 2: Goodness of fit indices

Model fit Statistics	Result	Recommended value	Decision
P	0.004	P < 0.05	Accepted
RMSEA (rms)	0.053 (0.030 - 0.076)	RMSEA < 0.08, rms <0.05	Accepted
GFI	0.97	GFI > 0.90	Accepted
AGFI	0.95	AGFI >0.90	Accepted
CFI	0.94	CFI >0.90	Accepted
NFI	0.89	NFI >0.90	Rejected

IV. RESULTS

4.1 Socio demographic characteristics of the respondents

The socio demographic data of the respondents (Table3) indicate that 61.1 % were male while 38.9 % were female. Most (32.2 %) of the participants were young adults aged between 26 and 30 years. The participants were all Christians with the majority of them affiliated to the Catholic Church. Most of the respondents (97.6 %) were literate. Eighty-four percent of them had acquired primary education while only 12.9 % of them achieved secondary school. This high level of education may be explained by the presence of many primary and secondary schools in the area. Monthly income was low as 87.1 % of the respondents earned under 75 000 FCFA (150 U.S $) per month. Agriculture was the main occupation of the respondents (80.2 %) followed by hunting (6.9%). The findings regarding income are not surprising because the majority of the respondents rely on subsistence farming as the main way of generating income activity, and only a small proportion of the production is sold.

Table 3: Socio demographic characteristics of respondents

Variables	N	%	Variables	N	%
Gender			Monthly income (FCFA)		
Male	204	61.1	Less than 30 000	129	38.6
Female	130	38.9	31000-75000	162	48.5
			76000-150000	38	11.4

			151000-200000 More than 200000	3 2	0.9 0.6
Age 18-25 years 26-30 years 31-35 years 36-40 years 41-45 years 46 and above	 48 111 60 36 25 54	 14.4 33.2 18.0 10.8 7.5 16.2	Main occupation Farmer Non timber forest product exploiter Hunter Fisher Village head Bush meat business man or woman Forest guard	 268 10 23 9 9 12 3	 80.2 3.0 6.9 2.7 2.7 3.6 0.9
Religion Catholic Presbyterian Protestant	 328 4 2	 98.2 1.2 0.6	Main source of income Sale of farm products Sale of household labour Hunting Petty trade	 261 24 25 24	 78.1 7.2 7.5 7.2
Level of formal education No formal education Primary Secondary University	 8 280 43 3	 2.4 83.8 12.9 0.9			

4.2 How do educational level, sensitization and attitude of local people through community involvement influences local people perceptions toward wildlife and conservation?

The results from the model estimation (Table 4) reveal a significant positive relationship between wildlife education, community wildlife sensitization, attitude of local people toward wildlife and community involvement in conservation activities. In other words, for a percent improvement on wildlife knowledge, wildlife sensitization and attitude of local people toward wildlife and conservation, community involvement will be enhanced by 14.8 percent, 18 percent and 14.6 percent, respectively. The results further reveal that community involvement has a strong and positive significant impact on the perception of local people towards wildlife and its conservation. The inner and the outer models were all found to be significant at 1%.

Table 4: T-values for the measurement and structural model estimate

	Original Sample (O)	Sample Mean (M)	Standard Deviation (STDEV)	Standard Error (STERR)	T Statistics (|O/STERR|)
Community Involvement -> Local People Perception	0.267116	0.270507***	0.011971	0.011971	22.313786
Local People Attitude -> Community Involvement	0.146514	0.148397***	0.009621	0.009621	15.228777
Wildlife Sensitization -> Community Involvement	0.189280	0.190536***	0.010493	0.010493	18.038105
Wildlife knowledge -> Community Involvement	0.148333	0.148537***	0.013009	0.013009	11.402364

4.3 Impact of local people perceptions on community discipline towards wildlife and conservation

The result shows that the perception of local people has a significant positive impact on the level of discipline toward wildlife and conservation. All the indicators that proxy perceptions and discipline were significant. The result in table 5 can be interpreted to mean that with a unit positive change in the measure of the perception of local people toward wildlife and conservation, the level of discipline toward it will be improved by 29 % (t = 28.16; p = 0.000).

Table 5: t-value of the measurement model: local people perceptions -> community discipline toward wildlife and conservation

	Original Sample (O)	Sample Mean (M)	Standard Deviation (STDEV)	Standard Error (STERR)	T Statistics (|O/STERR|)
LPP-> Community Discipline	0.292934	0.294829***	0.010402	0.010402	28.161522

4.4 Is perception of the local people index toward wildlife and its conservation uni-dimensional construct?

The results from the regression weight (Table 6) indicate that the perception index of local people is predicted by perceived wildlife threats, intention and community involvement. Their regression weight was significantly different from zero at 0.1 % (two-tailed). To verify if the local people perception index is one-dimensional suffice at this stage to test the constructs of evident of discriminant validity. Discriminant validity refers to the extent to which a construct is truly distinct from other constructs. The average variance extracted (AVE) of perceived wildlife threat is AVE = 0.40, *while* for intention is closed to the cut-off criteria (AVE = 0.63) and for community involvement, average variance extracted is 0.66. The correlation (r) between perceived wildlife threat and intention is 0.47; by comparing the average variance extracted of both constructs with the correlation square (r^2 = 0.22), the results indicate that the two constructs intention and wildlife threat exhibit sufficient discriminant validity. This is because both AVEs fall above the square of the correlation coefficient between them (Fornell and Larcker, 1981). Although two out of the 4 indicators predicting wildlife threat had a low and insignificant factor loading. Both AVEs of intention and community involvement are greater than the correlation coefficient between them (r^2=0.36). There is evidence of discriminant validity between these two constructs as well. This is interpreted to mean that local people perception index is not a one-dimensional construct but rather can be considered as three-dimensional constructs. As can be visualised from the Figure 3, intention is loading high (FL = 0.80) in the prediction model perception index of local people, followed by community involvement in conservation (FL=0.76) and perceived wildlife threat (FL= 0.59).

V. DISCUSSION

Our results indicate that the perception of local people toward wildlife and conservation is strongly influenced by their involvement in conservation activities, which in turn is influenced by education, wildlife sensitization and the attitude of local people. The perception of local people is therefore influenced by wildlife knowledge, attitude and community sensitization on wildlife and conservation. Similar results were reported by Vodouhê et *al* (2010), who concluded that the perception of local communities was strongly related to the management strategy of the park where local communities were effectively involved. Their results also pointed to education as the main factor in shaping positive perception toward wildlife among local communities. Wildlife sensitization was also reported by Steinmetz et *al* (2014) as one of the main factors leading to positive perception toward wildlife and conservation. According to this research, outreach can build trust, raise awareness, motivate, offer

opportunities for action, increase perceived behavioural control of villagers and generate social pressure against poaching. Our results reveal the importance of involving people in conservation. Strategies that aim to counteract, detect and punish poachers lead to loss of wildlife and money since interventions are almost always after animals are death. Educating people and raising awareness through sensitization can help prevent the loss of wildlife.

Rocha and Fortes (2015) also pointed to the role of education in determining the perception of local peoples toward wildlife and conservation. Their findings reveal that school-aged children had a positive perception toward monkeys. Many of them showed a strong understanding of the ecological importance of the monkeys. This understanding may be due to the environmental education they received at school. In the case of our study area, local people have been subjected to a multi-year education and sensitization through the intervention of local NGOs working in that area. Three conservation organisation work and have an established presence in the study area: Tropical Forest and Rural Development, the "Projet grands singes" and the Association Apes Assistance through its centre of agricultural training. All these organisations have been sensitizing local communities on the importance of preserving wildlife communities for their benefit and that of future generations for more than ten years. TF-RD, through its environmental education component, has been working on improving the perception of young students and school teachers. This was done by organising field trip with students in order to bring them in contact to animals in the National Park of Mefou. Children of the study area used to see animals after they have been killed. This environmental education program at the Mefou National Park allowed the children to meet and interact with the animals that are subject to conservation efforts to improve their perception toward wildlife and conservation.

Results also suggest that the perception of local people toward wildlife has a significant effect on their discipline toward it. People who have a positive perception toward wildlife are more likely to respect the conservation efforts and protected area agreements. Different results were reported by Nepal and Spiteri (2011) who concluded that despite their positive attitudes and perception, people did not necessarily behave in a way compatible with conservation. This was because positive attitude was derived by a perceived livelihood dependence on natural resources, but there was not a clear linkage to conservation. In the case of our study, local people are brought in a community-centred conservation strategy that place humans at the centre of conservation. Helping local people to meet livelihood requirements through cocoa farming and NTFP valorisation and building their capacities contribute to build good attitudes that produce good intentions to conserve wildlife and a good perception of wildlife and conservation. However, to create a clear linkage with conservation, communities were brought through this community-based conservation approach, to sign quid-pro-quo participatory agreement (Reciprocal Environmental Agreement, REA) for poaching reduction. Agreements specify that local communities will refrain from commercial hunting; cease hunting within the reserve; and support the Service de Conservation to stop outsider poaching (e.g., vigilance committees/intelligence through information on poachers). Indeed, local people whose perception is improved are not only more disciplined toward wildlife, but they also engage themselves in sensitizing their peers to refrain from poaching. This can be illustrated by many people in the study area who were very active in wildlife trafficking, but after their engagement in the project, some started to reduce their poaching activities; others stopped it and started to convince their fellow villagers to abandon poaching and rather engage in agriculture.

Result further reveal that the perception index of local people is not one dimensional but can be rather considered as a three-dimensional construct affected by intention to conserve, wildlife threat and community involvement. The perception of local people is therefore the result of combination of many factors that should be taken into consideration while designing conservation interventions. If local people think that wildlife is meat given by God and there is no alternative meat available, that the

government cares for wildlife more than the wellbeing of local people, that local people are not involved in conservation and that wildlife attacks livestock and destroys farms, then they will have a very bad perception toward wildlife. But if they understand that the main threat to wildlife is poaching and wildlife extinction is bad for ecosystem and for future generations, they will be more favourable to conservation. Knowing that should guide conservationists toward more integrated strategies that will act on all determinants of the perception of local people.

Table 6: regression weights from the measurement model of local people's perception index

			Estimate	S.E.	C.R.	P
Perceived Wildlife threat	<---	LPP_Index	0.299	0.066	4.54	0.000
Intention	<---	LPP_Index	0.667	0.097	6.859	0.000
Community Involvement	<---	LPP_Index	0.717	0.109	6.584	0.000
ILP1	<---	Intention	0.92	0.12	7.685	0.000
ILP2	<---	Intention	1.00			
ILP3	<---	Intention	0.747	0.097	7.732	0.000
CI2	<---	Community Involvement	0.936	0.16	5.859	0.000
CI3	<---	Community Involvement	1.00			
LPP2	<---	PWLT	1.00			
LPP3	<---	WLT	1.154	0.261	4.418	0.000
Q32	<---	WLT	0.49	0.172	2.849	0,004
Q34	<---	WLT	0.347	0.105	3.314	0.000

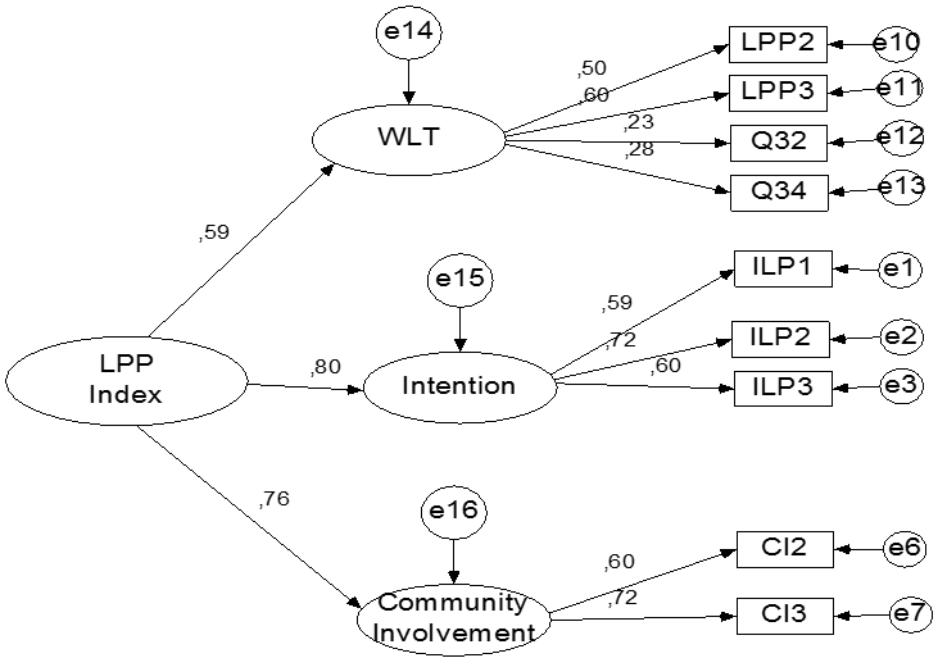

Figure 3: Predictive model of Local people Perception index

VI. CONCLUSION

This study assessed the perception of local people toward wildlife and conservation and the factors that can influence it. Overall, the study demonstrated that education, sensitisation and attitude of local people are very important factors that can influence the perception of local people which in turn can influence the discipline toward wildlife. Taking this into account benefits for conservation because this can help to save wildlife and money. We always intervene when animals are dead. This study also demonstrated that the implication of local people in wildlife management is crucial as it will lead to the improvement of their perception of wildlife and conservation and finally improve the discipline toward conservation rules. Anti-poaching strategies will be easier if local people had a good perception toward wildlife and its conservation. This study finally demonstrated that the perception of local people toward wildlife and conservation is not a one-dimensional construct, suggesting that issues concerning poaching need integrated responses. Working alongside with law enforcement to educate people, sensitising them on the importance of wildlife conservation, shaping bottom-up conservation strategies with local people, and improving their livelihoods through cocoa-based agroforestry and non-timber forest products valorisation will bring more successful conservation outcomes around the Dja Biosphere Reserve.

ACKNOWLEDGEMENTS

We are very thankful to the Small Initiative Program of the French Fund for the World Environment (PPI/FFEM) who provided fund for this research. We also Thank Thomas Bacha for constructive comments during the elaboration of this work. We also acknowledge the participation of the local population during data collection.

REFERENCES

1. Avila, E., et al. 2017. Interpreting long-term trends in bushmeat harvest in southeast Cameroon. *Acta Oecologica: 1-9*. http://dx.doi.org/10.1016/j.actao.2017.09.007
2. Badola, R., Barthwal, S., & Hussain, S. A. (2012). Attitudes of local communities towards conservation of mangrove forests: A case study from the east coast of India. Estuarine, Coastal and Shelf Science, 96, 188-196.
3. BUCREP (2011). Rapport national sur l'état de la population : enjeux et défis d'une population de 20 millions d'habitants au Cameroun en 2011. http://bucrep.cm/index.php/fr/ressources-et-documentations/telechargement/category/57-rnep-2011?download=89:rapport-national-sur-l-etat-de-la-population.
4. BUCREP (2005). Répertoire actualisé des villages du Cameroun : troisième recensement général de la population et de l'habitat du Cameroun.
5. Duan, W. ; Jiang, Yi. ; Shen, J. (2022). Impacts of Social Trust on Rural Household's Attitudes Towards Ecological Conservation-Example of the Giant Panda Nature Reserves in China. Forest 2022, 13, 53. https//doi.org/10.3390/f13010053.
6. Ebua, V. B., Agwafo, T. E., & Fonkwo, S. N. 2011. Attitudes and perceptions as threats to wildlife conservation in the Bakossi area, South West Cameroon. *International Journal of Biodiversity and Conservation*, *3*(12), 631-636. http://www.academicjournals.org/IJBC
7. Epanda, M.A. (2004). Projet intégré de conservation et de développement : chasse contrôlée pour une protection intégrale à la périphérie Nord de Réserve de Biosphère du Dja (RDB). Rapport intermediaire. P. 56.
8. Fornell, C. & Larcker, D. F. (1981). Evaluating structural equation models with unobservable variables and measurement error. *Journal of marketing research*, 39-50.

9. Gandiwa, E., et al. 2014. Local people's knowledge and perceptions of wildlife conservation in South-eastern Zimbabwe. *Journal of environmental protection, 5, 474-485*. http://dx.doi.org/10.4236/jep.2014.56050.
10. Geldmann, J., Barnes, M., Coad, L., Craigie, I. D., Hockings, M., & Burgess, N. D. (2013). Effectiveness of terrestrial protected areas in reducing habitat loss and population declines. *Biological Conservation*, *161*, 230-238. https://doi.org/10.1016/j.biocon.2013.02.018
11. Gemeda, D. O., Minstro, A. A., Feyessa, D. H., Sima, A. D., & Gutema, T. M. 2016. Community knowledge, attitude and practice towards black crowned crane (Balearica pavonina L.) conservation in Chora Boter district of Jimma Zone, Ethiopia. *Journal of Ecology and The Natural Environment*, *8*(4), 40-48.
12. Guéneau, S., & Jacobée, F. 2005. Conservation de la biodiversité forestière tropicale en Afrique centrale : dépassionner les débats. Institut du Développement Durable et des Relations Internationales (IDDRI), Workingpaper, 14.http://www.iddri.org/Publications/Collections /Idees-pour-le-debat/id_0514_gueneau&jacobee_depassionner.pdf
13. Hair, J. F., Black, W. C., Babin, B. J., Anderson, R. E., & Tatham, R. L. 1998. *Multivariate data analysis* (Vol. 5, No. 3, pp. 207-219). Upper Saddle River, NJ: Prentice hall. https://pdfs.semanticscholar.org/6885/bb9a29e8a5804a71bf5b6e813f2f966269bc.pdf.
15. Kumssa, T., & Bekele, A. 2014. Attitude and Perceptions of Local Residents toward the Protected Area of Abijata-Shalla Lakes National Park (ASLNP), Ethiopia. *J Ecosys Ecograph 4: 138*.
16. Knapp, E.J; Peace, N and Bechtel, L. 2017. Poachers and poverty: accessing objective and subjective measures of poverty among illegal hunters outside Ruaha National Park, Tanzania. *Conservation and society 15(1): 24-32. http://www.conservationandsociety.org/text.asp?2017/15/1/24/201393*
17. http://www.ceped.org/ireda/inventaire/ressources/cmr-2005rec_v4.7_repertoire_actualise_villages_cameroun.pdf
18. Nasi, R., Brown, D., Wilkie, D., Bennett, E., Tutin, C., Van Tol, G., and Christophersen, T. 441 2008. Conservation and use of wildlife-based resources: the bushmeat crisis. Secretariat of 442 the Convention on Biological Diversity, Montreal. And Center for International Forestry 443 Research (CIFOR), Bogor. Technical Series, 50 pages 444.
19. Nilsson, D., Baxter, G., Butler, J. R., & McAlpine, C. A. 2016. How do community-based conservation programs in developing countries change human behaviour? A realist synthesis. *Biological Conservation*, *200*, 93-103.
20. Rocha, l. c. & Fortes, v. b. (2015). Perceptions and attitudes of rural residents towards capuchin monkeys, in the area of influence of the Dona Francisca hydroelectric power plant, south Brazil. *Ambiente & Sociedade, 18(4), 19-34*.
21. Steinmetz, R; Srirattanaporn, S; Mor-Tip, J and Seuaturien, N. 2014. Can community outreach alleviate poaching pressure and recover wildlife in South-East Asian protected areas*? Journal of Applied Ecology 2014, 51, 1469–1478. http://onlinelibrary.wiley.com/doi/10.1111/1365-2664.12239/abstract*
22. Tichaawa, T. M., & Mhlanga, O. S. W. A. L. D. (2015). Community perceptions of a community-based tourism project: A case study of the CAMPFIRE programme in Zimbabwe. African Journal for Physical Health Education, Recreation and Dance, 21(Supplement 2), 55-67.
23. Vodouhê, F. G., Coulibaly, O., Adégbidi, A., & Sinsin, B. 2010. Community perception of biodiversity conservation within protected areas in Benin. *Forest Policy and Economics*, *12*(7), 505-512. *https://doi.org/10.1016/j.forpol.2010.06.008*
24. Willie, J., Petre, C.-A., Tagg, N., & Lens, L. (2012). Evaluation of species richness estimators based on quantitative performance measures and sensitivity to patchiness and sample grain size. *Acta oecologica, 45, 31-41*.

Theoretical Prerequisites for Optimizing the Spray Pattern Angles of an Adaptive Sprayer for a Field Sprayer

Rodimtsev S.A. & Dembovsky I.A

Orel State University

ABSTRACT

Vibrations of the sprayer field boom in the transverse-vertical plane result in a decrease in the quality of the technological operation. This is especially true in relation to the operation of small-sized single-support wheelbarrow-type sprayers. One of the possible solutions to compensate for the effect of transverse vibrations of the boom on the quality of spraying is the use of adaptive sprayers with a variable root angle of the spray torch, responding to the position occupied by the sprayer in relation to the surface being treated. The purpose of the work is to optimize the current values of the frontal spray angles of the nozzles of the adaptive distribution system of a small boom sprayer. The novelty of the study lies in the fact that, unlike industrial agricultural machinery, insufficient attention is paid to the implementation of technologies using small-scale mechanization tools. A prototype of a single-support boom motor sprayer was used as the object of study. The field experiment was carried out at the experimental sites of the Oryol State Agrarian University. Registration of data on the deviation of the sprayer from the vertical axis was carried out using a specially developed mathematical processing of the decrypted experimental data was carried out by a spreadsheet processor in the Microsoft Excel environment.

Keywords: small-sized sprayer, sprayer, spray angle, field boom, transverse vibrations, spray uniformity, nomogram.

Classification: DCC Code: 631.3

Language: English

Great Britain Journals Press

LJP Copyright ID: 925693
Print ISSN: 2631-8490
Online ISSN: 2631-8504

London Journal of Research in Science: Natural & Formal

Volume 24 | Issue 9 | Compilation 1.0

Theoretical Prerequisites for Optimizing the Spray Pattern Angles of an Adaptive Sprayer for a Field Sprayer

Rodimtsev S.A.[α] & Dembovsky I.A.[σ]

ABSTRACT

Vibrations of the sprayer field boom in the transverse-vertical plane result in a decrease in the quality of the technological operation. This is especially true in relation to the operation of small-sized single-support wheelbarrow-type sprayers. One of the possible solutions to compensate for the effect of transverse vibrations of the boom on the quality of spraying is the use of adaptive sprayers with a variable root angle of the spray torch, responding to the position occupied by the sprayer in relation to the surface being treated. The purpose of the work is to optimize the current values of the frontal spray angles of the nozzles of the adaptive distribution system of a small boom sprayer. The novelty of the study lies in the fact that, unlike industrial agricultural machinery, insufficient attention is paid to the implementation of technologies using small-scale mechanization tools. A prototype of a single-support boom motor sprayer was used as the object of study. The field experiment was carried out at the experimental sites of the Oryol State Agrarian University. Registration of data on the deviation of the sprayer from the vertical axis was carried out using a specially developed mathematical processing of the decrypted experimental data was carried out by a spreadsheet processor in the Microsoft Excel environment. The study of the obtained analytical dependencies was carried out in the environment of the mathematical calculation system Mathcad 14.0. The work used the method of nomogramming functions of several variables. It has been experimentally established that during operation the maximum deviations of the sprayer from the vertical can be up to 30°. At the same time, the average amplitude of the transverse operating vibrations of the boom of a single-support barrow-type boom sprayer ranges from +11° to -18°. The amplitude of lateral vibrations of a single-support sprayer depends on the operator's preparedness and the speed of movement of the unit. Balancing the sprayer is important, taking into account the moment of forces caused by the weight of the one-sided field boom. A formula has been derived for calculating the spray width of one sprayer, taking into account the geometric parameters of a single-support sprayer, as well as its angle of inclination in the transverse-vertical plane. An analytical relationship has been obtained that makes it possible to calculate the required limits of the root angle of the spray pattern of an adaptive sprayer, taking into account the installation distance of the sprayer, relative to the vertical plane passing through the support point of the sprayer. The values of the root spray angles were found for the deflectors of adaptive sprayers, with the amplitude of oscillations of the sprayer from -18° to +11° in the transverse-vertical plane. A nomogram has been developed to determine the optimal values of the frontal angles of the spray pattern of sprayer nozzles. An analytical technique for optimizing the current values of frontal spray angles has been proposed, taking into account the position of the distribution system and performed for the first time. The practical value of the study lies in the possibility of using a formula to determine the limits of change in root spray angles when designing and developing adaptive sprayers. The technique can be used to develop software for the control complex of a sprayer equipped with an adaptive system for distributing working fluid in changing conditions.

London Journal of Research in Science: Natural & Formal

Keywords: small-sized sprayer, sprayer, spray angle, field boom, transverse vibrations, spray uniformity, nomogram.

Author α : Doctor of Technical Sciences Orel State University named after I.S. Turgenev, Orel, Russia.
σ: Graduate student Oryol State Agrarian University named after N.V. Parakhin, Orel, Russia.

I. INTRODUCTION

In the processes of selection and primary seed production of plants, improvement of gardening and park farming, as well as on citizens' personal plots, single-support small-sized wheelbarrow-type boom sprayers are used. Among the most famous models offered by manufacturers are equipment from Wintersteiger (Austria), Euro Pulve (France), Walkover International (England), and a sprayer produced by JSC GSKB (Zernoochistka) Voronezh (Russia). Single-support sprayers have a number of advantages compared to a single-axle two-wheeled design: they are less metal-intensive, more maneuverable, do not require re-adjusting the track, and when switching to a different row spacing, they can be moved along narrow paths. At the same time, they are less stable in the transverse-vertical plane, which entails the need for constant monitoring of the horizontal position of the rod and excessive stress on the operator.

It is known that even slight vibrations of the boom lead to a deterioration in the quality of spraying: with increasing spray height, evaporation and drift of particles of the working fluid increase; The low height of the nozzles determines the absence of overlap zones and exceeding the rate of application of the active substance. As a result, conditions are created for insufficient inhibition of the development of weeds [1], acceleration of resistance (addiction) of pests [2, 3] to the drug and a decrease in its toxicological effect on pathogens [4] in the "under-application" zone. An increase in the concentration of the active substance causes burns of plant leaves [5]. For the environment, one of the main risk factors is the drift of small drops and the flow of large drops from the treated surface. It has been established that during spraying, the proportion of small droplets with a low rate of gravitational settling (less than 80 microns) ranges from 1...2% [6] to 5...6% [7] and more. In general, losses of herbicides during demolition can be 20...90%, and damage to crops that are not subject to this treatment is in some cases found at a distance of up to 20 km from the spraying sites [8].

Under these conditions, special attention should be paid to ensuring uniform application of protective equipment, regardless of elastic vibrations of the rod, resonance phenomena or current changes in the microrelief. Thus, for trailed, mounted and self-propelled sprayers, the problem of compensating for boom deflection has been systematically solved for many years. There are known technical and technological solutions based on copying the field topography using spring-lever suspensions [9], vibration dampers of the field rod [10], suppression of vibration of the distribution rod by combining its different cross sections [11], using a fan nozzle with a variable spray angle together with pulse-width modulation technology [12], changes in the merging of flows of adjacent nozzles, depending on the magnitude of the boom oscillations [13], etc. Means of small-scale mechanization have recently taken a stable place in the implementation of modern technologies. Therefore, issues of theoretical justification for the conditions of their functioning, design parameters and technological operating modes remain relevant and require reflection in new engineering projects.

The results of our earlier studies [14, 15] allow us to assert that a universal solution to the problem of compensating for deviations of the boom of a small-sized sprayer in the transverse-vertical plane can be the use of sprayers that adaptively respond to the position they occupy in relation to the surface being treated. In this case, there is no need to equip the sprayer with complex and massive lever copying devices, and maintaining the overlap pattern of the processed strips is achieved by changing the geometry of the spray torches of individual nozzles [16-19].

а б

Figure 1: A prototype of a single-support boom motor sprayer (a) and a device for measuring the magnitude of horizontal deviations of the field boom (b)

Based on the existing premises, the purpose and objectives of the study are formulated.

Purpose of the study: optimization of the spray pattern angles of the adaptive sprayer of a wheelbarrow-type field boom sprayer.

Research objectives:

1. Assessment of the amplitude of operating vibrations of the boom of a single-support sprayer in the transverse-vertical plane;
2. Analysis of the influence of the lateral deflection of the sprayer on the working width of the field sprayer;
3. Determination of the dependence of the values of the required spray pattern angle of the adaptive sprayer on the angle of inclination of the single-support sprayer in the transverse-vertical plane;
4. Determination of the limits for changing the root spray angles of the adaptive sprayer of a single-support boom sprayer of a wheelbarrow type;
5. Optimization of the current frontal spray angles of the distribution system nozzles, based on their functional relationships with influencing factors and the development of a nomogram for determining the optimal values of the frontal angles of the spray pattern of sprayer nozzles in production conditions.

II. MATERIALS AND METHODS

When solving the first problem, a prototype of a single-support boom motor sprayer (Fig. 1, a), which we had previously developed [20], was used as the object of study. The field experiment was carried out at the experimental sites of the Oryol State Agrarian University. Repetition of experiments - 3 times; measurement error - no more than 5%. Data recording on the deviation of the sprayer from the vertical axis was carried out using a specially designed inclinometer (Fig. 1, b). The latter consists of a measuring scale rigidly mounted on the sprayer frame and a hinged indicator arrow equipped with a plumb line [21]. The current readings of the protractor were recorded using a self-powered car recorder. Subsequent mathematical processing of the decrypted experimental data was performed by a spreadsheet processor in Microsoft Excel.

The theoretical substantiation of the influence of vibrations of the sprayer boom on the distribution parameters of the working fluid was carried out on the basis of generally accepted engineering calculation methods. The study of the obtained analytical dependencies was carried out in the environment of the mathematical calculation system Mathcad 14.0 (Russian version). The work used the method of nomogramming functions of several variables.

III. RESULTS AND DISCUSSION

The results of an experiment to evaluate the operating vibrations of a single-support sprayer with a right-handed boom in the transverse-vertical plane established the following. The maximum deviation angles of the sprayer from the vertical can range from +17° (left-side slope, in the direction of travel) to -30° (right-side slope, in the direction of travel). In this case, the arithmetic mean value of the transverse vibration angle is -3(±0.4)°. It is important to note that peak deviation values are quite rare and depend mainly on the operator's training and the speed of movement of the sprayer. The average values of the maximum inclination angles lie in the range from +11° to -18°. It is these values that will be decisive when choosing the operating modes of adaptive sprayers, which allow you to control the geometry of the spray plume.

In addition, analysis of the transverse vibration diagram (Fig. 2) indicates the clear presence of right-sided asymmetry. Obviously, the latter is caused by a slight shift in the center of gravity of the prototype sprayer, due to the imbalance of the moment of force from the weight of the one-sided field rod. One of the options for eliminating this design flaw could be to equip the sprayer with a tracking balancing mechanism [22]. Such a device is capable of adjusting the balancing of the sprayer by the spatial position of the tank, depending on the amount of working fluid in it.

In order to determine the theoretical width of the spray torch with one sprayer, we describe the geometric parameters of the sprayer with the diagram shown in Fig. 3.

Allowing for the possibility of deflection of the sprayer only in the plane of the drawing, the frame OA, height h, has transverse movements at an angle α relative to the hinge O. A horizontal rod AB of length l is installed perpendicular to the frame OA and is rigidly connected to it.

The spray torch is an isosceles triangle CBD with a constant angle β, at vertex B. The bisector VM drawn to the base of the triangle SVD is strictly perpendicular to the horizontal rod AB and, at the same time, is the height p of the triangle SVD. Here, the base CD=b0 is the line of contact of the spray torch with the surface being treated.

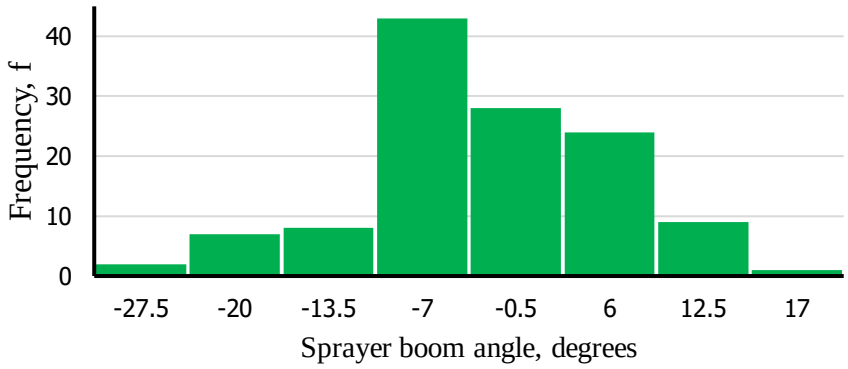

Figure 2: Histogram of the distribution of vibration values of the boom of a single-support sprayer in the transverse-vertical plane

As can be seen from Fig. 3, when the angle α of the position of the sprayer changes, a corresponding deviation of the SVD spray torch occurs from its original position. At the same time, the length of the contact line of the spray torch with the surface being treated will also change (CiDi=bi).

Let us analyze the influence of the lateral deviations of a single-support motorized sprayer on the working width of a field sprayer located at a distance l from the symmetry axis of the sprayer passing through its support point O.

From the cosine theorem it is known that the square of any side of a triangle is equal to the sum of the squares of its two other sides minus twice the product of these sides and the cosine of the angle between them. From here:

$$b_i = \sqrt{d^2 + c^2 - 2dc \times cos\beta} \tag{1}$$

where bi, d, c are the sides of the scalene triangle CiBiDi, formed by the spray torch and the surface being treated, when the sprayer frame is deflected at a certain angle α.

To determine the sides d and c of the triangle CiBiDi, we divide it into two rectangular ones CiBiMi and MiDiDi, with leg pi = BiMi.

Using the formulas for the relationship between the sides and angles of the right triangle CiBiMi, we write:

$$d = \frac{p_i}{sin\gamma}, \tag{2}$$

where γ is the angle at the base of the triangle.

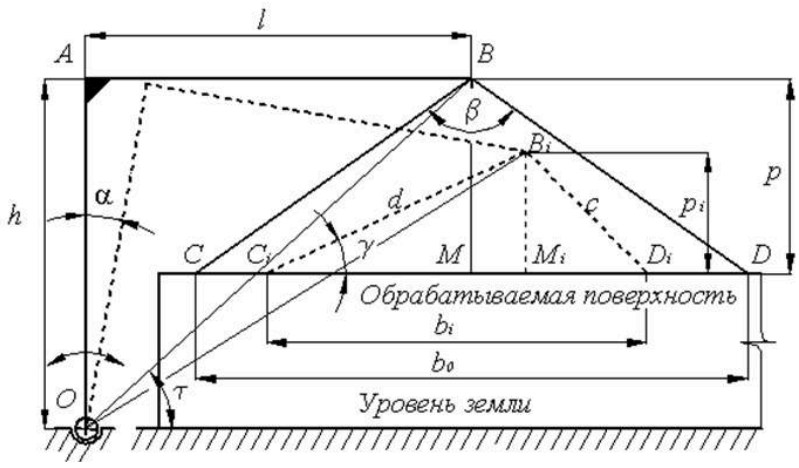

Figure 3: Scheme for calculating the change in the width of the spray torch of the sprayer nozzles when the boom oscillates in the transverse-vertical plane

The CiDiDi triangle is formed by the displacement of the CBD triangle due to the rotation of the frame by an angle α. Then, angle γ can be defined as the difference between angles α and one of the angles of the equilateral triangle CBD, at its base. From here:

$$\gamma = 90° - \frac{\beta}{2} - \alpha \tag{3}$$

By connecting points B and Bi with the support point O, we define pi as the difference in the heights of the triangles SVD and CiBiDi relative to the support surface.

It is obvious that the angle τ between the straight line OBi and the supporting surface is determined by the function.

$$tg\tau = \frac{h}{l}, \tag{4}$$

therefore, if

$$OB = OB_i = \sqrt{h^2 + l^2}, \tag{5}$$

That

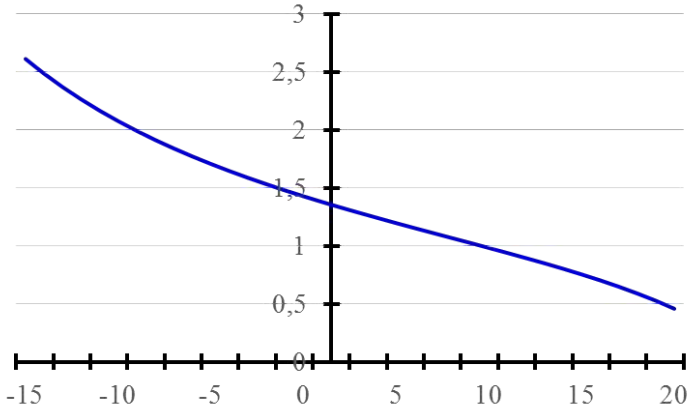

Figure 4: Dependence of the width of the processing strip with one sprayer on the deflection of the sprayer in the transverse-vertical plane

$$p_i = p - \left(h - \sqrt{h^2 + l^2} \times sin(\tau - \alpha)\right), \tag{6}$$

from where, taking into account (4)

$$d = \frac{p - \left(\left(h - \sqrt{h^2+l^2}\right) \times sin\left(arctg\frac{h}{l} - \alpha\right)\right)}{sin\left(90° - \frac{\beta}{2} - \alpha\right)} \tag{7}$$

To calculate the side c of the triangle CiBiDi, we will use the already known angle at the vertex Bi and height pi:

$$c = \frac{p_i}{cos\left(\frac{\beta}{2} - \alpha\right)} = \frac{p - \left(\left(h - \sqrt{h^2+l^2}\right) \times sin\left(arctg\frac{h}{l} - \alpha\right)\right)}{cos\left(\frac{\beta}{2} - \alpha\right)} \tag{8}$$

After some transformations, equality (1) for calculating the spray width, taking into account the geometric parameters of a single-support sprayer, as well as the angle of transverse inclination of the frame, will finally be written in the form:

$$b_i = \sqrt{\left(p - \left(h - \sqrt{h^2 + l^2}\right) \times sin\left(arctg\frac{h}{l} - \alpha\right)\right)\left(\left[\frac{1}{sin\left(90° - \frac{\beta}{2} - \alpha\right)}\right]^2 + \left[\frac{1}{cos\left(\frac{\beta}{2} - \alpha\right)}\right]^2 - -2\left(\frac{1}{sin\left(90° - \frac{\beta}{2} - \alpha\right)}\right)\left(\frac{1}{cos\left(\frac{\beta}{2} - \alpha\right)}\right) \times cos\beta\right)} \quad (9)$$

The graphical representation of formula (9) is illustrated in Fig. 4 for values p=0.5m; h=0.9m; l=1m; β=110°. As can be seen, with a horizontal position of the sprayer boom, the width b of the distribution strip of the working fluid with one sprayer is about 1.43 m. However, even when the sprayer is deviated by an angle α from -15° to +20° in the transverse-vertical plane, the width b varies from 2.60m to 0.46m, i.e. more than 1.8...3.1 times.

When setting the task of determining the necessary limits for changing the root spray angle β of the sprayer, we proceed from the premise of maintaining a constant working width bi. Due to the insignificance of the transverse deviations of the horizontal projection of the sprayer when the rod is tilted in the transverse-vertical plane, we do not take these deviations into account in the calculations. In addition, we accept the assumption that the vertical position of the sprayer axis is stable (provided by a vertical stabilization device).

In accordance with the theorem of sines we have (see Fig. 3):

$$\frac{BD}{sin90°} = \frac{b_0}{sin\beta}, \quad (10)$$

Where

$$\beta = arcsin\frac{b_0}{2BD} \quad (11)$$

From the Pythagorean theorem, the square of half the length of the hypotenuse BD is equal to the sum of the squares of the legs p and b0/2, or:

$$BD = \sqrt{p^2 + \left(\frac{b_0}{2}\right)^2} \quad (12)$$

Substituting (12) into (11) we get:

$$\beta = arcsin\frac{b_0}{2\left(\sqrt{p^2 + \left(\frac{b_0}{2}\right)^2}\right)} \quad (13)$$

From the diagram in Fig. 3 it is obvious that the current value of p will change in accordance with dependence (6). Taking into account that

$$\tau = arctg\frac{h}{l}, \quad (14)$$

the final record of the influence of the angle α of the position of a single-support sprayer on the required spray angle β, taking into account the distance l of the sprayer's projection, relative to the vertical axis passing through the sprayer's support point, can be represented in the form:

$$\beta = 2arcsin\frac{b_0}{2\left(\sqrt{\left[p - \left(\left(h - \sqrt{h^2 + l^2}\right) \times sin\left(arctg\frac{h}{l} - \alpha\right)\right)\right]^2 + \left(\frac{b_0}{2}\right)^2}\right)} \quad (15)$$

For the previously given numerical values included in formula (15) and the given value b0=1.43m, a graphical interpretation of the dependence β=f(α) is shown in Fig. 5. It is clearly seen that with a strictly vertical position of the sprayer (α=0°; horizontal position of the field boom), the root spray

angle β=110° allows for a treatment strip with an estimated width of 1.43 m. When the sprayer is tilted to the left, to the value α=- 15°, the distance from the spray nozzle to the surface being treated increases and, consequently, the width of the processing strip (see Fig. 3). As follows from the graph in Fig. 5, in

order to maintain the same working width b0, the required spray angle βi should be equal to 89°. Accordingly, the angle of inclination of the sprayer α=20° determines the opening of the spray angle to β=164°.

Using formula (15) makes it possible to calculate the required limits for changing the spray angle of one nozzle, with established average values of rod vibrations in the transverse-vertical plane. Thus, based on previously obtained experimental values of the rod oscillation angles and reducing their maximum operating values to average values, we obtain: α = +11°...-18°. For the given limits of vibration of the rod in the transverse-vertical plane, changes in the spray angle by the adaptive sprayer should be β=86°...135°, at a distance l=1 m.

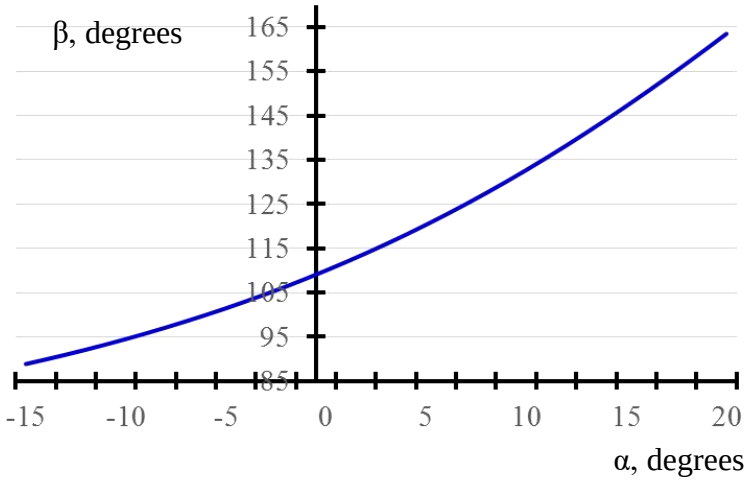

Figure 5: Dependence of the values of the required spray angle of the adaptive sprayer on the angle of inclination of the single-support sprayer in the transverse-vertical plane

For a deflector sprayer, the spray pattern angle in the form of a flat cone is formed by the cone angle of the restrictive collars at the periphery of the deflector [17]. Consequently, the angles of their taper formed by the outer sides of each reflective deflector will be determined by the calculated spray angles of a given adaptive atomizer deflector. Taking into account the distance of each sprayer from the symmetry plane of the sprayer passing through the support point, the numerical values of these angles are found using formula (15) and are summarized in table.

Table. Values of root angles β of spray for deflectors of adaptive sprayers, with values of α=-18°...+11°

Distance of the adaptive sprayer installation point from the sprayer support axis, m	Limits of change in spray pattern angles, degrees.		
	min	nom	max
0,5	99	110	123
1,0	86	110	135
1,5	76	110	149
2,0	67	110	164
2,5	60	110	179

Graphic interpretation of expressions (9; 15) was used to construct an optimization nomogram (Figure 6). The nomogram makes it possible to obtain the values of the current frontal spray angles that satisfy the permissible width of the processing strip, at any position of the sprayer boom.

Agrotechnical requirements for the spraying process allow uneven distribution (variation coefficient) of the working fluid - no more than 25% for low-volume and conventional spraying, and no more than 40% for ultra-low-volume spraying [23]. Then, taking into account the permissible unevenness of the application of the liquid preparation of 25%, the deviation limits of the width of the processing strip with one nozzle will be from 1.07 to 1.78 m, with a frontal spray angle of 110°. As can be seen from the upper sector of the nomogram, the liquid distribution parameters obtained by spraying nozzles located at a distance of l=2.5 m from the rolling center (at rod position angles ±2°) fit into the indicated interval; l=2.0 m (±3°); l=1.5 m (±4°); l=1.0 m (-6°...+7°). The spray pattern of the nozzle closest to the center of the rod's swing provides acceptable parameters for liquid distribution at rod slopes from -11° to +13°. The upper sector of the nomogram demonstrates the dependence of the width of the spray zone on the angle of inclination to the horizon of the distribution system (rod), with a corresponding distance of the nozzle from the rolling center. The lower sector shows a graphical formalization of the function of the influence of the angle of inclination of the rod on the required frontal spray angle, which ensures the optimal processing width with the corresponding nozzle.

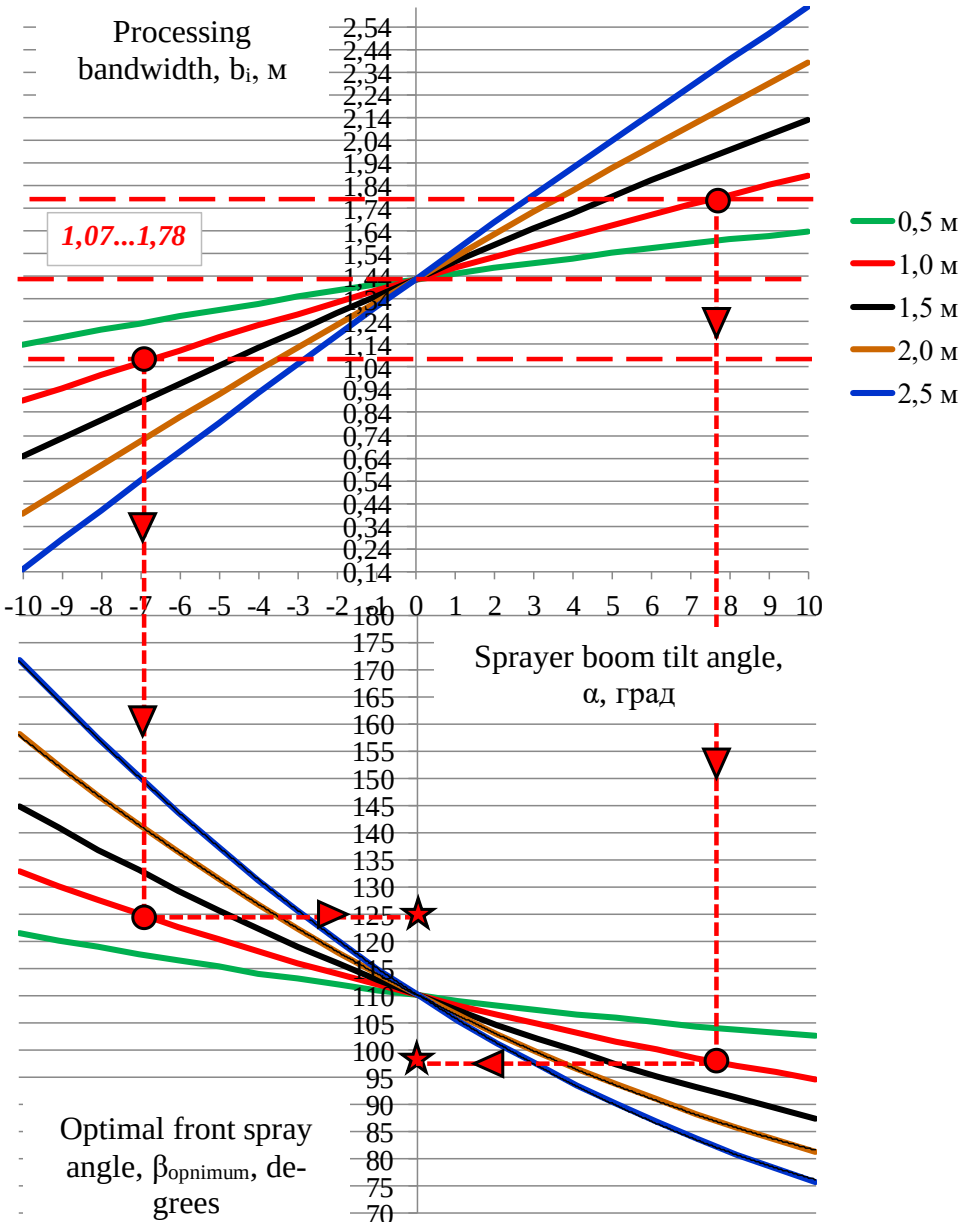

Fig. 6. Nomogram for determining the optimal current values of the front angles of the spray pattern of sprayer nozzles during vertical vibrations of the distribution system (for a spray angle of 110°)

IV. CONCLUSION

These studies have established that the maximum limits of lateral vibrations of a barrow-type boom single-support sprayer range from +17° (left-hand slope, in the direction of travel) to -30° (right-side slope, in the direction of travel). However, the average amplitude of operating vibrations is in the region =+11°...-18°. A formula has been obtained for calculating the spray width of one sprayer, taking into account the geometric parameters of a single-support sprayer, as well as its angle of inclination in the transverse-vertical plane. It has been established that one of the possible solutions to the problem of compensating for the quality of distribution of the working fluid during transverse vibrations of the sprayer boom can be the use of sprayers with a spray geometry that adaptively responds to the position occupied by the sprayer in relation to the surface being treated. An analytical relationship has been obtained that makes it possible to calculate the required limits of the root spray angle of the adaptive sprayer, taking into account the distance l of the sprayer's outreach, relative to the vertical axis passing through the sprayer's support point. The values of the root spray angles were found for the deflectors of

adaptive sprayers, for the limits of sprayer oscillations from -18° to +11° in the transverse-vertical plane. The proposed nomogram makes it possible to graphically obtain the optimal values of the frontal spray angles of spray nozzles located at different distances at any position of the sprayer distribution rod. The technique is applicable in the development of software for the control complex of a sprayer, equipped with an adaptive system for distributing working fluid in changing conditions. In addition, with proper refinement, the described methodological approaches can be used to quickly create the most preferred schemes for placing various sprayers on the boom and installing the latter in production conditions.

BIBLIOGRAPHY

1. Kireev I.M. Raspredelenie kapel'noj zhidkosti mezhdu raspylitelyami dlya tekhnologii opryskivaniya rastenij // Agro Forum. 2019. №4. S. 18-20.
2. Kovalenkov V.G. Rezistentnost' rapsovogo cvetoeda kak pokazatel' perestroj-ki geneticheskoj struktury populyacij vrednyh vidov pod vliyaniem insekticidov // Agro-himiya. 2018. №5. S. 54–62
3. Suhoruchenko G.I. Metody ocenki toksichnosti pesticidov dlya chlenistonogih, primenyaemyh v bor'be s vreditelyami kul'tur zashchishchennogo grunta // Entomologicheskoe obozrenie. 2018. № 4. S. 649-657.
4. Pobedinskaya M.A. Ustojchivost' vozbuditelej al'ternarioza kartofelya i to-mata k fungicidam // Mikologiya i fitopatologiya. 2012. T.46. V.6. S. 401-408.
5. Popov YU.V. Zashchita zernovyh kul'tur ot boleznej dolzhna byt' obosnovannoj // Zashchita i karantin rastenij. 2009. № 7. S. 42-45.
6. Lysov A.K., Kornilov T.V. Sovershenstvovanie tekhnologij primeneniya sredstv zashchity rastenij metodom opryskivaniya // Vestnik zashchity rastenij. 2017. №2(92). S. 50-53.
7. Nikitin N.V. Protivosnosnaya tekhnologiya vneseniya gerbicidov novogo poko-leniya // Vestnik zashchity rastenij. 2008. №3. S. 47-55.
8. Markevich A.E., Nemirovec YU.N. Osnovy effektivnogo primeneniya pestici-dov. Spravochnik v voprosah i otvetah po mekhanizacii i kontrolyu kachestva primeneniya pesticidov v sel'skom hozyajstve. Gorki: uchrezhdenie obrazovaniya «Mogilevskij gosudar-stvennyj uchebnyj centr podgotovki, povysheniya kvalifikacii, perepodgotovki kadrov, konsul'tirovaniya i agrarnoj reformy», 2004. 60 s.
9. Kuznecov V.V., Kuznecov A.V. Podveska shirokozahvatnoj shtangi polevogo oprys-kivatelya // Konstruirovanie, ispol'zovanie i nadezhnost' mashin sel'skohozyajstvennogo naznacheniya. 2012. № 1 (11). S. 5-9.
10. Kruk I.S., Karpovich S.K., Markevich A.E., Bolvanovich V.V., CHeshun P.V. Proekti-rovanie nesushchih konstrukcij, skhem podvesok i sistem stabilizacii shtang polevyh opryskivatelej. Rekomendacii. Minsk: BGATU, 2018. 172 s.
11. Junchao Yan. Analysis of Dynamic Behavior of Spray Boom under Step Excitation // Appl. Sci. 2021. 11. 10129.
12. Hamid Reza Ghasemzadeh, Daniel D. Humburg. Using variable spray angle fan nozzle on long spray booms // AgricEngInt. 2016. Vol. 18. No.1. RR. 82-90.
13. Borisenko I.B. Teoreticheskoe obosnovanie ravnomernosti naneseniya rabochego rastvora na ob"ekt vozdejstviya pri obrabotke propashnyh kul'tur sposobom polosovogo opryskivaniya // Izvestiya Nizhnevolzhskogo agrouniversitetskogo kompleksa: Nauka i vys-shee professional'noe obrazovanie. 2021. №4 (64). S. 296-305.
14. Dembovskij I.A., Rodimcev S.A. Opredelenie velichiny kolebanij shtangi ta-chechnogo opryskivatelya v poperechno-vertikal'noj ploskosti // Sostoyanie i perspektivy razvitiya agropromyshlennogo kompleksa. YUbilejnyj sbornik nauchnyh trudov XV Mezhdu-narodnoj nauchno-prakticheskoj konferencii. Rostov-na-Donu, 2022. S. 169-173.

15. Rodimcev S.A., Dembovskij I.A., Panin E.N. Razrabotka i obosnovanie paramet-rov mobil'nogo opryskivatelya dlya sadovo-parkovogo i landshaftnogo stroitel'stva // Mir transporta i tekhnologicheskih mashin. 2023. № 2 (81). S. 26-34.
16. CHencov V.V., Frumovich V.L.. Lagutin A.V., Sergeev YA.YU. SHtangovyj opryskiva-tel': avtorskoe svidetel'stvo № 1308307 SSSR; opubl. 07.05.1987, Byul. № 17.
17. Bilyk A.I., Maslo I.P., Sudak P.G. Raspylitel': avtorskoe svidetel'stvo № 650589 SSSR; opubl. 05.03.1979, Byul. № 9.
18. Dodson M. Ploskostrujnye forsunki dlya tekuchej sredy s reguliruemym razme-rom kapel', vklyuchayushchie postoyannyj ili peremennyj ugol raspyleniya: patent na izobre-tenie № 2515290 Rossijskaya Federaciya; opubl. 10.05.2014, Byul. № 13.
19. Gul'ko A.I. Kombinirovannaya raspylitel'naya golovka: patent na izobretenie № 2324348 Rossijskaya Federaciya; opubl. 20.05.2008, Byul. № 14.
20. YAndutova K.I., Rodimcev S.A. Optimizaciya uslovij raboty truda operatora ma-logabaritnogo shtangovogo opryskivatelya selekcionnogo naznacheniya // Ohrana truda 2011. Aktual'nye problemy i puti ih resheniya. Materialy Vserossijskoj nauchno-prakticheskoj konferencii. Orel, 2011. S. 128-138.
21. Rodimcev S.A., SHapenkova A.A. Ocenka i kontrol' polozheniya tachechnogo oprys-kivatelya v poperechno-vertikal'noj ploskosti //Agrotekhnika i energoobespechenie. 2015. № 3 (7). S. 233-238.
22. Rodimcev S.A., SHapenkova A.A., Timohin O.V., Patrin E.I. Obosnovanie ergo-nomicheskih harakteristik malogabaritnogo shtangovogo opryskivatelya tachechnogo tipa // Bezopasnost' zhiznedeyatel'nosti. 2014. № 12 (168). S. 17-23.
23. Zinchenko V.A. Agroekotoksikologicheskie osnovy primeneniya pesticidov. M., Izd-vo MSKHA, 2000. 180 s.

Tree Richness and Carbon Storage in Developing a Tropical Evergreen Forest after Slash-and-Burn in the Lacandon Region, Mexico

Mariana Zamudio-Guevara, Alexa Maillard-Méndez, Sandra Monserrat, Barragán-Maravilla, Gabriel Alejandro Hernández-Vallecillo y & Efraín R. Ángeles-Cervantes

Universidad Nacional Autónoma

ABSTRACT

The objectives were to quantify tree richness and estimate carbon stored during the recovery and development of tropical evergreen forest (BTP) affected by the traditional slash and burn (RTQ) system practiced by the Lacandon-Mayan ethnic group. This research was carried out in the Lacandona region of Mexico. The aim was to determine whether the RTQ system maintains tree species richness and whether stored C is recovered.

Methods. Dismantled areas were located with the RTQ system from 5, 10, and 20 years ago (BTR5, BTR10, and BTR20, respectively). To obtain tree richness, botanical collections of all tree species present in 0.1 ha plots of BTR5, BTR10, and BTR25, as well as two BTP plots (BTP1 and BTP2, respectively) were carried out. In each plot, height, diameter at breast height, and number of individuals of each tree species were recorded. To estimate the stored C, the equation proposed by Chave et al., (2005) was used, which relates the DAP and the density of the wood of each species.

Keywords: regeneration rainforest, environmental services, species richness, biodiversity, and tropical rainforest.

Classification: LCC Code: GE196

Language: English

Great Britain Journals Press

LJP Copyright ID: 925694
Print ISSN: 2631-8490
Online ISSN: 2631-8504

London Journal of Research in Science: Natural & Formal

Volume 24 | Issue 9 | Compilation 1.0

Tree Richness and Carbon Storage in Developing a Tropical Evergreen Forest after Slash-and-Burn in the Lacandon Region, Mexico

Mariana Zamudio-Guevara[α], Alexa Maillard-Méndez[σ], Sandra Monserrat[ρ], Barragán-Maravilla[ω], Gabriel Alejandro Hernández-Vallecillo y[§] & Efraín R. Ángeles-Cervantes[χ]

ABSTRACT

The objectives were to quantify tree richness and estimate carbon stored during the recovery and development of tropical evergreen forest (BTP) affected by the traditional slash and burn (RTQ) system practiced by the Lacandon-Mayan ethnic group. This research was carried out in the Lacandona region of Mexico. The aim was to determine whether the RTQ system maintains tree species richness and whether stored C is recovered.

Methods. Dismantled areas were located with the RTQ system from 5, 10, and 20 years ago (BTR5, BTR10, and BTR20, respectively). To obtain tree richness, botanical collections of all tree species present in 0.1 ha plots of BTR5, BTR10, and BTR25, as well as two BTP plots (BTP1 and BTP2, respectively) were carried out. In each plot, height, diameter at breast height, and number of individuals of each tree species were recorded. To estimate the stored C, the equation proposed by Chave et al., (2005) was used, which relates the DAP and the density of the wood of each species.

Results. A tree richness of 71 species was obtained in 0.1 ha. In BTP1, 47 species were recorded and in BTP2, 38 species were recorded. The number of species increased (20, 17, and 39 species) according to the recovery age of the BTR (5, 10, and 20 years respectively), so the rest period is adequate for the recovery of tree richness. The accumulation of C in the trees showed that the RTQ system must modify the recovery or rotation age since the carbon stored at 5, 10, and 20 years was 29, 35, and 74 Mg C ha^{-1} respectively, while in BTP1 and BTP2 they were 478 and 512 Mg C ha^{-1} respectively. The polynomial model obtained indicates rest periods between 40 and 50 years to recover the C stored in the mature BTP.

Keywords: regeneration rainforest, environmental services, species richness, biodiversity, and tropical rainforest.

Author α σ ρ ω § χ: Laboratorio de Ecología de Bosques e Hidrología. Facultad de Estudios Superiores Zaragoza. Universidad Nacional Autónoma de México. Dirección. Batalla 5 de mayo s/n esquina fuerte de Loreto, Colonia ejército de Oriente, Iztapalapa, CDMX, México. C.P. 09230.

I. INTRODUCTION

The Evergreen Tropical Forest (BTP) is the dominant vegetation in the Lacandona region of Mexico and one of the ecosystems with the greatest floristic diversity.

In tropical areas, food production is through the slash-and-burn (RTQ) system. RTQ is considered a use sustainable system of BTP, which is still practiced by the Maya-Lacandon indigenous people (Ochoa-Gaona *et al,*. 2007). And the rest or recovery periods are 15 to 20 years, which also allows the

recovery of soil fertility (Diemont *et al.,* 2006). However, it has also been pointed out that it is necessary to reduce the burning of agricultural waste because they are a source of Dioxins (*Comisión para la Cooperación Ambiental*, 2014).

Currently, the BTP rest or recovery times have been altered, and have even been reduced to seven years, so the question is: Does the tree wealth and the amount of carbon stored in a BTP recover in 20 years or less? To respond, the objectives of this work were: 1) Determine the variation and recovery of tree richness of the BTP, affected by the RTQ system in different years; and 2) To estimate how many years are required to recover the amount of C stored in a BTP after the RTQ system.

Answering these questions will help us develop better strategies for using and conserving BTP where this traditional farming system is practiced.

II. STUDY AREA DESCRIPTION

Location. This project was realized in the "Tres Lagunas" ecotourism center located in the town of San Javier, Municipality of Ocosingo, Chiapas, Mexico, which is located in the Lacandona region in the Montes Azules Biosphere Reserve, at the coordinates 16° 50´ 21.3´´ N, y 91° 8´ 36.6´´ W. Chiapas is located in the physiographic province of the highlands of Chiapas and Guatemala itself, which is divided into five subprovinces: Sierras Plegadas del Norte, Meseta de Chiapas, Central Depression, Coastal Plain of Chiapas and Sierra de Chiapas (Instituto Nacional de Ecología INE, 2000).

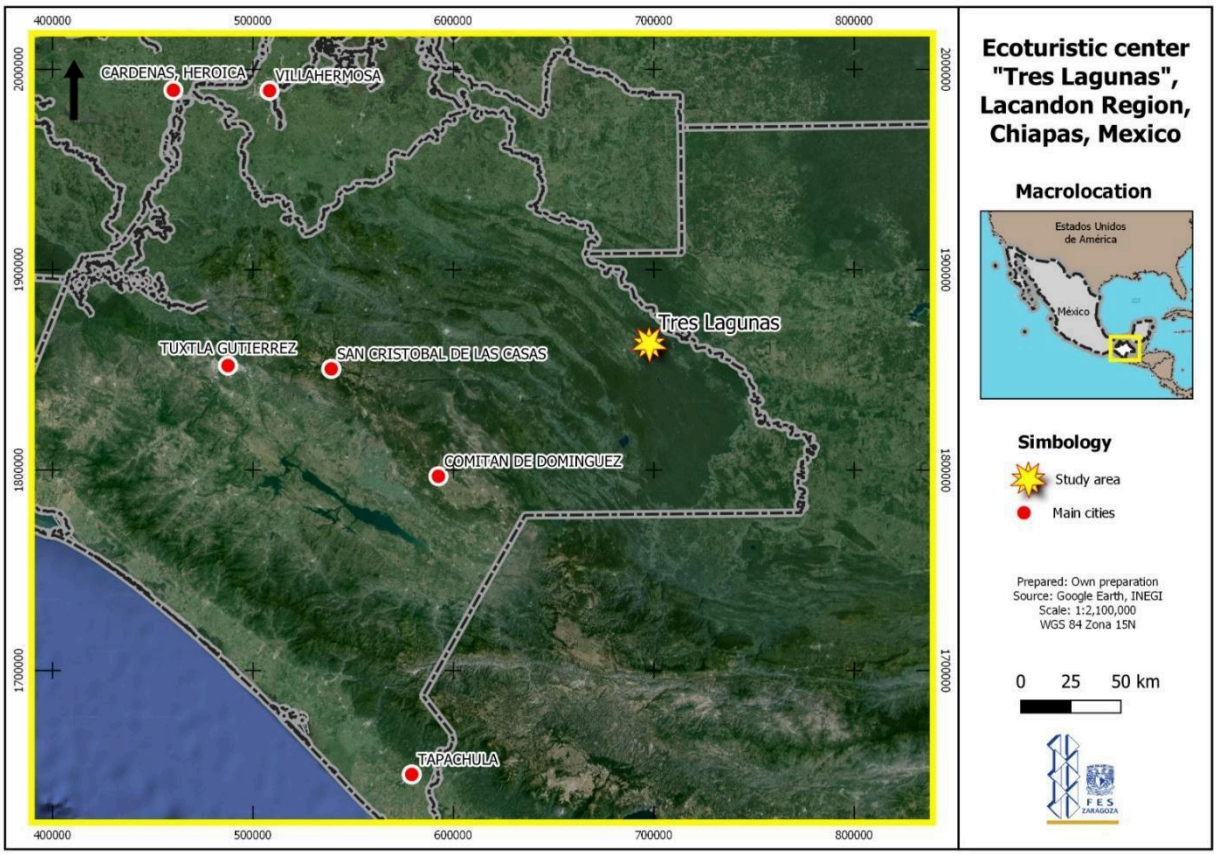

Figure 1. Location of the Ecotourism center "Tres Lagunas", in the Lacandona Region, Chiapas, Mexico.

Clime: The average annual temperature varies from 24 to 26 °C. Precipitation in the Lacandona region varies from 1,500 to 3,500 mm per year and is affected by the rugged relief of the mountains of Chiapas (INE, 2000).

Geology: It presents limestone rocks, with breaks, fractures, faults, and joints being, the elements that control the position of the karst forms. (INE, 2000).

Edaphology: Rendzines predominate in areas whose main geological substrates are limestone and sandstone. Its soils are shallow (3 cm thick), predominantly relatively acidic Lithosols (Leptsosols), with little organic matter, low fertility, and silt-clay texture (INE, 2000).

Hydrology: The hydrological region belongs to the Grijalva-Usumacinta system, which is one of the largest in the country (1550,200 ha), according to INE (2000).

Vegetation: This Evergreen Tropical Forest is characterized by having a closed and evergreen canopy where the trees in the upper layer have an average height of 30 m, although they can reach between 65 and 75 m. In this type of vegetation, woody climbing plants are abundant. The dominant tree species are canshán (*Terminalia amazonia*), guapaque (*Dialium guianense*), ramón (*Brosimum alicastrum*), chicozapote (*Manilkara zapota*), barí (*Calophyllum brasilense*), caoba (*Swietenia macrophylla*), palo mulato (*Bursera simaruba*), tinco (*Vatairea lundellii*) y bayo (*Aspidosperma cruentum*) (INE, 2000).

III. MATERIALS AND METHODS

Site selection: Sites locally called "acahuales" were selected, which are Tropical Forests in Recovery (BTR) of 5, 10, and 20 years (BTR20). The owner of the land, Mr. Pablo Chankin proportionated some data on the age and location of the BTR. Likewise, two areas of conserved and mature tropical forest (BTP) were located to have reference sites, which are characterized by the presence of trees with diameters at chest height between 30 and 60 cm, with well-developed buttresses and wide, which according to Pennington and Sarukhán (2005) correspond to mature phases of the development of a forest. The BTR and BTP are relatively close and on the edge of a conserved forest, under the same management system, soil group, and geology, based on the digital map provided by GEODATA (2008).

Tree species sample collection: Circular plots with an area of 0.1 ha were delimited which were divided into eight subplots. The five plots (0.5ha) correspond to two evergreen tropical forest sites (BTP1 and BTP2) and three plots of acahuales or tropical forests in recovery, 5, 10, and 20 years after being affected by the RTQ system (BTR5, BTR10, and BTR20). The location of each plot can be seen in Figure 2. In each subplot, the common name, basal area, and density of the tree species were recorded. Diameter at breast height (DBH) and coverage (in centimeters) were measured for each individual.

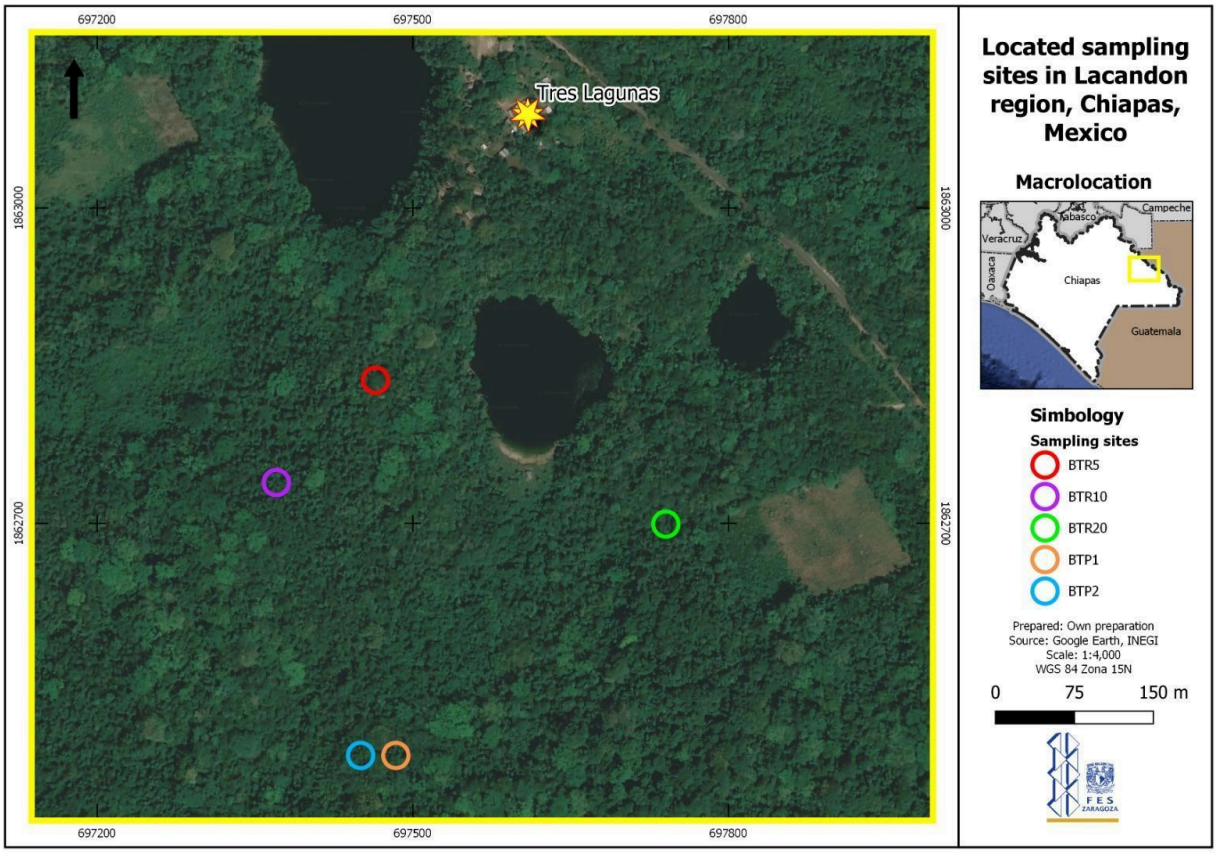

Figure 2: Location of sampling sites.

Subsequently, with the recorded data, the relative values of the frequency, density, basal area, and ecological importance value index of the species were obtained, by applying the following formulas:

Relative frequency (Fr). It was estimated as the number of subplots in which each species appeared.

$$Fr = \frac{No.\ of\ subplots\ in\ which\ the\ species\ is\ present}{No.\ of\ subplots\ from\ all\ species} \times 100$$

Relative density (RD). The relative density was calculated as follows:

RD= (Absolute density per species/Absolute density of all species) × 100

Where:

Absolute density *DA* = Number of individuals of a species / Area sampled

Relative basal area (AB). It is the basal area of each species divided by the total basal area in the subplot times

The basal area (AB) is given by the formula: AB = π r², where r is the tree radio = ½ DAP (diameter at chest height) of each species.

$$AB = \pi\left(\frac{DAP}{2}\right)^2$$

ABR= (AB of each specie/ AB of all species) x 100.

Importance value (VIR). It is defined as the sum of the values of frequency, density and, relative basal area.

$$VIR = \frac{1}{3}(ABr + Dr + Fr)$$

Likewise, the tree diameter structure was obtained in each BTR, which is obtained from a graph of the number of individuals per diameter class.

Diversity index (DI): The Chao2 index was used. This estimator is based on the presence-absence of a species in a given sample, that is, only if the species is present and how many times that species is present in the set of subplots. According to Escalante-Espinoza (2003), it is calculated with the following formula:

$$Sest = Sobs + \left(\frac{L^2}{M \times 2}\right)$$

where:

Sest= estimated number of species
Sobs= number of species observed
L= number of species occurring in a subplot (single species), and
M= number of species occurring in exactly two subplots (double or duplicate species).

The Chao2 index is an estimator of species diversity and tells us how diversity changes in each BTR and at what point it will resemble the BTP.

Similarity analysis. This analysis is carried out to evaluate the similarity of the tree composition of each BTR with the BTP. A cluster or hierarchical grouping analysis was used to obtain a dendrogram: Using the Stata V.8 package, the similarity index (SI) was applied as follows:

$$ID = \frac{(a+b)}{a+b+c+d}$$

where:
a = number of species present at all sampling sites: A, B, C, D.
b= number of species present at one site A but absent at another B, C, D.
c = number of species present at site B but absent at A, C, D.
d = number of species that are not present in the two samples that are compared.

Determination of species and comparison of specimens. With the help of local parataxonomists, the species with the common name were determined, subsequently, specimens were collected for identification, based on Pennington and Sarukhán (2005) and they were collated in the INIF Herbarium (National Forest Herbarium) Mexico.

Carbon sequestration estimate $(ABD)_{est}$. One of the approaches to quantifying the carbon stored in biomass consists of converting the data inventoried in the field through regression models. The equation developed by Chave *et al.* (2005) relates the density of the wood and the diameter at breast height to calculate the total aerial biomass, with the following formula:

$$(ABG)_{est} = \rho * \exp(-1.499 + 2.148 * \ln(D) + 0.207 (\ln(D))^2 - 0.0281 (\ln(D))^3)$$

where:

ABG = Total aerial biomass.
ρ = Wood density.
D = diameter at breast height.

The value obtained is multiplied by the percentage of carbon contained in the trees, which is 47% (according to Kirby and Potvin, 2007), with which the amount of carbon stored in a tree.

The value obtained from each tree is multiplied by the number of plants per tree species. You do the same for each species and add up the total C stored at each sampling point and multiply it by 10 to get the amount of carbon per hectare of the BTR and BTP was obtained.

IV. RESULTS

A total of 1,662 stems corresponding to 71 species belonging to 33 botanical families were recorded.

Estructura diamétrica: Diametric structure. BTP1 has trees with DBH less than 0.01 m and up to 1.23 and 1.71 m, the latter corresponding to *Terminalia amazonia*. Trees with DBH less than 0.01 m, 1.03 m, and up to 1.60 m, corresponding to *Manikara zapota* and *Dialium guanine*, were also recorded in Tropical Evergreen Forest 2 (BTP2).

In the 5 and 10-year BTRs, diameter categories of 0.01 to 0.3 m are presented. In BTR20 there are trees with DAP less than 0.01 m and up to 0.6 m (of the species, *Crysophillum mexicanum*). In all cases, the predominant diameter category is 0.01 to 0.1 m and a lesser extent 0.11 to 0.2 m. Only in the BTPs do individuals appear with a DBH greater than 0.7. Table 1 shows the number of individuals with diameter intervals at chest height for each site sampling.

Table 1: Variation in the diameter structure and number of trees, in BTR of 5, 10, and 20 years and two evergreen tropical forests (BTP1 and BTP2) in the Lacandon Region, Chiapas.

Site		Diameter at breast height DAP (cm)									
	<1	1-10	11-20	21-30	31-40	41-50	51-60	61-70	71-80	81-90	>100
BTR5	0	120	70	1	0	0	0	0	0	0	0
BTR10	0	263	90	9	0	0	0	0	0	0	0
BTR20	18	333	44	18	3	0	1	0	0	0	0
BTP1	64	328	25	12	4	1	2	0	1	0	2
BTP2	52	226	20	19	9	2	0	0	0	1	2

Note: BTR5=Tropical Forest in Recovery, 5 years; Tropical Forest in Recovery, 10 years; Tropical Forest in Recovery, 20 years; BTP1=Tropical Evergreen Forest 1; BTP2=Tropical Evergreen Forest 2.

Structure and composition of the vegetation: The structure in BTP1 is composed of 47 species. The species *Terminalia amazonia* recorded the highest VIR value of 18.8. The next six species with VIR greater than three were: *Metopium brownei*, *Spondias mombin*, *Astrocaryum mexicanum*, *Quercus sp.*, *Sloanea schippii*, and *Trichospermum mexicanum*.

Table 2: Tree vegetation structure, relative density, relative frequency, and relative Basal Area, and relative importance value in the BTP1, of the Lacandona region, Chiapas.

Species	Dr	Fr	ABr	VIR
	(%)			
Terminalia amazonia (J.F.Gmel.) Exell	1.5	3.8	51.1	18.8
Metopium brownei (Jacq.) Urban.	17.4	6.9	13.6	12.6
Spondias mombin L.	9	6.3	0.2	5
Astrocaryum mexicanum Lieb. Ex Mart.	6.8	6.3	1.9	5
Quercu ssp.	8.6	5.6	0.4	4.9
Sloanea schippii Standl.	7.1	5	2	4.7
Trichospermum mexicanum (DC.) Baill.	1.5	3.8	8	4.4
Chrysophillum mexicanum Brandegee	4.9	4.4	0.7	3.3
Nectandra ambigens (Blake) C.K. Allen	4.2	5	0.6	3.2
Dialium guianense (Aubl.) Sandw.	3.9	3.8	1.7	3
Psidium guajava L.	3.2	3.8	1.8	2.9
Vatairea lundelli (Standl.) Killip ex Record	4.6	3.8	0.2	2.9
Ampelocera hottlei (Standl.) Standl.	3.9	3.8	0.8	2.8
Brosimum alicastrum Sw.	3.4	3.8	0.5	2.6
Enterolobium cyclocarpum (Jacq.) Griseb.	0.2	0.6	6.2	2.4
Bursera simaruba (L.) Sarg.	0.5	1.3	3.8	1.8
Ficus cotinifolia Kunth	0.7	1.9	2.8	1.8
Mortoniodendron guatemalense Standl. & Steyerm	1.7	2.5	0.6	1.6
Swietenia macrophylla King	1.5	3.1	0.1	1.6
Simira salvadorensis (Standl.) Steyerm	1	1.9	1.1	1.3
Stemmadenia donnell-smithii (Rose) Woodson	1	2.5	0.3	1.2
Pithecellobium arboreum (L.) Urban.	1.2	1.9	0	1
Parathesis serrulata Mez.	1	1.9	0.1	1
Calophyllum brasiliense Cambess.	1	1.9	0	1
Astronium graveolens Jacq.	0.7	1.9	0.1	0.9
Hampea nutricia Fryxell	0.7	1.9	0.1	0.9
Alseis yucatanensis Standl.	0.7	1.9	0	0.9
Garcinia intermedia (Pittier) Hammel	0.7	1.9	0	0.9
Bola de perro **ND**	0.7	1.3	0.1	0.7
Pimenta dioica (L.) Merrill	0.5	1.3	0.1	0.6
Geonoma binervia Oerst.	0.5	1.3	0	0.6
Vernonia deppeana Less.	0.5	1.3	0	0.6
Sommera grandis (Bertl.) Standl.	0.5	1.3	0	0.6
Pachira aquatica Aubl.	0.7	0.6	0.2	0.5
Cecropia obtusifolia Bertol.	0.2	0.6	0.4	0.4
Schefflera morototonii (Aubl.) Maguire, Steyerm. &Frodin	0.5	0.6	0.1	0.4
Mata blanca **ND**	0.5	0.6	0.1	0.4
Ceratonia siliqua L.	0.5	0.6	0	0.4
Tabebuia rosea (Bertol.) DC.	0.2	0.6	0.1	0.3
Cassia holwayana Rose.	0.2	0.6	0	0.3
Aspidosperma megalocarpon Müll. Arg.	0.2	0.6	0	0.3
Quararibea funebris (La Llave) Vischer	0.2	0.6	0	0.3
Ficus máxima Mill.	0.2	0.6	0	0.3
Lysiloma acapulcensis (Kunth) Benth.	0.2	0.6	0	0.3

Byrsonima crassifolia (L.) Kunt.	0.2	0.6	0	0.3
Majab **ND**	0.2	0.6	0	0.3
Lysiloma latisiliquum (L.) Benth.	0.2	0.6	0	0.3

Note: Dr: Relative density; Fr= Relative frequency; AB= Relative basal area; VIR= Importance value; ND= undetermined species.

The BTP2 structure is composed of 38 species. The species *Dialium guianense* has a relative density of 3.0%, a relative frequency of 3.7%, and a relative basal area of 34.4%. *D. guianense* also obtained the highest VIR; followed by *Metopium brownei, Quercus sp., Spondias mombin, Terminalia amazonia, Brosimum alicastrum, Manikara zapota, Psidium guajava* and *Swietenia macrophylla* (Table 3).

Table 3: Tree vegetation structure, relative density, relative frequency, and relative Basal Area, and relative importance value in the BTP2, of the Lacandona region, Chiapas.

Species	Dr	Fr	AB	VIR
	(%)			
Dialium guianense (Aubl.) Sandw.	3	3.7	33.4	13.4
Metopium brownei (Jacq.) Urban.	10.8	7.5	19	12.4
Quercus sp.	20.5	9	2.2	10.6
Spondias mombin L.	10.8	7.5	0.1	6.1
Terminalia amazonia (J.F.Gmel.) Exell	9.9	5.2	0.2	5.1
Brosimum alicastrum Sw.	5.4	6	3.3	4.9
Manilkara zapota (L.) Royen	0.3	0.7	13.2	4.8
Psidium guajava L.	6.3	6.7	0.5	4.5
Swietenia macrophylla King	0.9	2.2	10.2	4.4
Vernonia deppeana Less.	4.2	6.7	0.8	3.9
Astrocaryum mexicanum Lieb. Ex Mart.	4.2	5.2	1.2	3.5
Nectandra ambigens (Blake) C.K. Allen	4.5	4.5	1.2	3.4
Simira salvadorensis (Standl.) Steyerm	1.2	1.5	4	2.2
Bursera simaruba (L.) Sarg.	0.9	1.5	4.3	2.2
Mortoniodendron guatemalense Standl. &Steyerm	1.8	3.7	0.1	1.9
Chrysophillum mexicanum Brandegee	2.4	3	0.1	1.8
Hampea nutricia Fryxell	1.2	3	1.1	1.8
Ampelocera hottlei Standl.	1.2	2.2	1.1	1.5
Sloanea schippii Standl.	1.2	2.2	0.1	1.2
Zuelania guidonia (Sw.) Britt. & Millisp.	0.9	1.5	0.6	1
Parathesis serrulata Mez.	1.2	1.5	0	0.9
Schefflera morototonii (Aubl.) Maguire, Steyerm. &Frodin	0.6	1.5	0.6	0.9
Lonchocarpus cruentus Lundell	0.9	1.5	0	0.8
Majasté **ND**	0.6	1.5	0.1	0.7
Calophyllum brasiliense Cambess.	0.6	1.5	0	0.7
Cassia holwayana Rose.	0.3	0.7	1	0.7
Trichospermum mexicanum (DC.) Baill.	0.3	0.7	0.9	0.7
Mata blanca **ND**	0.6	0.7	0.2	0.5
Stemmadenia donnell-smithii (Rose) Woodson	0.3	0.7	0.1	0.4
Astronium graveolens Jacq.	0.3	0.7	0.1	0.4
Sapindus saponaria L.	0.3	0.7	0	0.4
Alseis yucatanensis Standl.	0.3	0.7	0	0.4
Pseudolmedia oxyphyllaria Donn.Sm.	0.3	0.7	0	0.4
Cydista aequnoctilis (L.) Miers.	0.3	0.7	0	0.3

	Pachira aquatica Aubl.	0.3	0.7	0	0.3
	Vatairea lundelli (Standl.) killip ex Record	0.3	0.7	0	0.3
	Garcinia intermedia (Pittier) Hammel	0.3	0.7	0	0.3
	Pimenta dioica (L.) Merrill	0.3	0.7	0	0.3

Note: Dr: Relative density; Fr= Relative frequency; AB= Relative basal area; VIR= Importance value; ND= undetermined species.

The BTR5 structure is composed of 20 species. The species *Trichospermum mexicanum* presents a relative density, frequency, and basal area of 72.3%, 17%, and 66%, respectively, and a VIR of 51.8, followed by *Heliocarpus donnell-smithii, Cecropia obtusifolia*, *Ficus maxima and Sommera grandis* (Table 4).

Table 4: Tree vegetation structure, relative density, relative frequency, and relative Basal Area, and relative importance value in the BTR5, of the Lacandona region, Chiapas.

Species	Dr	Fr	AB	VIR
	(%)			
Trichospermum mexicanum (DC.) Baill.	72.3	17	66	51.8
Heliocarpus donnell-smithii Rose	4.7	12.8	6.8	8.1
Cecropia obtusifolia Bertol.	4.7	10.6	5.9	7.1
Ficus máxima Mill.	4.7	10.6	3	6.1
Sommera grandis (Bertl.) Standl.	3.1	8.5	4.2	5.3
Dialium guianense (Aubl.) Sandw.	1	4.3	2.1	2.5
Quercus sp.	1	4.3	0.9	2.1
Astronium graveolens Jacq.	1	4.3	0.8	2
Piscidia piscipula (L.) Sarg.	1	4.3	0.4	1.9
Alseis yucatanensis Standl.	0.5	2.1	2.6	1.7
Oreopanax liebmanii Marchal.	1	2.1	1.5	1.5
Cydista aequnoctilis (L.) Miers.	0.5	2.1	2	1.5
Brosimum alicastrum Sw.	0.5	2.1	1.4	1.4
Castilla elástica Cerv.	0.5	2.1	1.3	1.3
ND	0.5	2.1	0.5	1.1
Luehea speciosa Willd.	0.5	2.1	0.1	0.9
Lonchocarpus cruentus	0.5	2.1	0.1	0.9
Tabebuia rosea (Bertol.) DC.	0.5	2.1	0.1	0.9
Cassia holwayana Rose.	0.5	2.1	0.1	0.9
Nectandra ambigens (Blake) C.K. Allen	0.5	2.1	0.1	0.9

Note: Dr: Relative density; Fr= Relative frequency; AB= Relative basal area; VIR= Importance value; ND= undetermined species.

The structure of BTR10 is composed of 17 species. The species *Trichospermum mexicanum* and *Zexmenia frutescens* are the species that present the highest values of density and relative frequency. The species with the highest VIR were *Trichospermum mexicanum* and *Zexmenia frutescens*, *Bursera simaruba*, and *Nectandra ambigens* (Table 5).

Table 5: Tree vegetation structure, relative density, relative frequency, and relative Basal Area, and relative importance value in the BTR10, of the Lacandona region, Chiapas.

Species	Dr	Fr	AB	VIR
	(%)			
Trichospermum mexicanum (DC.) Baill.	28.2	17	65.3	36.8
Zexmenia frutescens Blake.	58.7	17	29.5	35.1
Bursera simaruba (L.) Sarg.	2.6	10.6	0.5	4.6
Nectandra ambigens (Blake) C.K. Allen	2.6	8.5	1.9	4.3
Ficus máxima Mill.	1.3	6.4	0.5	2.7
Astronium graveolens Jacq.	1	6.4	0.8	2.7
Spondias mombin L.	1.3	6.4	0.4	2.7
Aspidosperma megalocarpon Müll. Arg.	1	6.4	0.1	2.5
Alseis yucatanensis Standl.	0.6	4.3	0.1	1.7
Árbol ND	0.6	2.1	0.1	1
Schefflera morototonii (Aubl.) Maguire, Steyerm. &Frodin	0.3	2.1	0.3	0.9
Sommera grandis (Bertl.) Standl.	0.3	2.1	0.2	0.9
Swietenia macrophylla King.	0.3	2.1	0.2	0.9
Cecropia obtusifolia Bertol.	0.3	2.1	0.1	0.9
Topotste ND	0.3	2.1	0.1	0.8
Alchornea latifolia Swartz	0.3	2.1	0.1	0.8
Pithecellobium arboreum (L.) Urban.	0.3	2.1	0.03	0.8

Note: Dr: Relative density; Fr= Relative frequency; AB= Relative basal area; VIR= Importance value; ND= undetermined species.

The BTR20 structure is composed of 39 species. The species *Trichospermum mexicanum* presented a relative density, frequency, and basal area of 16.5%, 6.7%, and 52.9%, the VIR for *T. mexicanum* was 25.4. Other species that presented a VIR > 3 were: *Sommera grandis*, *Quercus sp.*, *Nectandra ambigens*, *Hampea nutricia*, *Chrysophillum mexicanum*, *Astronium graveolens*, *Swietenia macrophylla*, *Alseis yucatanensis* and *Schefflera morototonii* (Table 6).

Table 6: Tree vegetation structure, relative density, relative frequency, and relative Basal Area, and relative importance value in the BTR20, of the Lacandona region, Chiapas.

Specie	Dr	Fr	AB	VIR
	(%)			
Trichospermum mexicanum (DC.) Baill.	16.5	6.7	52.9	25.4
Sommera grandis (Bertl.) Standl.	11.2	6.7	8.1	8.7
Quercus sp.	16.5	6.7	1.6	8.3
Nectandra ambigens (Blake) C.K. Allen	13.2	5.2	3	7.1
Hampea nutricia Fryxell.	5.7	4.5	2.3	4.2
Chrysophillum mexicanum Brandegee.	0.7	1.5	10.3	4.2
Astronium graveolens Jacq.	2.6	4.5	4.6	3.9
Swietenia macrophylla King.	4.3	5.2	1.3	3.6
Alseis yucatanensis Standl.	4.3	4.5	1.1	3.3
Schefflera morototonii (Aubl.) Maguire, Steyerm. & Frodin	2.6	3.7	2.7	3
Calophyllum brasiliense Cambess.	3.1	4.5	0.2	2.6
Bursera simaruba (L.) Sarg.	2.2	3.7	1.4	2.4
Tabebuia rosea (Bertol.) DC.	0.5	0.7	5.3	2.2

Palo rayo **ND**	2.2	3.7	0.5	2.1
Vatairea lundelli (Standl.) killip ex Record	1.9	3.7	0.7	2.1
Psidium guajava L.	1.2	3.7	0.4	1.8
Alchornea latifolia Swartz	1	3	0.3	1.4
Vernonia deppeana Less.	1	3	0.1	1.4
Bola de perro **ND**	1.4	2.2	0.4	1.4
Acosmium panamense (Benth.) Yakovlev	1	3	0.1	1.3
Terminalia amazonia (J.F.Gmel.) Exell	1	2.2	0.4	1.2
Lonchocarpus cruentus Lundell.	0.7	1.5	0.8	1
Spondias mombin L.	0.7	2.2	0	1
Manilkara zapota (L.) Royen	0.5	1.5	0.1	0.7
Eschweilera mexicana Wendt, Mori and Prance.	0.5	1.5	0	0.7
Simira salvadorensis (Standl.) Steyerm	0.5	1.5	0	0.7
Pithecellobium arboreum (L.) Urban.	0.5	0.7	0.3	0.5
Dialium guianense (Aubl.) Sandw.	0.2	0.7	0.5	0.5
Pimenta dioica (L.) Merrill	0.2	0.7	0.2	0.4
Sapindus saponaria L.	0.2	0.7	0.2	0.4
Aspidosperma megalocarpon Müll. Arg.	0.2	0.7	0.1	0.4
Blepharidium mexicanum Standl.	0.2	0.7	0	0.3
Lysiloma acapulcensis (Kunth) Benth.	0.2	0.7	0	0.3
Zit-it **ND**	0.2	0.7	0	0.3
Palo morado **ND**	0.2	0.7	0	0.3
Platymiscium yucatanum Standl.	0.2	0.7	0	0.3
Centradenia floribunda Planchon.	0.2	0.7	0	0.3
Parathesis serrulata Mez.	0.2	0.7	0	0.3
Sloaneaschippii Standl.	0.2	0.7	0	0.3

Note: Dr: Relative density; Fr= Relative frequency; AB= Relative basal area; VIR= Importance value; ND= undetermined species.

Species diversity (Chao2) and tree density (number of stems) are similar between BTR recovered 20 years later and conserved evergreen tropical forests. Table 7 shows the diversity index for the five sampled sites.

Table 7: Chao 2 diversity index, in VTR and evergreen tropical forest, of the Lacandona region, Chiapas.

Sitio	Species number	Stems number	Chao2 diversity index
BTR5	20	191	21
BTR10	17	312	49
BTR20	38	418	55
BTP1	47	409	63
BTP2	38	332	50
TOTAL	71	1662	

Note: BTR5=Tropical Forest in Recovery, 5 years; Tropical Forest in Recovery, 10 years; Tropical Forest in Recovery, 20 years; BTP1=Tropical Evergreen Forest 1; BTP1=Tropical Evergreen Forest 2.

Tree richness: In BTP1, 47 species were recorded, and in BTP2 38 species. In the 20-year BTR the species richness is similar to that of the conserved sites (39 species); while for sites with a shorter recovery time, the species richness is lower (Figure 3).

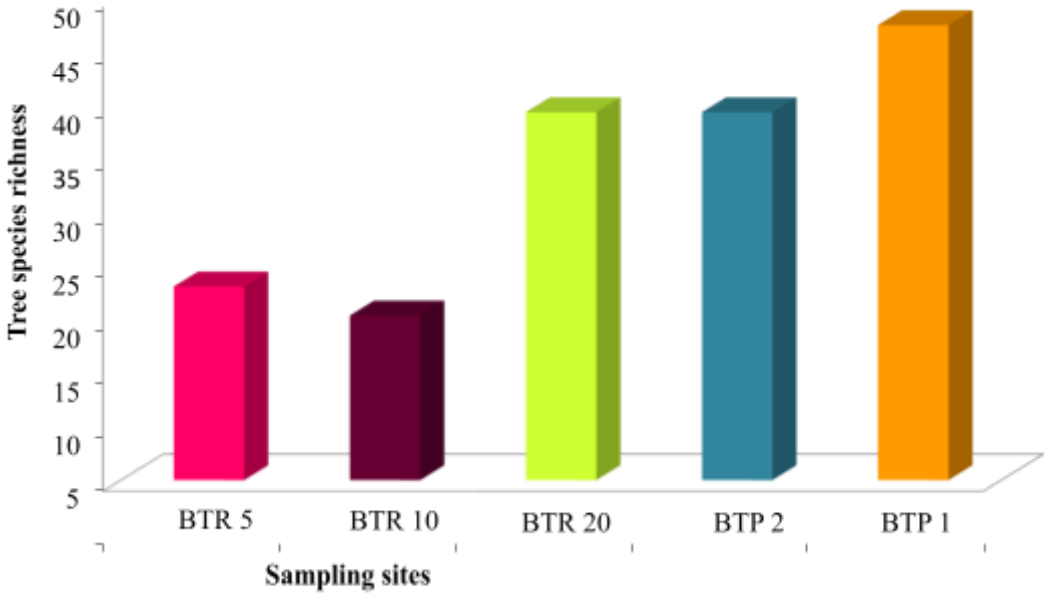

Figure 3: Tree richness in BTR of different ages and two evergreen tropical forests, in the Lacandon region, Chiapas.

Tree density: The results showed 4,090 and 3,220 individuals ha^{-1} for BTP1 and BTP2, respectively. After 20 years of recovery, in the BTR the tree density was 4,810; while in BTR5 it was 1,910 and in BTR10 it was 3,120 individuals.

Variation of tree composition: In BTR 5 one and then two species dominate. After 20 years the tree richness becomes very similar to that of the conserved and mature BTP. In BTR5 the species *Trichospermum mexicanum* covers 73% of the tree composition, the remaining 28% is made up of other species. In BTR10, the species *Zexmenia frutescens* and *Trichospermum mexicanum* represent 87% and 13% respectively of the tree species composition. In BTR 20 the species *T. mexicanum*, *Quercus sp.*, *Nectandra ambigens*, and *Sommera grandis* represent 57% of the tree composition, but the remaining 43% is composed of other species. In BTP1, Species *Metopium brownei*, *Spondias mombin*, *Quercus sp.*, *Sloanea schipii*, and *Astrocaryum mexicanum* represent 49% of the tree composition, while 51% is composed of other species. In BTP2 the species *Quercus sp.*, *Metopium brownei*, *Spondias mombin*, and *Terminalia amazonia* represent 52% of the tree composition and the remaining 48% is covered by other species (Figure 4).

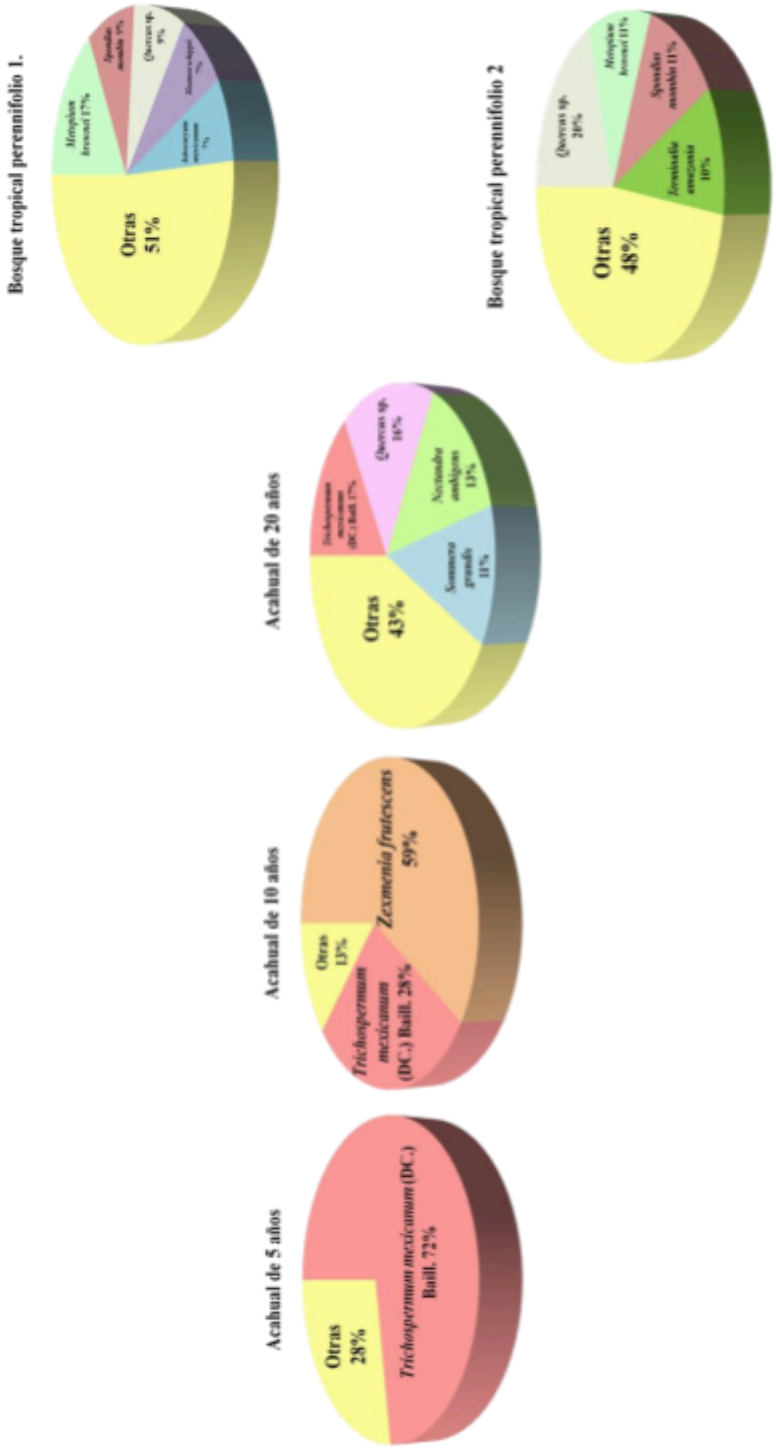

Figure 4: Variation of tree composition in acahuales of 5, 10, and 20 years, derived from a tropical evergreen forest subjected to slash-and-burn systems and two tropical evergreen forest sites, in the Lacandona region, Chiapas.

Similarity analysis. The dendrogram shows two groups. In the first, BTP1 and BTP2 show 68% similarity and 50% with BTR20. The other group is composed of BTR5 and BTR10 with 39% similarity. According to the Jaccard index, there is the same number of groups, however, the similarity between BTR5 and BTR10 was lower.

*Stored carbon***.** The amount of carbon stored in BTP1 and BTP2 was estimated to be a total of 479 and 513 Mg C ha^{-1} respectively. In BTR5, BTR10, and BTR20, the stored carbon obtained was 29, 35, and 80 Mg C ha^{-1} respectively (Figure 5). The polynomial equation obtained was: $y = 0.033x^3 - 0.9451x^2 + 9.6731x + 4E - 12$, con $R^2 = 0.99$, and describes the increase in stored carbon concerning the age of the BTR (Figure 5).

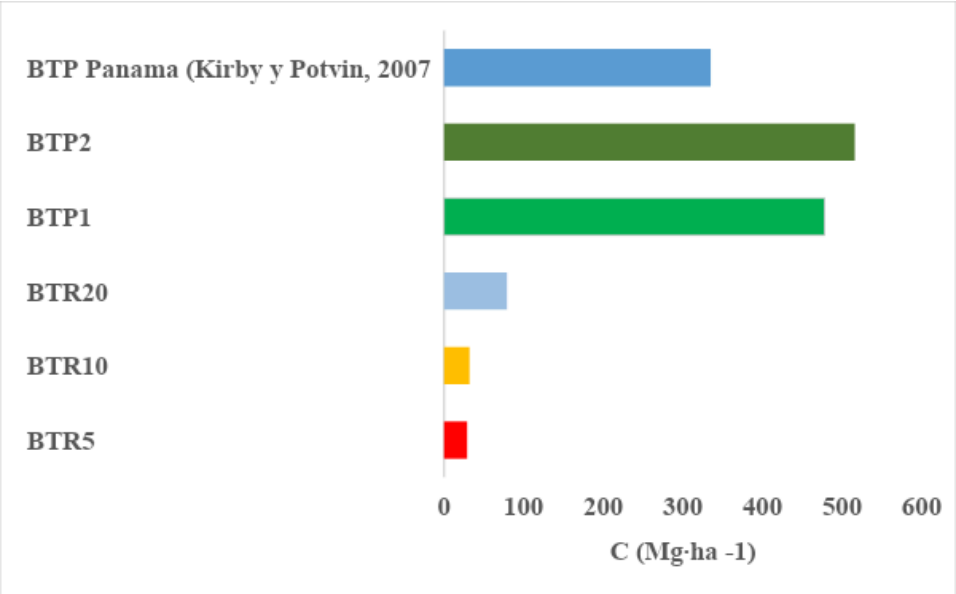

Figure 5: Stored carbon (Mg C ha^{-1}) in BTR of 5, 10, and 20 years and in two evergreen tropical forests, concerning that captured in the Panama BTP. The BTRs are a product of the application of the slash-and-burn system.

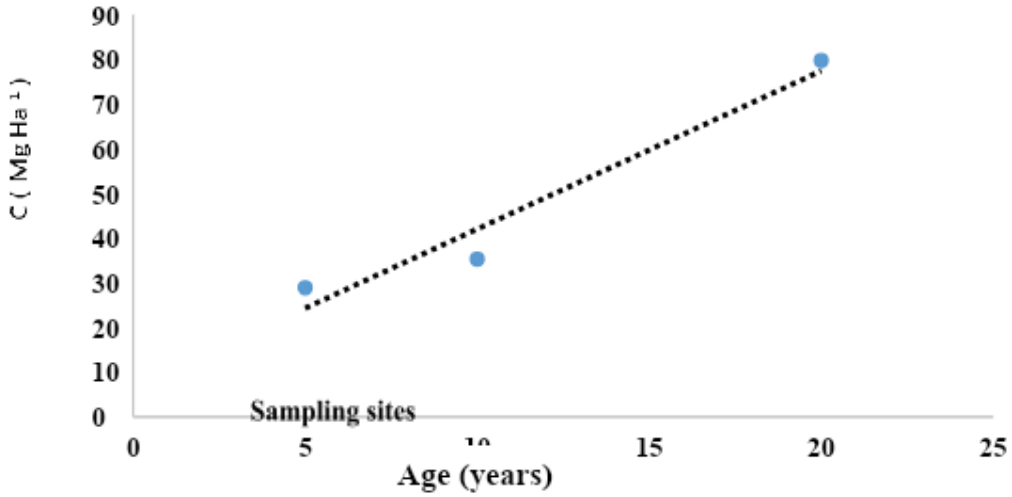

Figure 6: Hypothetical polynomial model of carbon stored during the development of the BTR in the first 20 years, in a tropical forest in the Lacandona Region, Chiapas.

To know the time that must elapse for a BTR to store C similar to that of a tropical evergreen forest subjected use RTQ, the equation shown in Figure 7 was used. According to this extrapolation, at least 50 years are required for BTR to reach stored carbon values similar to those of mature BTP.

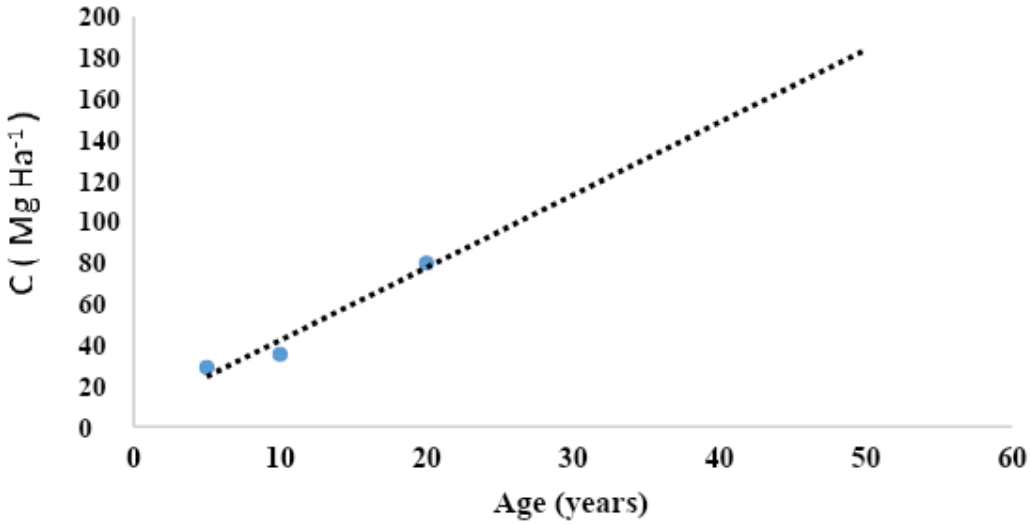

Figura 7: Modelo polinómico hipotético de años necesarios para volver a recuperar el carbono almacenado, similar a un de BTP en la Región Lacandona Chiapas México.

V. DISCUSSION

The RTQ system did not record species during the first three years, which is why acahuales or recovering tropical forests (BTR) were sampled up to five years later. In BTR5 there is the presence of *Trichospermum mexicanum*, *Heliocarpus donnellsmithii*, *Cecropia obtusifolia*, *Castilla elastica*, *Luehea speciosa*, and *Tabebuia rosea*. These species are considered pioneers in disturbed ecosystems (Pennington and Sarukhán, 2005). The seeds of these species arrive through birds, and in the case of *C. obtusifolia*, *C. elastica*, *L. speciosa*, and *Tabebuia rosea* by bats and some rodents (Vázquez-Yanes *et al.*, 1984), so seed dispersal for zoochory it is very important.

For birds to reach these sites, they require the presence of shrubs, and for this reason, they do not appear in the first three years when weak herbaceous plants are abundant. The dominance of fast-growing herbaceous plants does not allow the arrival of birds and therefore seeds of tree species, as reported by the owners of the plots studied. Pioneer species show accelerated growth in clearings where they can receive full sunlight and spread quickly over disturbed areas since they present early seed production (Pennington and Sarukhán, 2005; Turner, 2001).

It is important to note that in the first five years, species typical of high and medium evergreen forests were recorded, such as *Astronium graveolens*, *Alseis yucatanensis*, and *Nectandra ambigens*, as well as species considered climax (25% of the species) as *Dialium guianense*, *Brosimum alicastrum* and *Lonchocarpus cruentus*. The seeds of these species arrive through wind dispersal and the rest by birds, bats, and monkeys (Pennington and Sarukhán, 2005). *A. graveolens* is a threatened species included in NOM-059-SEMARNAT-2001). The germination of these species in these conditions is since they only require humidity, for example, for *N. ambigens* (Barajas-Guzmán and Álvarez-Sánchez, 2004) and *B.*

alicastrum (Vázquez-Yanes *et al.,* 1984). Meanwhile, *D. guianense* requires passage through the digestive tract of birds for its germination (Vázquez-Yanes *et al.,* 1984).

The above suggests that the initial presence of species with advanced stages of succession and even climax depends on dispersal syndromes, in the case of the RTQ system in the Lacandona region, it is due to zoochory.

The presence of pioneer species, species typical of the middle stratum of, and climax species of the BTP (22, 25, and 53% mean of the species, respectively). In the early stages of succession, they coincide with what has been recorded in other tropical forests. According to Whitmore (1998), when a clearing is opened, the seeds of pioneer and climax species arrive simultaneously for colonization after a disturbance, but the pioneer species dominate until they are progressively displaced by the climax species. In a study in Atewa, Ghana, it was found that colonization began with 90% pioneer species, but already 60% climax species were also present during the first year). The two groups grew together and progressively became enriched with the remaining 40% of the climax species and were subsequently dominant in the older evergreen tropical forests (Swaine and Hall, 1983). Something similar occurred in Barro Colorado, when the presence of climax and pioneer species occurred after the opening of a clearing, and they grew together during the first five years (Brokaw, 1987).

In BTR10, pioneer species decline and constitute only 25% of the species. The dominance of *Trichospermum mexicanum* is maintained and that of *Zexmenia frutescens* and *Bursera simaruba* increases, but *Cecropia obtusifolia* decreases. The arrival of *Z. frutescens* is by wind and zoochory (Standley, 1926). The increase in *B. simaruba* indicates that recruitment is continuous, and its growth occurs due to its greater ecological breadth (Vázquez-Yanes *et al.,* 1984).

When the pioneer species develop and form a canopy, they allow a greater presence of shade-tolerant BTP species (33.33%) such as *Nectandra ambigens*, *Astronium graveolens*, *Alseis yucatanenses*, and *Alchornea latifolia*; advanced secondary vegetation species (16.66%) such as *Spondias mombin* and *Schefflera morototonii* and even climax species (25%) such as *Aspidosperma megalocarpon*, *Swietenia macrophylla* and *Pithecellobium arboreum* (Pennington and Sarukhán, 2005).

The arrival of seeds of *S. mombin*, *S. morototonii*, is attributed to the fact that its dispersal syndrome is carried out by birds (Vázquez-Yanes *et al.*, 1984) and the dispersal of seeds of *A. latifolia* occurs by birds and bats because It requires the bird's gastric juices to germinate. In *A. megalocarpon*. *S. macrophylla* and *P. arboreum* dispersion is anemochorous (wind) (Pennington and Sarukhán, 2005; Vázquez-Yanes *et al.,* 1984). The presence and greater abundance of these species are because they are adapted to more humid, protected, and fertile areas (Pennington and Sarukhán, 2005), therefore, they only occur under the canopy, and can potentially replace pioneer species.

In BTR20, pioneer species continue to constitute 25% of the total species. *T. mexicanum*, *Bursera simaruba*, *Tabebuia rosea*, *Psidium guajava* and *Lysiloma acapulcensis* (VIR 25.4, 2.4, 2.2, 1.8, 1.0, 0.3 and 0.3 respectively). Meanwhile, the middle stratum species *Nectandra ambigens*, *Hampea nutricia*, *Chrysophillum mexicanum*, and *Blepharidium mexicanum* among others registered a VIR of 7.1, 4.2, 4.2, and 0.3 respectively, but continued to increase their dominance and reach 40%.

Regarding the species of climax vegetation, for example, *Vatairea lundelli*, *Acosmium panamense*, and *Terminalia amazonia* mainly (VIR 2.1, 1.3, 1.2% respectively) constitute 32.14%. Finally, only *Schefflera morototonii* and *Spondias mombin* were recorded as characteristic species of advanced secondary vegetation (Pennington and Sarukhán, 2005).

The arrival of *P. guajava*, *L. acapulcensis*, *Hampea nutricia*, *Chrysophillum mexicanum*, and *Blepharidium mexicanum* is because they present a zoochory dispersal syndrome (Vázquez-Yanes *et al.,* 1984; Ávila *et al.,* 2005; Rodríguez-Velázquez *et al.,* 2009) and the species *Vatairea lundelli*, *Acosmium panamense* and *Terminalia amazonia* present a dispersal syndrome due to anemocoria (Salazar and Soihet, 2001; Rodríguez Velázquez *et al.,* 2009).

The increase in tree species of different sizes that represent a greater diversity of fruits also means a greater number of perching sites, which favors the arrival of new species of birds and therefore a greater dispersal of seeds, and this may explain why They find new species in more developed stages. In this regard, Bojorges-Baños and López-Mata (2006) found in the jungles of Veracruz that the abundance, diversity, and composition of bird communities are closely related to tree richness. Shankar-Raman *et al.* (1998) found that richness, diversity, and abundance increase as post-disturbance succession develops, similar to the slash-and-burn system in Indian tropical forests. The above helps to explain why the similarity of the 20-year-old acahual with BTP1 and BTP2 increases.

In BTP*1,* middle stratum species predominate and constitute 50% of the species. *Metopium brownei, Chrysophillum mexicanum*, and *Nectandra ambigens* stand out (VIR 12.6, 3.3, and 3.2, respectively), while the climax species constitute 23.52%, such as *Terminalia amazonia*, *Dialium guianense* and *Vatairea lundelli* the most characteristic, with VIR 18.8, 3.1 and 2.9, respectively. *Spondias mombin* has been frequently recorded in advanced secondary vegetation (Pennington and Sarukhán, 2005).

In BTP1, pioneer species are also present such as *Trichospermum mexicanum* and *Psidium guajava*, among others (VIR 4.4 and 2.9 respectively). It should be noted that the pioneer and climax species are present in the same proportion.

In BTP2 the VIR for *Metopium brownei*, *Swietenia macrophylla*, and *Nectandra ambigens* were 12.4, 4.4, and 3.4, respectively, which are species of the middle stratum (57.14%) and are dominant. The climax species constitute 25% (*Dialium guianense*, *Terminalia amazonia*, and *Brosimum alicastrum*, with VIR 13.4, 5.1 and 4.9 respectively). *Schefflera morototoni and Spondias mombin* are found as advanced secondary vegetation species (Pennington and Sarukhán 2005). The pioneer species that dominate are *P. guajava, B. simaruba,* and *T. mexicanum* with VIR 6.1, 4.5, 2.2, and 0.7%, respectively, and composed 14.28%.

Based on the above, we can infer that the process of repopulating the tropical forest affected by the RTQ system in the Lacandona region begins with the arrival of seeds, both of pioneer species and advanced stages, and even climaxes, through birds and bats (mainly up to three years old). This occurs since seeds dispersed by birds have a greater chance of reaching fields that are surrounded by remnants of jungle, in addition to the fact that their flight in open fields is conditioned by the presence of food sources and perches (Martínez-Ramos and García-Orth, 2007).

In this regard, Wunderle (1997) found that the greatest flight activity in birds was recorded between 1 and 80 m from the edges of the secondary forest towards the open field, and therefore the opening of small clearings during the RTQ system also allows be quickly colonized.

Based on the above, it can be said that pioneer tree species develop and tend to dominate in the first 10 years, and then form a canopy that offers new shelters and seed dispersal sites, mainly by ornithochory; either by species from the middle stratum, advanced secondary vegetation and climax. These species germinate due to the greater humidity offered by this new condition, which, combined with a lower intensity of light, allows their development. Subsequently, seeds of shade-tolerant species arrive, both

from advanced secondary vegetation, middle stratum, and from climax species (mainly by zoochory), which grow and are favored by the opening of new clearings. In the Lacandona region, Chiapas, the set of species of advanced stages grows until it reaches the height of the canopy, and becomes dominant after 20 years, so the abundance of the pioneer species decreases, and the similarity of the tree composition with the evergreen tropical forest.

In general, the results obtained demonstrate that the management scheme of the traditional RTQ system, with 20-year cycles and openings of less than 1ha, does not alter the process of maintaining the richness of tree species. The richness found in the two BTP and BTR sampled was 71 species in 0.5 ha and is located within the average range of that recorded for the BTP.

In the Lacandona Forest, the number of tree species per hectare recorded by other authors is variable, for example, 160 (Meave, 1983), 79 (Levy-Tacher *et al.,* 2006), and 31 (Ochoa-Gaona *et al.,* 2007). In other tropical forests in Ecuador, between 44 species per hectare have been recorded (Wright, 2002) and up to 620 in Colombia (Giraldo, 2000).

BTR development and carbon sequestration.

Trees assimilate and store large amounts of carbon throughout their lives, mainly in the tree trunk and it´s related to the diameter structure and tree density (Chave *et al.,* 2005).

Tropical agricultural systems have the greatest potential for carbon (C) sequestration (Albrecht and Kandji, 2003). In the Lacandona region, acahuales or BTR are generated after the practice of slashing, slashing, and burning, which by increasing their age after the disturbance (5, 10, and 20 years), increases the density of stems and therefore stored carbon. Something similar to what was recorded by Huges *et al.* (1999), during the development of BTR that are within the intervals reported by (Albrecht and Kandji, 2003) which are between 12 to 228 Mg C ha^{-1}, and are greater than those recorded by Eaton and Lawrence (2009). For three-year secondary forests in Yucatán (4.8 Mg C ha^{-1}) and twenty-four years (37.7 Mg C ha^{-1}). Williams *et al.* (2008) recorded values between 10.1 and 22.2 Mg C ha^{-1} for plots of more than 20 years of abandonment in Mozambique. However, in Lacandona, Chiapas, the high stored carbon content is attributed to the species richness and tree density.

In BTP 1 and BTP2, the amount of C stored was 478.73 and 512.53 Mg C ha^{-1}, respectively, higher than that recorded by other authors. For example, in the forest plots in Mozambique recorded 4.3 to 33.4 Mg ha^{-1} (Willimas *et al.,* 2008). In a primary and secondary forest in Panama 251.7 Mg C ha^{-1} (Chave, 2004). In the Amazon rainforest, with values from 335 Mg C ha^{-1} (Kirby and Potvin, 2007); 144.5 Mg C ha^{-1} (de Alencastro *et al.* 2005); to 145 to 232 Mg C ha^{-1} (Houghton *et al.* 2000). Xiao-Tao *et al.* (2010) recorded 163 to 258 Mg C ha^{-1} es in a seasonal tropical forest in China; Meanwhile, Glenday (2006) in East Africa obtained 330 ±65 Mg C ha^{-1}. Finally, Eaton and Lawrence (2009), in a conserved forest in Yucatán 73.5 Mg C ha^{-1}.

The higher carbon values obtained in the BTPs of the Lacandona region can be attributed to: i) Selva Lacandona can be more productive than other areas; ii) Other allometric equations are used in most of the works cited; iii) There may be a difference in the productivity of the BTP and the density of the wood of each species since although the BTP1 and BTP2 are contiguous, they have a difference of 30 Mg C ha^{-1}; iv) The age of the forests in conservation has not been specified, but some, such as Holz *et al.* (2009), consider a forest in conservation to be between 25 and 50 years old; vi) In this work, areas with large-diameter trees are selected. These are indicators of a mature state and can be used for the following purposes, and vii) BTPs affected by Mercury (Hg), such as those from Central and South America, tend to lose their fertility and productivity (Carvalho *et al.,* 2019; Mainville *et al.,* 2006).

The results indicate that the 20-year cycle of the RTQ system allows tree richness to be restored, but does not allow C to be stored at a rate similar to that of BTPs, which store eight times more. The above has strong implications because this type of agriculture is considered sustainable, but in this 20-year cycle, the amount of C stored in a mature evergreen tropical forest is not recovered. According to our estimates, it takes approximately 50 years for stored carbon to recover, 10 years than estimated by Chazdon *et al.* (2016) for tropical forests.

To reduce the recovery time of C storage in BTR, we consider as a possible strategy, leaving the trees alive at the ages of 10 to 20 years and then applying the RTQ system. Likewise, fast-growing and commercial pioneer species such as *Bursera simaruba*, a timber species, are planted, and the resin is used for incense and varnish (Toledo-Aceves *et al.,* 2009). These species are propagating by cuttings (Vázquez-Yanes *et al.,* 1984) and the use of similar species could imply rapid growth and C storage in less time.

VI. CONCLUSIONS

Based on the results of this study it can be concluded that:

1. The RTQ system traditionally applied by the Lacandon Maya, with periods of rest of 20 years, allows the recovery of the richness, diversity, and tree density of the Lacandon jungle.
2. The RTQ system practiced with 20-year rest periods does not allow the regeneration of the amount of C stored in tropical evergreen forests; this would be achieved with 50-year rest periods.
3. The development of the BTR and the regeneration of the tree cover is gradual and depends largely on the dispersal of seeds by fauna, particularly birds.

ACKNOWLEDGMENTS

This work was funded by the PAPIIT-IN 217308 project of the UNAM and the FES Zaragoza UNAM-Biology. We thank Mr. Pablo Chankin Njabor and his family for the support and facilities provided for the proper development of this research on his property. Janelle Sacnité Chávez-Barrera, Juan M. Castro-García, Sandra E. Aldana-Pérez, Jesús A. Lugo Aldana, Adriana Vallejo Fernández, Juan A. Poblano-Olivares, and Tania González-Vargas supported during the sampling and fieldwork.

REFERENCES.

1. Albrecht, A. y Kandji, S.T. 2003. Carbon sequestration in tropical agroforestry systems. Agriculture, Ecosystems and Environment 99: 15-27.
2. Barajas-Guzmán, G. y Álvarez-Sánchez, J. 2004. Asignación de recursos e influencia de los cotiledones en el crecimiento de plántulas de Nectandra ambigens (Blake) C.K. Allen (Lauraceae) en una selva tropical húmeda. Bol. Soc. Bot. Mex. 74: 5-11.
3. Bojorges-Baños, J.C. y López-Mata, L. 2006. Asociación de la riqueza y diversidad de especies de aves y estructura de la vegetación en una selva mediana subperennifolia en el centro de Veracruz, México. Anales del Instituto de Biología. Serie Botánica. 77: 235-249.
4. Brokaw, N.V.L. 1987. Gap-phase regeneration of three pioneer tree species in a tropical forest. Journal of Ecology. 75: 9-19. En Davy, A.S., Hutchings, M.J., Watkinson, A.R.(Eds.). Plant population ecology. Blackwell Scientific Publications, Oxford UK, pp. 271-287.
5. Carvalho G.S., Oliveira J. R., Cury N., Schulze D.G., Marques J.J., 2019. Selenium and mercury in Brazilian Cerrado soils and their relationships whith physical and chemical soil characteristics. Chemosfera 218: 412-415.

6. Chave, J., Andalo, C., Brown, S., Cairns, M. A., Chambers, J. Q., Eamus, D., Fölster, H., Fromard, F., Higuchi, N., Kira, T., Lescure, J.P., Nelson, B. W., Ogawa, H., Puig, H., Riéra, B. y Yamakura, T. 2005. Tree allometry and improved estimation of carbón stocks and balance in tropical forests. Oecologia 145:87-99.
7. Chave, J., Condit, R., Aguilar, S., Hernandez, A., Lao, S., Perez, R., 2004. Error propagation and scaling for tropical forest biomass estimates. Phil. Trans. Roy. Soc. Lond. B 359, 409–420.
8. Chazdon, R.L., E. N. Broadbent, D. M. A. Rozendaal, F. Bongers, A. M. A. Zambrano,T. M. Aide, P. Balvanera, J. M. Becknell, V. Boukili, P. H. S. Brancalion, D. Craven,J. S. Almeida Cortez, G. A. L. Cabral, B. de Jong, J. S. Denslow, D. H. Dent, S. J. DeWalt,J. M. Dupuy, S. M. Durán, M. M. Espírito-Santo, M. C. Fandino, R. G. César, J. S. Hall,J. L. Hernández-Stefanoni, C. C. Jakovac, A. B. Junqueira, D. Kennard, S. G. Letcher, M. Lohbeck, M. Martínez-Ramos, P. Massoca, J. A. Meave, R. Mesquita, F. Mora, R. Muñoz, R. Muscarella, Y. R. F. Nunes, S. Ochoa-Gaona, E. Orihuela-Belmonte, M. Peña-Claros, E. A. Pérez-García, D. Piotto, J. S. Powers, J. Rodríguez-Velazquez, I. Eunice Romero-Pérez, J. Ruíz, J. G. Saldarriaga, A. Sanchez-Azofeifa, N. B. Schwartz, M. K. Steininger, N. G. Swenson, M. Uriarte, M. van Breugel, H. van der Wal, M. D. M. Veloso, H. Vester, I. C. G. Vieira, T. V. Bentos, G. B. Williamson, L. Poorter. 2016. Carbon sequestration potential of second growth forest regeneration in the Latin American tropics. Sci. Adv.2, el 501639 (2016).
9. Comisión para la Cooperación Ambiental CCA. 2014. La quema de residuos agrícolas: fuente de dioxinas, Canadá, 6 pp. de Alencastro G. P.M.,Vieira D. L., Neeff T. and da Costa F. C. 2005. Carbon budget estimation in Central Amazonia: Successional forest modeling from remote sensing data. Remote sensing enviromental. 94:4: 608-522.
10. Diemont, S. A.W., Martina, J. F, Levy-Tacher, S. I., Nigh, R.B., Ramirez Lopez, P. J. y Golicher D. 2006. Lacandon Maya forest management: Restoration of soil fertility using native tree species. Ecological Engineering. 28: 205-212.
11. Eaton, J. M. y Lawrence D. 2009. Loss of carbon sequestration potential after several decades of shifting cultivation in the Southern Yucatán. Forest Ecology and Management. 258: 949–958.
12. Escalante-Espinoza, T. 2003. ¿Cuántas especies hay? Los estimadores no paramétricos de Chao. Elementos. 52:53-56.
13. Glenday, J. 2006. Carbon storage and emissions offset potential in an East African tropical rainforest. Forest Ecology and Management. 235:72–83
14. Holz S., Placci G. y Quintana R.D. 2009. Effects of history on secondary forest regeneration in the Upper Parana Atlantic Forest (Misiones, Argentina). Forest Ecology and Management. 258: 1629-1642.
15. Houghton, R., Skole, D., Nobre, C., Hackler, J., Lawrence, K., & Chomentowski, W. 2000. Annual fluxes of carbon from deforestation and regrowth in the Brazilian Amazon. Nature. 403(20): 301–304.
16. Huges, Flint R., Kauffman, Bonne J.y Jaramillo Victor J. 1999. Biomass, carbon and nutrient dynamics of secondary forests in a humid tropical region of Mexico. Ecology. 80 (6): 1892-1907
17. Instituto Nacional de Ecología INE. 2000. Programa de Manejo Reserva de la Biosfera Montes Azules. México. INE, 256 p.
18. Kirby, K.R. y Potvin, C. 2007. Variation in carbon storage among tree species: Implications for the management of a small-sale carbon sink project. Forest Ecology and Management. 246: 208-221.
19. Mainville N., Webb J., Lucotte M., Davidson R., Betancourt O., Cueva E. and Mergler D. 2006. Decrease sof soil fertility and release of mercury following deforestacion in the Andean Amazon, Napo River Valley, Ecuador. Science of The Total Environment 368: 99-98.
20. Martínez-Ramos, M. 2006. Aspectos Ecológicos de la selva húmeda en la Región Lacandona: Perspectivas para su estudio y conservación. En: Oyama K. y A. Castillo. 2006. Manejo

conservación y restauración de recursos naturales en México: perspectivas desde la investigación científica. México: Siglo XXI, UNAM, Centro de investigaciones en Ecosistemas.
21. Martínez- Ramos, M. y García-Orth, X. 2007. Sucesión ecológica y restauración de las selvas húmedas. Boletín de la Sociedad Botánica de México. 80:69-84.
22. Meave, J. 1983. Estructura y composición de la selva alta perennifolia de Bonampak, Chiapas. Tesis profesional, Facultad de Ciencias, UNAM, México.
23. Norma Oficial Mexicana NOM-059-ECOL-2001, Protección ambiental-Especies nativas de México de flora y fauna silvestres-Categorías de riesgo y especificaciones para su inclusión, exclusión o cambio-Lista de especies en riesgo.
24. Ochoa-Gaona S., Francisco H.V., Bernardus H., De J., Francisco D.G.G. 2007. Pérdida de diversidad florística ante un gradiente de intensificación del sistema de roza-tumba-quema: un estudio en el caso en la selva Lacandona, Chiapas, México. Boletín de la Sociedad Botánica de México. 81:65-80
25. Pennington, T.D. y Sarukhán, J., 2005. Árboles tropicales de México. Manual para la identificación de las principales especies. 3ª. ed. México, UNAM, FCE. 523 p.
26. Rodríguez-Velázquez, J., Sinaca Colín, P. y Jamangapé G., G. 2009. Frutos y semillas de árboles tropicales de Mexico. SEMARNAT,México, pp. 119.
27. Salazar R. y C. Soihet. 2001. Manejo de semillas de 75 especies forestales de América Latina. Vol. II. Centro Agronómico Tropical de Investigación y Enseñanza (CATIE), Costa Rica pp. 79-80.
28. Shankar-Raman, T.R., Rawat, G.S. y Johnsingh, A.J.T. 1998. Recovery of Tripical Rainforest Avifauna in relation to vegetation succesion following shifting cultivation in Mizoram, North-East India. Journal of Applied Ecology. 35 (2):214231.
29. Standley, P.C. 1926. Trees and Shrubs of Mexico. V.23. Smithsonian Institution. United States National Museum, Washington, pp 1566.
30. Swaine, M.D. y Hall, J.B. 1983. Early succession on cleared forest land in Ghana. Journal of Ecology. 71: 601-28.
31. Toledo-Aceves, T., Purata-Velarde, S y Peters, C.M. 2009. Regeneration of commercial tree species in a logged forest in the Selva Maya, México. Forest Ecology and Management. 258: 2481-2489.
32. Turner, I.M. 2001. The ecology of Trees in the Tropical Rain Forest. Cambridge University Press, 228 p.
33. Vázquez-Yanes, C., Batis-Muñoz, A. I., Alcocer-Silva, M. I., Díaz, M. G. y Sánchez-Dirzo, C. 1984. Árboles y arbustos nativos potencialmente valiosos para la restauración ecológica y la reforestación. PROYECTO J-084 – CONABIO.
34. Williams, M., Ryan, C.M., Rees, R.M., Sambane, E., Fernando, J., Grace, J. 2008. Carbon sequestration and biodiversity of re-growing miombo woodlands in Mozambique. Forest Ecology and Management. 254: 145-155.
35. Whitmore, T.C. 1998. The influence of tree population dynamics on forest species composition. In: Davy, A.S., Hutchings, M.J., Watkinson, A.R.(Eds.). Plant population ecology. Blackwell Scientific Publications, Oxford UK, pp 271-287.
36. Wright, J. S. 2002. Plant diversity in tropical forests: a review of mechanisms of species coexistence. Oecologia. 130: 1-14.
37. Wunderle, J.M. 1997. The role of animal seed dispersal in accelerating native forest regeneration on degraded tropical lands. Forest Ecology and Management. 99: 223-235.
38. Xiao-Tao Lüa, Jiang-Xia Yina, Martin R. Jepsenc, Jian-Wei Tanga. 2010. Ecosystem carbon storage and partitioning in a tropical seasonal forest in Southwestern China. Forest Ecology and Management. 260:1798–1803.

This page is intentionally left blank

On Multiverses (or Parallel Universes) of Matrix Triple Solutions of the Diophantine Equation $X^3 + Y^6 = Z^6$

Joachim Moussounda Mouanda

Blessington Christian University

ABSTRACT

We show that the Diophantine equation

$$X^3 + Y^6 = Z^6 \tag{0.1}$$

admits matrix triple solutions from M3(N) and M6k(N), $k \in N$. We construct infinite universes made of these solutions. We introduce different construction structures sets of matrix solutions associated to the Diophantine equation (0.1). These construction structures sets of matrix solutions allow us to show that there exists an infinite number of multiverses (parallel universes) of the matrix solutions of the Diophantine equation (0.1) containing each a finite number of universes of matrix triples.

Keywords: matrices of integers, diophantine equations.

Classification: MSC Code: 11D09, 15A03, 11C20

Language: English

Great Britain Journals Press

LJP Copyright ID: 925691
Print ISSN: 2631-8490
Online ISSN: 2631-8504

London Journal of Research in Science: Natural & Formal

Volume 24 | Issue 9 | Compilation 1.0

On Multiverses (or Parallel Universes) of Matrix Triple Solutions of the Diophantine Equation $X^3 + Y^6 = Z^6$

Joachim Moussounda Mouanda

ABSTRACT

We show that the Diophantine equation

$$X^3 + Y^6 = Z^6 \tag{0.1}$$

admits matrix triple solutions from M3(N) and M6k(N), $k \in N$. We construct infinite universes made of these solutions. We introduce different construction structures sets of matrix solutions associated to the Diophantine equation (0.1). These construction structures sets of matrix solutions allow us to show that there exists an infinite number of multiverses (parallel universes) of the matrix solutions of the Diophantine equation (0.1) containing each a finite number of universes of matrix triples.

Keywords: matrices of integers, diophantine equations.

Author: Blessington Christian University, Mathematics Department Nkayi, Republic of Congo

I. INTRODUCTION AND MAIN RESULT

A multiverse (or parallel universes) is the collection of alternate universes that share a universal hierarchy. The idea of the existence of the multiverse has been around for long time. An idea which many theoretical physicists have been trying to prove by using string theory which is a branch of theoretical physics that attempts to reconcile gravity and general relativity with quantum physics. In 2018, Stephen Hawking on his paper entitled "A smooth exit from eternal inflation?" predicted that there are not infinite parallel universes in the multiverse, but instead a limited number and these universes would have laws of physics like our own [4]. The idea of multiverse is not sufficiently understood to the most mathematicians. Perhaps the lack of understanding the existence of the multiverse is due to the fact that mathematicians never deeply study the idea of multiverse in terms of tuples of numbers satisfying an equation (E) which represents the universal stability law of universes contained in the multiverse. Generating universes of tuples of numbers (or matrices) which satisfy a certain equation (E) is an interesting approach. In 2021, Mouanda introduced a new method of computing the Galaxies of sequences of Pythagorean triples [5]. He constructed the multiverse $\mathcal{F}_{2,2,2}(\mathbb{C})$ of Pythagorean triples of complex numbers which has a finite number of universes since

London Journal of Research in Science: Natural & Formal

$$\mathcal{F}_{2,2,2}(\mathbb{N}) \subset \mathcal{F}_{2,2,2}(\mathbb{Z}) \subset \mathcal{F}_{2,2,2}(\mathbb{Q}) \subset \mathcal{F}_{2,2,2}(\mathbb{R}) \subset \mathcal{F}_{2,2,2}(\mathbb{C}).$$

This lead to the introduction of the new theory called "Galaxies Number Theory". This new theory provides us a better understanding of the laws and structures of different universes. The study of the galaxies of the universe of Pythagorean triples of positive integers (matrices or polynomials) gives us a clear understanding of parallel universes. Pythagorean triples have been known and developed since ancient times with the oldest record dating back to 1900 BC [1]. Finding methods for generating Pythagorean triples have been of great interest to mathematicians since Babylonians (from 1900 to 1600 BC). In the literature, there are three classical methods of generating Pythagorean triples. Namely, Pythagoras' method (c. 540BC), Plato's Formula (c. 380 BC) [8] and Euclid's formula (c. 300BC) [2]. There are in three post-classical methods which are Fibonacci's method (c. 1170 - c. 1250), Stifel's method (1544) [11] and Ozanam's Method (1694)[9]. There are two modern methods which are Portia's method and Dickson's method [10, 3]. Recent Mouanda's work on finding the matrix solutions of Diophantine equations shows that matrix exponential Diophantine equations always admit an infinite number of matrix solutions [6].

In this paper, we show that the Diophantine equation $X^3 + Y^6 = Z^6$ admits not only matrix solutions from the set $M_3(\mathbb{N})$ but also matrix solutions from the set $M_{6k}(\mathbb{N}), k \in \mathbb{N}$. We give some examples of matrix solutions. We construct universes made of these solutions. We introduce different construction structures sets of matrix solutions associated to this Diophantine equation. These construction structures sets of matrix solutions allow us to construct the multiverses (parallel universes) of matrix triple solutions of the Diophantine equation $X^3 + Y^6 = Z^6$ containing each a finite number of universes.

Theorem 1.1. *There exists an infinite number of multiverses (parallel universes) of matrix triple solutions of the Diophantine equation $X^3 + Y^6 = Z^6$ containing each a finite number of universes of matrix triples.*

II. PROOF OF THE MAIN RESULT

In this section, we construct universes of matrix triple solutions of the Diophantine equation (0.1). We introduce the construction structures sets of matrix triple solutions of this equation. We construct the multiverses of matrix triple solutions of the equation (0.1).

2.1 The Universe of Matrix Triple Solutions of the Diophantine Equation $X^3 + Y^6 = Z^6$

Let $f : \mathbb{N}^3 \longrightarrow \mathbb{N}$ be a function of three variables. Define by

$$\mathcal{F}(\mathbb{N}^3) = \{(x, y, z) : f(x, y, z) = 0\}.$$

The set $\mathcal{F}(\mathbb{N}^3)$ is called the universe of triples of positive integers. Every element of the set $\mathcal{F}(\mathbb{N}^3)$ is called a planet.The equation $f(x,y,z)=0$ is called the stability law of the universe $\mathcal{F}(\mathbb{N}^3)$.

Example 1: Let $f_{n,m,k}:\mathbb{N}^3\longrightarrow\mathbb{N}$ be a function of three variables such that

$$(x,y,z)\longmapsto f_{n,m,k}(x,y,z)=x^n+y^m-z^k.$$

In this case,

$$\mathcal{F}_{n,m,k}(\mathbb{N}^3)=\left\{(x,y,z)\in\mathbb{N}^3 : f(x,y,z)=0\right\}=\left\{(x,y,z)\in\mathbb{N}^3 : x^n+y^m=z^k\right\}.$$

Fermat's Last Theorem allows us to say that $\mathcal{F}_{n,n,n}(\mathbb{N}^3)=\{\}$, with $n\geq 3$.

Example 2: The universe

$$\mathcal{F}_{2,2,2}(\mathbb{N}^3)=\left\{(x,y,z)\in\mathbb{N}^3 : x^2+y^2=z^2\right\}$$

has an infinite number of elements. The set $\mathcal{F}_{2,2,2}(\mathbb{N}^3)$ is called the universe of Pythagorean triples.

Mouanda's recent work on finding matrix solutions of Diophantine equations shows that the universe

$$\mathcal{F}_{n,m,k}(M_{nmk}(\mathbb{N})^3)=\left\{(X,Y,Z)\in M_{nmk}(\mathbb{N})^3 : X^n+Y^m=Z^k\right\}$$

is not empty at all for every triple (n,m,k) of positive integers. Assume that $n=3$ and $m=k=6$. Let us construct subsets of the universe

$$\mathcal{F}_{3,6,6}(M_6(\mathbb{N})^3)=\left\{(X,Y,Z)\in M_6(\mathbb{N})^3 : X^3+Y^6=Z^6\right\}.$$

Definition 2.1. *[7] A matrix $B\in M_n(\mathbb{N})$ is a construction structure of matrix solutions of Diophantine equations if there exist two positive integers m,β such that $B^m-\beta\times I_n=0$.*

Denote by

$$D_n(\mathbb{N})=\{B\in M_n(\mathbb{N}) : B^m-\beta\times I_n=0, m,\beta\in\mathbb{N}\}$$

the set of all construction structures of matrix solutions of Diophantine equations from $M_n(\mathbb{N})$. A matrix Diophantine equation can admit several construction structures. Let α be a positive integer. Let

$$A_\alpha=\begin{pmatrix}0&1&0&0&0&0\\0&0&1&0&0&0\\0&0&0&1&0&0\\0&0&0&0&1&0\\0&0&0&0&0&1\\\alpha&0&0&0&0&0\end{pmatrix}$$

be a Rare matrix of order 6 and index 1 [6]. The matrix A_α allows us to construct an infinite number of matrix solutions of the Diophantine equation $X^3 + Y^6 = Z^6$. Indeed, let us notice that $A_\alpha^6 = \alpha \times I_6$. This implies that

$$\begin{cases} A_\alpha^{2\times 3} = \alpha \times I_6 \\ A_\beta^6 = \beta \times I_6 \\ A_{\alpha+\beta}^6 = (\alpha+\beta) \times I_6 \\ (A_\alpha^2)^3 + A_\beta^6 = (\alpha+\beta) \times I_6 = A_{\alpha+\beta}^6, \forall \alpha, \beta \in \mathbb{N}. \end{cases}$$

Therefore, the matrix triples $(A_\alpha^2, A_\beta, A_{\alpha+\beta}), \alpha, \beta \in \mathbb{N}$, are solutions of the Diophantine equation $X^3 + Y^6 = Z^6$. In other words, for $\alpha, \beta \in \mathbb{N}$, the matrix triples

$$\left(\begin{pmatrix} 0 & 0 & 1 & 0 & 0 & 0 \\ 0 & 0 & 0 & 1 & 0 & 0 \\ 0 & 0 & 0 & 0 & 1 & 0 \\ 0 & 0 & 0 & 0 & 0 & 1 \\ \alpha & 0 & 0 & 0 & 0 & 0 \\ 0 & \alpha & 0 & 0 & 0 & 0 \end{pmatrix}, \begin{pmatrix} 0 & 1 & 0 & 0 & 0 & 0 \\ 0 & 0 & 1 & 0 & 0 & 0 \\ 0 & 0 & 0 & 1 & 0 & 0 \\ 0 & 0 & 0 & 0 & 1 & 0 \\ 0 & 0 & 0 & 0 & 0 & 1 \\ \beta & 0 & 0 & 0 & 0 & 0 \end{pmatrix}, \begin{pmatrix} 0 & 1 & 0 & 0 & 0 & 0 \\ 0 & 0 & 1 & 0 & 0 & 0 \\ 0 & 0 & 0 & 1 & 0 & 0 \\ 0 & 0 & 0 & 0 & 1 & 0 \\ 0 & 0 & 0 & 0 & 0 & 1 \\ \alpha+\beta & 0 & 0 & 0 & 0 & 0 \end{pmatrix} \right)$$

are planets of the universe $\mathcal{F}_{3,6,6}(M_6(\mathbb{N})^3)$. In fact,

$$\mathcal{F}_{A_\alpha, A_\alpha, A_\alpha} = \left\{ (A_\delta^2, A_\beta, A_{\delta+\beta}) : \delta, \beta \in \mathbb{N} \right\} \subset \mathcal{F}_{3,6,6}(M_6(\mathbb{N})^3).$$

The matrix A_α is called a construction structure of matrix solutions of the Diophantine equation $X^3 + Y^6 = Z^6$ and the triple $(A_\alpha, A_\alpha, A_\alpha)$ is called a construction structure triple of matrix solutions of the Diophantine equation $X^3 + Y^6 = Z^6$. The matrix A_α is not only the unique construction structure of matrix solutions of the Diophantine equation $X^3 + Y^6 = Z^6$. The matrix transpose of the matrix A_α noted by A_α^T is also a construction structure of matrix solutions of this equation. Therefore, the triples

$$(A_\alpha, A_\alpha, A_\alpha), (A_\alpha, A_\alpha, A_\alpha^T), (A_\alpha, A_\alpha^T, A_\alpha), (A_\alpha, A_\alpha^T, A_\alpha^T), (A_\alpha^T, A_\alpha, A_\alpha),$$

$$(A_\alpha^T, A_\alpha, A_\alpha^T), (A_\alpha^T, A_\alpha^T, A_\alpha), (A_\alpha^T, A_\alpha^T, A_\alpha^T)$$

are 8 construction structures of matrix solutions of the Diophantine equation $X^3 + Y^6 = Z^6$. Every construction structure triple of matrix solutions allows the construction of an infinite universe of matrix solutions of the Diophantine equation $X^3 + Y^6 = Z^6$. For example, the construction structure triple $(A_\alpha, A_\alpha^T, A_\alpha^T)$ allows the construction of the infinite universe

$$\mathcal{F}_{A_\alpha, A_\alpha^T, A_\alpha^T} = \left\{ (A_\delta^2, A_\beta^T, A_{\delta+\beta}^T) : \delta, \beta \in \mathbb{N} \right\}.$$

We can see that the matrix A_α generates 8 infinite universes.

2.2 Construction Structures Set of Matrix Solutions of the Diophantine Equation $X^3 + Y^6 = Z$

In this section, we show that the matrix Diophantine equation $X^3+Y^6 = Z^6$ admits matrix solutions in $M_3(\mathbb{N})$ and $M_{6\times k}(\mathbb{N}), k \in \mathbb{N}$. In the case where the matrix solutions are elements of the set $M_3(\mathbb{N})$, we can choose the matrix

$$A_\alpha = \begin{pmatrix} 0 & 1 & 0 \\ 0 & 0 & 1 \\ \alpha & 0 & 0 \end{pmatrix}$$

to generate construction structures associated to this equation. The set of matrix triples

$$\mathcal{F}_{A_\alpha,A_\alpha,A_\alpha} = \left\{ \left(\begin{pmatrix} 0 & 1 & 0 \\ 0 & 0 & 1 \\ 2\delta\beta+\delta^2 & 0 & 0 \end{pmatrix}, \begin{pmatrix} 0 & 1 & 0 \\ 0 & 0 & 1 \\ \beta & 0 & 0 \end{pmatrix}, \begin{pmatrix} 0 & 1 & 0 \\ 0 & 0 & 1 \\ \delta+\beta & 0 & 0 \end{pmatrix} \right) : \delta, \beta \in \mathbb{N} \right\}$$

are solutions of the equation $X^3 + Y^6 = Z^6$. Let us consider the matrices

$$A_{\alpha,1} = \begin{pmatrix} 0 & 1 & 0 \\ 0 & 0 & 1 \\ \alpha & 0 & 0 \end{pmatrix}, A_{\alpha,2} = \begin{pmatrix} 0 & \alpha & 0 \\ 0 & 0 & 1 \\ 1 & 0 & 0 \end{pmatrix}, A_{\alpha,3} = \begin{pmatrix} 0 & 1 & 0 \\ 0 & 0 & \alpha \\ 1 & 0 & 0 \end{pmatrix}.$$

The construction structures set $CS(A_{\alpha,1}) = \left\{A_{\alpha,j}, A_{\alpha,j}^T : j = 1, 2, 3\right\}$ is non-commutative. The set $CS(A_{\alpha,1})$ is called the construction structures set of matrix solutions of the Diophantine equation $X^3 + Y^6 = Z^6$ associated to the matrix $A_{\alpha,1}$. We can now construct the set

$$\{\mathcal{F}_{P_\alpha,Q_\alpha,H_\alpha} : P_\alpha, Q_\alpha, H_\alpha \in CS(A_{\alpha,1})\}$$

of universes of matrix triple solutions of the Diophantine equation

$$X^3 + Y^6 = Z^6.$$

Assume that the matrix solutions are elements of the set $M_6(\mathbb{N})$, in this case, we can consider the matrices

$$A_{\alpha,1} = \begin{pmatrix} 0 & 1 & 0 & 0 & 0 & 0 \\ 0 & 0 & 1 & 0 & 0 & 0 \\ 0 & 0 & 0 & 1 & 0 & 0 \\ 0 & 0 & 0 & 0 & 1 & 0 \\ 0 & 0 & 0 & 0 & 0 & 1 \\ \alpha & 0 & 0 & 0 & 0 & 0 \end{pmatrix}, A_{\alpha,2} = \begin{pmatrix} 0 & \alpha & 0 & 0 & 0 & 0 \\ 0 & 0 & 1 & 0 & 0 & 0 \\ 0 & 0 & 0 & 1 & 0 & 0 \\ 0 & 0 & 0 & 0 & 1 & 0 \\ 0 & 0 & 0 & 0 & 0 & 1 \\ 1 & 0 & 0 & 0 & 0 & 0 \end{pmatrix},$$

$$A_{\alpha,3}=\begin{pmatrix}0&1&0&0&0&0\\0&0&\alpha&0&0&0\\0&0&0&1&0&0\\0&0&0&0&1&0\\0&0&0&0&0&1\\1&0&0&0&0&0\end{pmatrix},A_{\alpha,4}=\begin{pmatrix}0&1&0&0&0&0\\0&0&1&0&0&0\\0&0&0&\alpha&0&0\\0&0&0&0&1&0\\0&0&0&0&0&1\\1&0&0&0&0&0\end{pmatrix},$$

$$A_{\alpha,5}=\begin{pmatrix}0&1&0&0&0&0\\0&0&1&0&0&0\\0&0&0&1&0&0\\0&0&0&0&\alpha&0\\0&0&0&0&0&1\\1&0&0&0&0&0\end{pmatrix},A_{\alpha,6}=\begin{pmatrix}0&1&0&0&0&0\\0&0&1&0&0&0\\0&0&0&1&0&0\\0&0&0&0&1&0\\0&0&0&0&0&\alpha\\1&0&0&0&0&0\end{pmatrix}.$$

The set $CS(A_{\alpha,1})=\left\{A_{\alpha,j},A_{\alpha,j}^{T}:j=1,2,...,5,6\right\}$ is non-commutative. The set $CS(A_{\alpha,1})$ is another construction structures set of matrix solutions of the Diophantine equation $X^3+Y^6=Z^6$ associated to the matrix $A_{\alpha,1}$.

2.3 Construction Structures Set of Matrix Solutions of Diophantine Equations

Let α be a positive integer. Assume that $A_{\alpha,1}\in M_n(\mathbb{N})$ is a square matrix of order n and let introduce the associated construction structures set of matrix solutions. Let

$$A_{\alpha,1}=\begin{pmatrix}0&1&0&0&\ldots&0&0&0&0\\0&0&1&0&\ldots&0&0&0&0\\0&0&0&1&\ldots&0&0&0&0\\0&0&0&0&\ldots&0&0&0&0\\\vdots&\vdots&\vdots&\vdots&\ldots&\vdots&\vdots&\vdots&\vdots\\0&0&0&0&\ldots&0&1&0&0\\0&0&0&0&\ldots&0&0&1&0\\0&0&0&0&\ldots&0&0&0&1\\\alpha&0&0&0&\ldots&0&0&0&0\end{pmatrix}$$

be a Rare matrix of order n and index 1. Denote by

$$A_{\alpha,2}=\begin{pmatrix}0&\alpha&0&0&\ldots&0&0&0&0\\0&0&1&0&\ldots&0&0&0&0\\0&0&0&1&\ldots&0&0&0&0\\0&0&0&0&\ldots&0&0&0&0\\\vdots&\vdots&\vdots&\vdots&\ldots&\vdots&\vdots&\vdots&\vdots\\0&0&0&0&\ldots&0&1&0&0\\0&0&0&0&\ldots&0&0&1&0\\0&0&0&0&\ldots&0&0&0&1\\1&0&0&0&\ldots&0&0&0&0\end{pmatrix},A_{\alpha,3}=\begin{pmatrix}0&1&0&0&\ldots&0&0&0&0\\0&0&\alpha&0&\ldots&0&0&0&0\\0&0&0&1&\ldots&0&0&0&0\\0&0&0&0&\ldots&0&0&0&0\\\vdots&\vdots&\vdots&\vdots&\ldots&\vdots&\vdots&\vdots&\vdots\\0&0&0&0&\ldots&0&1&0&0\\0&0&0&0&\ldots&0&0&1&0\\0&0&0&0&\ldots&0&0&0&1\\1&0&0&0&\ldots&0&0&0&0\end{pmatrix},$$

$$A_{\alpha,4} = \begin{pmatrix} 0 & 1 & 0 & 0 & \dots & 0 & 0 & 0 & 0 \\ 0 & 0 & 1 & 0 & \dots & 0 & 0 & 0 & 0 \\ 0 & 0 & 0 & \alpha & \dots & 0 & 0 & 0 & 0 \\ 0 & 0 & 0 & 0 & \dots & 0 & 0 & 0 & 0 \\ \vdots & \vdots & \vdots & \vdots & \dots & \vdots & \vdots & \vdots & \vdots \\ 0 & 0 & 0 & 0 & \dots & 0 & 1 & 0 & 0 \\ 0 & 0 & 0 & 0 & \dots & 0 & 0 & 1 & 0 \\ 0 & 0 & 0 & 0 & \dots & 0 & 0 & 0 & 1 \\ 1 & 0 & 0 & 0 & \dots & 0 & 0 & 0 & 0 \end{pmatrix}, \dots, A_{\alpha,n-2} = \begin{pmatrix} 0 & 1 & 0 & 0 & \dots & 0 & 0 & 0 & 0 \\ 0 & 0 & 1 & 0 & \dots & 0 & 0 & 0 & 0 \\ 0 & 0 & 0 & 1 & \dots & 0 & 0 & 0 & 0 \\ 0 & 0 & 0 & 0 & \dots & 0 & 0 & 0 & 0 \\ \vdots & \vdots & \vdots & \vdots & \dots & \vdots & \vdots & \vdots & \vdots \\ 0 & 0 & 0 & 0 & \dots & 0 & \alpha & 0 & 0 \\ 0 & 0 & 0 & 0 & \dots & 0 & 0 & 1 & 0 \\ 0 & 0 & 0 & 0 & \dots & 0 & 0 & 0 & 1 \\ 1 & 0 & 0 & 0 & \dots & 0 & 0 & 0 & 0 \end{pmatrix},$$

$$A_{\alpha,n-1} = \begin{pmatrix} 0 & 1 & 0 & 0 & \dots & 0 & 0 & 0 & 0 \\ 0 & 0 & 1 & 0 & \dots & 0 & 0 & 0 & 0 \\ 0 & 0 & 0 & 1 & \dots & 0 & 0 & 0 & 0 \\ 0 & 0 & 0 & 0 & \dots & 0 & 0 & 0 & 0 \\ \vdots & \vdots & \vdots & \vdots & \dots & \vdots & \vdots & \vdots & \vdots \\ 0 & 0 & 0 & 0 & \dots & 0 & 1 & 0 & 0 \\ 0 & 0 & 0 & 0 & \dots & 0 & 0 & \alpha & 0 \\ 0 & 0 & 0 & 0 & \dots & 0 & 0 & 0 & 1 \\ 1 & 0 & 0 & 0 & \dots & 0 & 0 & 0 & 0 \end{pmatrix}, A_{\alpha,n} = \begin{pmatrix} 0 & 1 & 0 & 0 & \dots & 0 & 0 & 0 & 0 \\ 0 & 0 & 1 & 0 & \dots & 0 & 0 & 0 & 0 \\ 0 & 0 & 0 & 1 & \dots & 0 & 0 & 0 & 0 \\ 0 & 0 & 0 & 0 & \dots & 0 & 0 & 0 & 0 \\ \vdots & \vdots & \vdots & \vdots & \dots & \vdots & \vdots & \vdots & \vdots \\ 0 & 0 & 0 & 0 & \dots & 0 & 1 & 0 & 0 \\ 0 & 0 & 0 & 0 & \dots & 0 & 0 & 1 & 0 \\ 0 & 0 & 0 & 0 & \dots & 0 & 0 & 0 & \alpha \\ 1 & 0 & 0 & 0 & \dots & 0 & 0 & 0 & 0 \end{pmatrix}.$$

The set $CS(A_{\alpha,1}) = \left\{A_{\alpha,j}, A_{\alpha,j}^T : j = 1, 2, ..., n-1, n\right\}$ is called the construction structures set of matrix solutions of Diophantine equations. In this case, the set $CS(A_{\alpha,1})$ contains exactly $2n$ matrices.

2.4 Multiverses Associated to the Construction Struc-tures Sets of Matrix Solutions of the Diophantine Equation $X^3 + Y^6 = Z$

The Diophantine equation $X^3 + Y^6 = Z^6$ has an infinite number of construction structures sets of different sizes. In particular, matrices from the sets $M_{6k}(\mathbb{N}), k \in \mathbb{N}$ are matrix solutions of this Diophantine equation.

Definition 2.2. *A multiverse (or parallel universes) is the collection of alternate universes that share a universal hierarchy.*

Let $CS(A_{\alpha,1}) = \left\{A_{\alpha,j}, A_{\alpha,j}^T : j = 1, 2, ..., 5, 6\right\}$ be a construction structures set of matrix solution of the Diophantine equation $X^3 + Y^6 = Z^6$. The set

$$\mathcal{M} = \{\mathcal{F}_{P_\alpha, Q_\alpha, H_\alpha} : P_\alpha, Q_\alpha, H_\alpha \in CS(A_{\alpha,1})\}$$

is called the multiverse of matrix triple solutions of the Diophantine equation $X^3 + Y^6 = Z^6$. The set $\mathcal{M}$ is finite. We can now show that every multiverse of matrix triple solutions of the Diophantine equation $X^3 + Y^6 = Z^6$ is finite.

Proof of Theorem 1.1

We need to construct multiverses of matrix solutions elements of the set $M_{6k}(\mathbb{N})$.

• Assume that $k = 1$. In this case, the matrix solutions are elements of the set $M_6(\mathbb{N})$, we can consider the matrix

$$A_{\alpha,1} = \begin{pmatrix} 0 & 1 & 0 & 0 & 0 & 0 \\ 0 & 0 & 1 & 0 & 0 & 0 \\ 0 & 0 & 0 & 1 & 0 & 0 \\ 0 & 0 & 0 & 0 & 1 & 0 \\ 0 & 0 & 0 & 0 & 0 & 1 \\ \alpha & 0 & 0 & 0 & 0 & 0 \end{pmatrix}$$

and the construction structures set

$$CS_1(A_{\alpha,1}) = \left\{A_{\alpha,j}, A_{\alpha,j}^T : j = 1, 2, ..., 5, 6\right\}$$

has 12 matrices. The universe

$$\mathcal{F}_{P_\alpha,Q_\alpha,H_\alpha} = \left\{(P_\delta^2, Q_\beta, H_{\delta+\beta}) : \delta, \beta \in \mathbb{N}\right\}, P_\alpha, Q_\alpha, H_\alpha \in CS_1(A_{\alpha,1})$$

is an infinite set. The set

$$\mathcal{M}_1 = \{\mathcal{F}_{P_\alpha,Q_\alpha,H_\alpha} : P_\alpha, Q_\alpha, H_\alpha \in CS_1(A_{\alpha,1})\}$$

is called the first multiverse of matrix solutions of the equation $X^3 + Y^6 = Z^6$. This multiverse has exactly $12 \times 12 \times 12 = 1,728$ universes.

• Assume that $k = 2$. Let

$$A_{\alpha,1} = \begin{pmatrix} 0 & 1 & 0 & 0 & 0 & 0 & 0 & 0 & 0 & 0 & 0 & 0 \\ 0 & 0 & 1 & 0 & 0 & 0 & 0 & 0 & 0 & 0 & 0 & 0 \\ 0 & 0 & 0 & 1 & 0 & 0 & 0 & 0 & 0 & 0 & 0 & 0 \\ 0 & 0 & 0 & 0 & 1 & 0 & 0 & 0 & 0 & 0 & 0 & 0 \\ 0 & 0 & 0 & 0 & 0 & 1 & 0 & 0 & 0 & 0 & 0 & 0 \\ 0 & 0 & 0 & 0 & 0 & 0 & 1 & 0 & 0 & 0 & 0 & 0 \\ 0 & 0 & 0 & 0 & 0 & 0 & 0 & 1 & 0 & 0 & 0 & 0 \\ 0 & 0 & 0 & 0 & 0 & 0 & 0 & 0 & 1 & 0 & 0 & 0 \\ 0 & 0 & 0 & 0 & 0 & 0 & 0 & 0 & 0 & 1 & 0 & 0 \\ 0 & 0 & 0 & 0 & 0 & 0 & 0 & 0 & 0 & 0 & 1 & 0 \\ 0 & 0 & 0 & 0 & 0 & 0 & 0 & 0 & 0 & 0 & 0 & 1 \\ \alpha & 0 & 0 & 0 & 0 & 0 & 0 & 0 & 0 & 0 & 0 & 0 \end{pmatrix}$$

be a Rare matrix of order 12 and index 1. The construction structures set

$$CS_2(A_{\alpha,1}) = \left\{A_{\alpha,j}, A_{\alpha,j}^T : j = 1, 2, ..., 11, 12\right\}$$

has 24 matrices. The universe

$$\mathcal{F}_{P_\alpha,Q_\alpha,H_\alpha} = \left\{(P_\delta^4, Q_\beta^2, H_{\delta+\beta}^2) : \delta, \beta \in \mathbb{N}\right\}, P_\alpha, Q_\alpha, H_\alpha \in CS_2(A_{\alpha,1})$$

is an infinite set. The set

$$\mathcal{M}_2 = \{\mathcal{F}_{P_\alpha,Q_\alpha,H_\alpha} : P_\alpha, Q_\alpha, H_\alpha \in CS_2(A_{\alpha,1})\}$$

is called the second multiverse of matrix solutions of the equation $X^3 + Y^6 = Z^6$. This multiverse has exactly $24 \times 24 \times 24 = 13,824$ universes.

• Let k be a positive integer and let

$$A_{\alpha,1} = \begin{pmatrix} 0 & 1 & 0 & 0 & \dots & 0 & 0 & 0 & 0 \\ 0 & 0 & 1 & 0 & \dots & 0 & 0 & 0 & 0 \\ 0 & 0 & 0 & 1 & \dots & 0 & 0 & 0 & 0 \\ 0 & 0 & 0 & 0 & \dots & 0 & 0 & 0 & 0 \\ \vdots & \vdots & \vdots & \vdots & \dots & \vdots & \vdots & \vdots & \vdots \\ 0 & 0 & 0 & 0 & \dots & 0 & 1 & 0 & 0 \\ 0 & 0 & 0 & 0 & \dots & 0 & 0 & 1 & 0 \\ 0 & 0 & 0 & 0 & \dots & 0 & 0 & 0 & 1 \\ \alpha & 0 & 0 & 0 & \dots & 0 & 0 & 0 & 0 \end{pmatrix} \in M_{6k}(\mathbb{N}), \alpha \neq 0,$$

be a Rare matrix of order $6k$ and index 1. Denote by

$$A_{\alpha,2} = \begin{pmatrix} 0 & \alpha & 0 & 0 & \dots & 0 & 0 & 0 & 0 \\ 0 & 0 & 1 & 0 & \dots & 0 & 0 & 0 & 0 \\ 0 & 0 & 0 & 1 & \dots & 0 & 0 & 0 & 0 \\ 0 & 0 & 0 & 0 & \dots & 0 & 0 & 0 & 0 \\ \vdots & \vdots & \vdots & \vdots & \dots & \vdots & \vdots & \vdots & \vdots \\ 0 & 0 & 0 & 0 & \dots & 0 & 1 & 0 & 0 \\ 0 & 0 & 0 & 0 & \dots & 0 & 0 & 1 & 0 \\ 0 & 0 & 0 & 0 & \dots & 0 & 0 & 0 & 1 \\ 1 & 0 & 0 & 0 & \dots & 0 & 0 & 0 & 0 \end{pmatrix}, A_{\alpha,3} = \begin{pmatrix} 0 & 1 & 0 & 0 & \dots & 0 & 0 & 0 & 0 \\ 0 & 0 & \alpha & 0 & \dots & 0 & 0 & 0 & 0 \\ 0 & 0 & 0 & 1 & \dots & 0 & 0 & 0 & 0 \\ 0 & 0 & 0 & 0 & \dots & 0 & 0 & 0 & 0 \\ \vdots & \vdots & \vdots & \vdots & \dots & \vdots & \vdots & \vdots & \vdots \\ 0 & 0 & 0 & 0 & \dots & 0 & 1 & 0 & 0 \\ 0 & 0 & 0 & 0 & \dots & 0 & 0 & 1 & 0 \\ 0 & 0 & 0 & 0 & \dots & 0 & 0 & 0 & 1 \\ 1 & 0 & 0 & 0 & \dots & 0 & 0 & 0 & 0 \end{pmatrix}$$

$$A_{\alpha,4}=\begin{pmatrix}0&1&0&0&\dots&0&0&0&0\\0&0&1&0&\dots&0&0&0&0\\0&0&0&\alpha&\dots&0&0&0&0\\0&0&0&0&\dots&0&0&0&0\\\vdots&\vdots&\vdots&\vdots&\dots&\vdots&\vdots&\vdots&\vdots\\0&0&0&0&\dots&0&1&0&0\\0&0&0&0&\dots&0&0&1&0\\0&0&0&0&\dots&0&0&0&1\\1&0&0&0&\dots&0&0&0&0\end{pmatrix},\dots,A_{\alpha,6k-2}=\begin{pmatrix}0&1&0&0&\dots&0&0&0&0\\0&0&1&0&\dots&0&0&0&0\\0&0&0&1&\dots&0&0&0&0\\0&0&0&0&\dots&0&0&0&0\\\vdots&\vdots&\vdots&\vdots&\dots&\vdots&\vdots&\vdots&\vdots\\0&0&0&0&\dots&0&\alpha&0&0\\0&0&0&0&\dots&0&0&1&0\\0&0&0&0&\dots&0&0&0&1\\1&0&0&0&\dots&0&0&0&0\end{pmatrix},$$

$$A_{\alpha,6k-1}=\begin{pmatrix}0&1&0&0&\dots&0&0&0&0\\0&0&1&0&\dots&0&0&0&0\\0&0&0&1&\dots&0&0&0&0\\0&0&0&0&\dots&0&0&0&0\\\vdots&\vdots&\vdots&\vdots&\dots&\vdots&\vdots&\vdots&\vdots\\0&0&0&0&\dots&0&1&0&0\\0&0&0&0&\dots&0&0&\alpha&0\\0&0&0&0&\dots&0&0&0&1\\1&0&0&0&\dots&0&0&0&0\end{pmatrix},A_{\alpha,6k}=\begin{pmatrix}0&1&0&0&\dots&0&0&0&0\\0&0&1&0&\dots&0&0&0&0\\0&0&0&1&\dots&0&0&0&0\\0&0&0&0&\dots&0&0&0&0\\\vdots&\vdots&\vdots&\vdots&\dots&\vdots&\vdots&\vdots&\vdots\\0&0&0&0&\dots&0&1&0&0\\0&0&0&0&\dots&0&0&1&0\\0&0&0&0&\dots&0&0&0&\alpha\\1&0&0&0&\dots&0&0&0&0\end{pmatrix}.$$

It is well known that $A_{\alpha,j}^{6k}=\alpha\times I_{6k}, j=1,\dots,6k$ [5]. The set

$$CS_k(A_{\alpha,1})=\left\{A_{\alpha,j},A_{\alpha,j}^T:j=1,2,\dots,6k\right\}\subset M_{6k}(\mathbb{N})$$

is the k^{th} construction structures set of the matrix solutions of the Diophantine equation $X^3+Y^6=Z^6$. The Diophantine equation

$$X^{6k}+Y^{6k}=Z^{6k},$$

allows us to deduce that

$$(X^{2k})^3+(Y^k)^6=(Z^k)^6.$$

Therefore,

$$(A_{\alpha,j}^{2k})^3+(A_{\beta,j}^k)^6=(A_{\alpha+\beta,j}^k)^6, j=1,2,\dots,6k,\alpha,\beta\in\mathbb{N}.$$

The matrix triples $(A_{\alpha,j}^{2k},A_{\beta,j}^k,A_{\alpha+\beta,j}^k),\alpha,\beta\in\mathbb{N}$, satisfy the Diophantine equation $X^3+Y^6=Z^6$. The universe

$$\mathcal{F}_{P_\alpha,Q_\alpha,H_\alpha} = \left\{(P_\delta^{2k}, Q_\beta^k, H_{\delta+\beta}^k) : \delta, \beta \in \mathbb{N}\right\}, P_\alpha, Q_\alpha, H_\alpha \in CS_k(A_{\alpha,1}) \subset M_{6k}(\mathbb{N}),$$

is an infinite set. The set

$$\mathcal{M}_k = \{\mathcal{F}_{P_\alpha,Q_\alpha,H_\alpha} : P_\alpha, Q_\alpha, H_\alpha \in CS_k(A_{\alpha,1})\}$$

is called the k^{th} multiverse of matrix solutions of the Diophantine equation $X^3 + Y^6 = Z^6$. The multiverse $\mathcal{M}_k$ has

$$12k \times 12k \times 12k = 1,728 \times k^3$$

universes of matrix solutions. This yields us the desired result. □

REFERENCES

1. J. H. Barnett, Generating Pythagorean triples: the methods of Pythagoras and of Plato via Gnomons, 2017.
2. L.C. Bruno, Math and Mathematicians: The History of Math Discoveries Around the World. Math and Mathematicians, U X L, 2002.
3. L. E. Dickson, History of the theory of numbers: Diophantine Analysis, vol. 2. Courier Corporation, 2013.
4. S. W. Hawking, Thomas Hertog, "A Smooth exist from eternal inflation?", Journal of High Energy Physics, 147(2018).
5. J. Moussounda Mouanda, On Fermat's Last Theorem and Galaxies of sequences of positive integers, American Journal of Computational Mathematics, 12(2022), 162-189.
6. J. Moussounda Mouanda. On Beal's Conjecture for Matrix Solutions and Multiplication Commutative Groups of Rare Matrices. Turkish Journal of Analysis and Number Theory, Vol. 12(1), 1-7, 2024.
7. J. Moussounda Mouanda. On Construction Structures of Matrix Solutions of Diophantine Equations. Journal of Advances in Mathematics and Computer science, Vol. 39 (5), 1-14, 2024.
8. G. R. Proclus et al, A commentary on the first book of Euclid's Elements, 1970.
9. Ozanam, Recreat ons n Mat emat cs an Natura P osop y. Mat an Mathematicians, G. Kearsley; 49, 1814.
10. J. Rukavicka, Dickson's method for generating Pythagorean triples revisited, European Journal of Pure and Applied Mathematics, vol. 6, no.3, 2013.
11. F. J. Swetz et al, Mathematical treasures - Michael Stifel's Arithmetica Integra, 2011.